SOME CURRENT TOPICS IN CONDENSED MATTER PHYSICS 2016

M.E. MORA-RAMOS
R. PÉREZ-ÁLVAREZ
L. M. GAGGERO-SAGER
(editors)

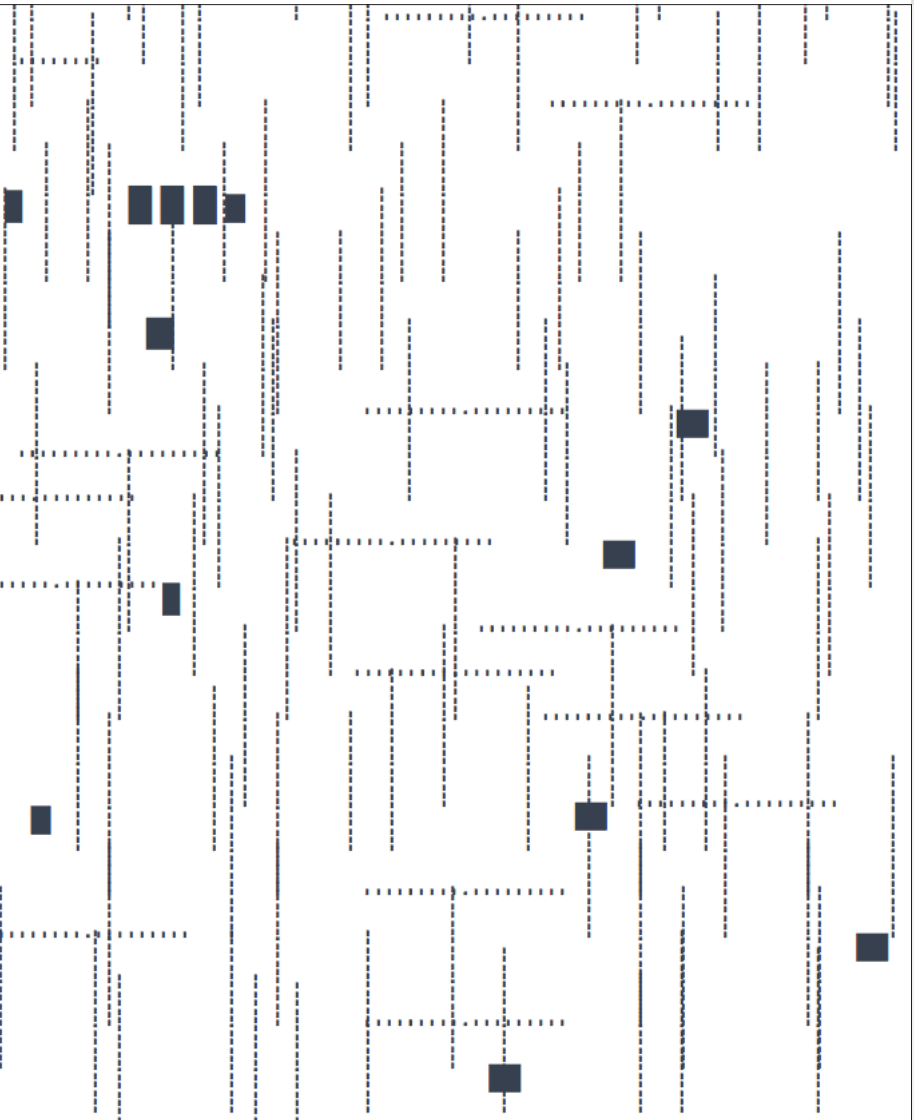

UNIVERSIDAD AUTÓNOMA DEL ESTADO DE MORELOS
Colección: *Contemporary Condensed Matter Physics: Selected Topics*

Some current topics in condensed matter physics

2016

M. E. Mora-Ramos, R. Pérez-Álvarez,
L. M. Gaggero-Sager
(Eds.)

Universidad Autónoma del Estado de Morelos
Cuernavaca. México
2018

Some current topics in condensed matter physics, 2016.
Colección: Contemporary Condensed Matter Physics: Selected Topics

D.R. 2018, Universidad Autónoma del Estado de Morelos
Av. Universidad 1001, Col. Chamilpa
62210, Cuernavaca, Morelos
publicaciones@uaem.mx
libros.uaem.mx

ISBN: 978-607-8519-73-6
ISBN (colección): 978-607-8434-78-7

Imagen de portada: Ernesto Ríos. De la serie Faebook
dr@wings. Gráfica digital con teclado de celular, 2007

Cuerpo Académico de Física del Estado Sólido
Universidad Autónoma del Estado de Morelos

Foreword

For some years, professors belonging to the Group of Solid State Physics in the Morelos Autonomous State University (UAEM), have edited a series of compilations of selected talks that were presented at the Workshop of Molecular and Condensed Matter Physics, held at UAEM since 2008 (http://web.fc.uaem.mx/ tallerfmcm/temas.htm). The present is the fourth of this series of electronic books, which corresponds to the selection made in 2016. It contains some recent contributions in several areas of the research frontier in Condensed Matter Physics.

Since the first edition we have decided to keep the bilingual format (english-spanish) with the purpose of achieving a wider diffusion of the contents via electronic means.

Cuernavaca, Mexico. May 2017

M. E. Mora-Ramos
(memora@uaem.mx)
R. Pérez-Álvarez (rpa@uaem.mx)
L. M. Gaggero-Sager (lgaggero@uaem.mx)

Durante varios años, un grupo de profesores del Cuerpo Académico de Física del Estado Sólido de la Universidad Autónoma del Estado de Morelos, hemos realizado compilaciones de algunas de las conferencias impartidas en el Taller de Física de la Materia Condensada y Molecular, que se celebra desde 2008 en predios de la mencionada Institucin. Luego de la publicación de los dos primeros volúmenes (http://web.fc.uaem.mx/ tallerfmcm/temas.htm) de esta serie de libros electrónicos, presentamos a la comunidad cuarto, correspondiente a la selección del año 2016. Esta vez, las contribuciones abarcan áreas de actividad de vanguardia de la Física de la Materia Condensada que no haban sido abordadas en los libros anteriores.

Como comentamos en el prefacio del primer volumen de la serie, hemos mantenido con toda intención el formato bilingüe (español-inglés), en aras de que los materiales publicados puedan encontrar mayor difusión vía *internet*.

Cuernavaca, México. May 2017

M. E. Mora-Ramos
(memora@uaem.mx)
R. Pérez-Álvarez (rpa@uaem.mx)
L. M. Gaggero-Sager (lgaggero@uaem.mx)

Contents

Anomalous diffusion in phase space: Relation to the entropy growth rate

Oscar Sotolongo-Costa, Oscar Sotolongo-Grau, L. M. Gaggero-Sager and I. Rodríguez-Vargas

Abstract

In this work it is shown that the time dependence of entropy can be intricate, more than the well-known linear dependence for chaotic systems. With the help of fractional calculus and considering a phase space with anomalous diffusion a close expression for the entropy was derived. This expression is quite general, since the equiprobability postulate is not longer assumed, the system dynamic in the phase space is not necessarily Markovian and the system is not in a steady state at all. Different possibilities for the time evolution of entropy by considering different features of the phase space and processes involved in the system dynamic are obtained.

En este trabajo se muestra que la dependencia temporal de la entropía puede ser compleja, mucho más incluso que la bien conocida dependencia lineal para sistemas caóticos. Con la ayuda del cálculo fraccionario y considerando un espacio de fase con difusión anómala se pudo derivar analíticamente una expresión para la entropía como función del tiempo. Esta expresión es general, ya que en ningún momento se asume el postulado de iguales probabilidades a priori, la dinámica del sistema en el espacio de fase no necesariamente es Markoviana e igualmente el sistema no está necesariamente en un estado estacionario. También se presentan casos específicos para la evolución temporal de la entropía, los cuales son el resultado de con-

(OSC, IRV) Centro de Investigaciones en Ciencia-(IICBA), Universidad Autónoma del Estado de Morelos, Av. Universidad 1001, 62209 Cuernavaca, Morelos, México. (OSG) Alzheimer Research Center and Memory Clinic, Fundacio ACE, Institut Catala de Neurociencies Aplicades, Barcelona, Spain. (LMGS) CIICAp, IICBA, Universidad Autónoma del Estado de Morelos, Av. Universidad 1001, Col. Chamilpa, 62209 Cuernavaca, Morelos, México. (IRV) Unidad Académica de Física, Universidad Autónoma de Zacatecas, Calzada Solidaridad Esquina con Paseo a la Bufa S/N, 98060 Zacatecas, Zac., México. e-mail: osotolongo@uaem.mx

siderar características particulares del espacio fase y los procesos involucrados en la dinámica del sistema.

1 Introduction

Entropy is one of the most fascinating, abstract and complex concepts in physics. So much so that several entropies have arisen. Among the most important characteristics of entropy its extensive and non-conserved character stand out. From a microscopic stand point entropy can be linked to the probabilistic features of the accessible microstates of a system, or in other words to the peculiarities of the corresponding phase space. In non-linear dynamics the evolution of entropy is a linear function of time or equivalently the entropy production rate is constant, better known as Kolmogorov-Sinai entropy [1, 2], and specifically given by the sum of positive Lyapunov exponents, known as Pesin identity [3]. Even in the onset of chaos, in which the Pesin identity fails, it is possible to find a direct relation between the production rate of the Tsallis entropy and the so called generalized Lyapunov exponents or q-Lyapunov exponents [4]. In the case of the statistical entropy -also known as physical entropy-, $S(t)$, three general stages for far-from-equilibrium processes have been identified [5, 6]: 1) $S(t)$ depends strongly on the dynamical system and the initial probability distribution, and the rate of variation can be positive, negative, large or small; 2) $S(t)$ is a linear increasing function of time; 3) physical entropy tends to a constant value, typical of equilibrium. By giving the same weights to the initial probability distribution from all regions of phase space (coarse graining) a direct connection between the physical entropy and the Kolmogorov-Sinai entropy can be established [6]. However, there are other possibilities such as the gradual evolution of the probability density in space and time, or the anomalous diffusion of the representative points in the phase space. The aim of the present work is to address the latter scenario.

2 Fundamentals of anomalous diffusion

Let's start with general considerations. It is well known that the time evolution of the entropy of an arbitrary system is analyzed by studying the system evolution towards equilibrium, through the diffusion of the representative points in the phase space. The possible set of initial

conditions of the system are represented by a set of phase space points. The time evolution of these points takes place in diffusion fashion. Here, the diffusion process obeys a waiting times distribution with infinite variance, which is typical of Levy processes or also called continuous-time random walks (CTRWs) [7]. In the case of normal diffusion the probability distribution comes as

$$\rho(x,t) = \frac{1}{\sqrt{4\pi K t}} \exp\left(-\frac{x^2}{4Kt}\right), \tag{1}$$

where K is the diffusion coefficient and ρ represent the particle density at position x and time t. In terms of probability $\rho(x,t)$ is the probability that the particle be located at the point x and at the instant t. Besides, the corresponding diffusion equation is

$$\frac{\partial \rho}{\partial t} = K \frac{\partial^2 \rho}{\partial x^2}, \tag{2}$$

with $K = \sigma^2/\tau$.

In order to generalize the preceding equation to anomalous diffusion the CTRW will be used as starting point. This model is based on the idea that the length of a particle jump from one site to another as well as the waiting time between jumps are described by a function $\psi(x,t)$. Specifically, the jumps probability density is given as,

$$\lambda(x) = \int_0^\infty \psi(x,t)dt, \tag{3}$$

and the corresponding one for waiting times

$$\omega(t) = \int_{-\infty}^\infty \psi(x,t)dx, \tag{4}$$

Here, $\lambda(x)dx$ can be interpreted as the probability of a jump of length x in the interval $[x, x+dx]$, and $\omega(t)dt$ in the same way as the probability of a waiting time t in the interval $[t, t+dt]$. It is also assumed that the spatial and temporal processes are independent, that is, $\psi(x,t) = \lambda(x)\omega(t)$. In the same footing, the characteristic waiting time and the jumps variance can be defined as:

$$\tau = \int_0^\infty t\omega(t)dt, \tag{5}$$

and

$$\left\langle x^2 \right\rangle = \int_{-\infty}^{\infty} x^2 \lambda(x) dx. \tag{6}$$

With this definitions a CTRW can be written as

$$\eta(x,t) = \int_{-\infty}^{\infty} dx' \int_0^{\infty} dt' \eta(x',t') \psi(x-x',t-t'), \tag{7}$$

where $\eta(x,t)$ the probability of reaching x at exactly the time t. Then,

$$W(x,t) = \int_0^t \eta(x,t') \psi(t-t') dt', \tag{8}$$

is the probability to be at x at the time t, which is different from $\eta(x,t)$. In addition,

$$\psi(t) = 1 - \int_0^t W(t') dt', \tag{9}$$

is the probability that the particle does not move up to t.

With all this definitions in mind it is possible to obtain the probability density $\rho(x,t)$ in the reciprocal spaces of the variables x and t by Fourier and Laplace transforming it, respectively:

$$\rho(k,u) = \frac{1-\omega(u)}{u} \frac{\rho_0(k)}{1-\psi(k,u)}. \tag{10}$$

Here, $\omega(u)$ can be approximated as $\omega = 1-(u\tau)^{\alpha}$. This approximation is possible by assuming that the distribution of waiting times has the asymptotic form $\omega(t) = \left(\frac{\tau}{t}\right)^{1+\alpha}$. For the jumps a gaussian distribution is considered, hence $\lambda(k) = 1-\sigma^2 k^2$. Then,

$$\psi(k,u) = 1-(u\tau)^{\alpha} - \sigma^2 k^2, \tag{11}$$

and

$$\rho(k,u) = \frac{\rho_0(k)/u}{1+u^{-\alpha} K_{\alpha} k^2}, \tag{12}$$

with $K_{alpha} = \frac{\sigma^2}{\tau^{\alpha}}$. By taking the inverse Fourier transform of the latter equation the following equation is get

$$u\rho(x,u)-\rho_0 = K_\alpha u^{1-\alpha}\rho''(x,u). \tag{13}$$

The term on the left hand side can be identified as the Laplace transform of the temporal derivative of $\rho(x,t)$ and the term on the right hand side with the second derivative with respect to x of the Laplace transform of the fractional integral of $\rho(x,t)$. Explicitly,

$$\mathscr{L}\left(\frac{\partial\rho(x,t)}{\partial t}\right) = K_\alpha \frac{\partial^2}{\partial x^2}\mathscr{L}\left[{}_0D_t^{1-\alpha}\rho(x,t)\right], \tag{14}$$

where $\mathscr{L}$ stands for the Laplace transform. Eq. (14) can be written in equivalent ways as

$$\frac{\partial\rho(x,t)}{\partial t} = {}_0D_t^{1-\alpha} K_\alpha \frac{\partial^2\rho(x,t)}{\partial x^2}. \tag{15}$$

This equation represent a fractional diffusion equation. By taking the Fourier transform of eq. (15),

$$\frac{\partial\rho(k,t)}{\partial t} = {}_0D_t^{1-\alpha} K_\alpha k^2\rho(k,t). \tag{16}$$

Taking into account the definition of the fractional integral

$${}_0D_t^{1-\alpha} f(t) = \frac{1}{\Gamma(\nu)}\int_0^t (t-u)^{\nu-1} f(u)du, \tag{17}$$

eq. (16) can be expressed as

$$\rho(k,t)-\rho(k,0) = \frac{K_\alpha k^2}{\Gamma(\alpha-1)}\int_0^t (t-u)^{\alpha-2}\rho(k,u)du. \tag{18}$$

For more details about anomalous diffusion from a fractional dynamical approach see [8].

3 Anomalous diffusion in the phase space and the entropy growth rate

With the fundamentals of the preceding section it is possible to tackle the problem of anomalous diffusion of representative points in the phase space of an arbitrary system. It is worth saying that if we want to calculate the entropy in terms of the phase space volume increase

we must notice that fine-grained quantities do not vary with time, since, by Liouville's Theorem, the volume of phase space occupied by the system during its evolution is constant. Instead, under coarse-graining; *i.e.*, smearing or smoothing of the probability distribution in phase space, the volume occupied keeps increasing.

The simplest way to produce a coarse-graining is to divide the phase space in cells such that the sum of their volumes equals the total volume of the available phase space. Then, we consider the process of diffusion as random walkers successively occupying different cells, so that the initial configuration smears out and the entropy increases [6, 12]. By knowing the time variation of the mentioned points, more specifically the time dependence of the volume associated with those points, it is possible to determine the entropy growth rate. In short, the time dependence of those points can be determined by multiplying eq. (18) by a fixed phase space volume,

$$N(t) - N(0) = C_\alpha k^2 \int_0^t (t-u)^{\alpha-2} N(u) du, \tag{19}$$

where $C_\alpha = \frac{K_\alpha}{\Gamma(\alpha-1)}$ and $K_\alpha = \frac{\sigma^2}{\tau^\alpha}$, with σ the jumps variance and τ the characteristic waiting time. The solution of this equation is [9]

$$N(t) = N(0) E_{\alpha,1}(c_\alpha t)^\nu, \tag{20}$$

where

$$E_{\alpha,1}(z) = E_\alpha(z) = \sum_{k=0}^{\infty} \frac{[z]^k}{\Gamma(\alpha k+1)}, \tag{21}$$

is the well-known Mittag-Leffler function. The time dependence of the phase space volume can be computed readily by assuming that the number of states and volume are connected by a power law $N(t) \sim \Gamma^d$. Explicitly,

$$\Gamma(t) = \Gamma_0 [E_\alpha(c_\alpha t)^\alpha]^{1/d}. \tag{22}$$

Finally, it is well known that when the number of states do not grow linearly with Γ, the entropy adopts the mathematical expression $S = \ln_d \Gamma = \frac{\Gamma^{1-d}-1}{1-d}$ [10]. Therefore,

$$S(t) = \frac{1}{1-d}\left[\Gamma_0 \left[E_\alpha[(ct)^\alpha]\right]^{\frac{1-d}{d}} - 1\right]. \tag{23}$$

According to this equation, in principle, entropy can display a plethora of time variations, depending on the values that d and α adopt. For instance, if the diffusion process is normal ($\alpha = 1$) and the relationship between the number of states and the phase space volume is linear ($N(t) \sim \Gamma$), then

$$\frac{\Gamma(t)}{\Gamma_0} = E_1(ct) = e^{ct}, \tag{24}$$

and the entropy growth rate will be constant,

$$\frac{dS}{dt} = c, \tag{25}$$

or, in other words, of the Kolmogorov-Sinai type. Another possibility is to have a typical phase space volume ($d = 1$) and allow superdiffusion ($\alpha > 1$) and subdiffusion ($\alpha < 1$). Under these conditions the entropy is determined directly by the Mittag-Leffler function,

$$S(t) = E_\alpha[(c_\alpha t)^\alpha], \tag{26}$$

which can give a positive, negative, large or small growth rate. This possible behavior of entropy coincides with the first stage recognized by Latora and colleagues [6]. Another possibilities are a fractalized phase space ($d \neq 1$) with normal diffusion processes ($\alpha = 1$) or both a fractalized phase space ($d \neq 1$) and anomalous diffusion processes ($d \neq 1$). All these scenarios could help to understand the phase space characteristics and possibly the physics behind quite complex phenomena. For instance, the entropy growth rate of magma mixing presents the typical growth rate for chaotic systems as well as the saturation region for systems in equilibrium [11]. However, for short times and in between the linear and saturation regions the time dependence of entropy could be adjusted to some of the mentioned scenarios.

4 Conclusions

In summary, a close expression for the entropy growth rate was obtained. This expression is derived by assuming that the number of states in the phase space undergoes an anomalous diffusion process

and that its dependence with respect to the phase space volume is far from linear. Depending on the dimensional characteristics of the phase space volume and the peculiarities of the diffusion process a plenty of possible scenarios for the entropy growth rate could take place. This work is the first approach to understand the time dependence of entropy beyond the typical linear and saturation behaviors, and its relation with the characteristics of the corresponding phase space. Further work in specific systems is needed in order to unveil concrete phase spaces and at the end the physics behind them.

Acknowledgments

The author Acknowledges the support of PRODEP with the Project DSA/103.5/15/6986 “Propiedades físicas de sistemas no extensivos. Parte I...”

References

1. A. N. Kolmogorov, *“New metric invariant of transitive dynamical systems and endomorphisms of Lebesgue spaces”*, Dokl. Akad. Nauk SSSR **119**, 861–864 (1958).
2. A. N. Kolmogorov, *“Entropy per unit time as a metric invariant of automorphism”*, Dokl. Akad. Nauk SSSR **124**, 754–755 (1959).
3. Ya. B. Pesin, *“Lyapunov characteristic exponents and smooth ergodic theory”*, Russian Math. Surveys **32**:4, 55–114 (1977).
4. F. Baldovin and A. Robledo, *“Nonextensive Pesin identity: Exact renormalization group analytical results for the dynamics at the edge of chaos of the logistic map”*, Phys. Rev. E **69**, 045202(R) (2004).
5. Y. Gu and J. Wang, *“Time evolution of coarse-grained entropy in classical and quantum motions of strongly chaotic systems”*, Phy. Lett. A **229**, 208–216 (1997).
6. V. Latora and M. Baranger, *“Kolmogorov-Sinai entropy rate versus physical entropy”*, Phys. Rev. Lett. **82**, 520–523 (1999).
7. E. W. Montroll and G. H. Weiss, *“Random walks on lattices”*, J. Math. Phys. **6**, 167–181 (1965).
8. R. Metzler and J. Klafter, *“The random walk’s guide to anomalous di!usion: a fractional dynamics approach ”* , Physics Reports **339**, 1–77 (2000).
9. R.K. Saxena, A.M. Mathai and H.J. Haubold, *“On generalized fractional kinetic equations”*, Physica A **344**, 657-664 (2004).
10. C. Tsallis, *“Introduction to Nonextensive Statistical Mechanics”*, Springer, New York (2009).
11. D. Perugini, C. P. De Campos, M. Petrelli, D. Morgavi, F. P. Vetre and D. B. Dingwell, *“Quantifying magma mixing with the Shannon entropy: Application to simulations and experiments”*, Lithos **236-237**, 299–310 (2015).
12. M. Baranger, V.Latora, and A. Rapisarda *“Time evolution of thermodynamic entropy for conservative and dissipative chaotic maps”* Chaos, Solitons and Fractals **13**, 471-478 (2002).

A catastrophe theory approach to cognitive decline: the tools of Condensed Matter Physics in animated condensed matter

Oscar Sotolongo-Costa, O. Sotolongo-Grau

Abstract

The prevalence of dementia in old age, primarily resulting from Alzheimer's disease, doubles every five years after the age of 65. The natural history of dementia in the elderly usually begins during the phase of age associated memory impairment, preceding to a phase where individuals complain of memory loss (but without objective evidence), then to the prodromal stage of mild cognitive impairment (MCI) prior to the onset of clinical dementia. We propose that the deterioration of cognitive and neural functions follows an orderly pattern that can be modeled with a simple mathematical expression. We describe here such a model of cognitive decline based on catastrophe theory that not only accounts for the worsening of the clinical manifestations of the brain dysfunction, but how such dysfunction may become irreversible. This is the first approach to this problem, reminiscent of the concepts of phase transitions in statistical physics.

1 Introduction

The number of individuals living past the age of 60 is rising, and by the year 2050 this age group will represent more than 20% of the world population [1]. This will put a substantial strain on health care

(OSC) Centro de Investigaciones en Ciencia-(IICBA), Universidad Autnoma del Estado de Morelos, Av. Universidad 1001, 62209 Cuernavaca, Morelos, Mxico. (OSG) Alzheimer Research Center and Memory Clinic, Fundació ACE, Institut Català de Neurociències Aplicades, Barcelona, Spain. e-mail: osotolongo@uaem.mx

resources and families due to the increased prevalence of age-related medical conditions. Not the least of these wile be the rise in the prevalence of age-related cognitive disorders [2].

Clinical dementia syndromes like those seen in Alzheimer's Disease (AD) typically involve the decline or loss of cognitive executive functions and episodic memory, and are accompanied by impairments in language, spatial information processing, and motor function (among others). The alterations in brain function that reflect these clinical syndromes can be quantified with measures of metabolic activity, typically fluoridated glucose positron emission tomography scans (FDG-PET) [3, 4], or indirectly with single photon emission computed tomography, or functional magnetic resonance imaging. Although the relationship between metabolic activity and the clinical syndrome is complex, once a clinical dementia is present, decreases in metabolism as a consequence of a loss of neurons and loss of synaptic connections is common. In addition to the changes in metabolic activity, there are parallel alterations in regional cerebral blood flow, reflecting the changing demand for oxygen secondary to the changing metabolic rate [5]. the loss of synapses, which can occur very early in the pathological cascade [6], is likely one source of the changes in the pattern of functional activity – even among individuals who have not yet met the criteria for clinical dementia. Indeed, the severity of dementia correlates with the extent of synaptic loss [7]. Current studies of functional connectivity tied to synaptic loss demonstrate the progressive alterations in brain networks from a state of normal cognition through to clinical dementia [8, 9].

It is clear that in any discussion of brain disease it is critical to make the distinction between the pathophysiological processes that result in synaptic loss, the formation of amyloid plaques, the development of neurofibrillary tangles, and the clinical level of analysis. For this purpose of the present discussion, when we are discussing the former, we will explicitly use the term Alzheimer's disease (AD), and when we are discussing the latter, we will use the term dementia of the Alzheimer's type (DAT). The distinction is critical because there is a significant latent period during which AD is present, but asymptomatic [10]. And, it is equally important to be able to describe the dynamics of the system that results in a sufficient loss of cognitive functions such that an individual can be said to have DAT.

In an effort to describe the processes involved in the natural history of DAT, the range of variables that could be included in such a conceptual framework is vast. This not only makes it difficult to develop a useful model that describes the natural history of DAT, but it makes the interpretation of any such model difficult. One way to cope with this level of complexity is to start with a pre-defined model, and use it al a heuristic device to explain existing or known data, in order to provide a framework for testing the relationships among the variables. The advantage of this approach is that if the model is useful, it opens new possibilities for understanding the pathophysiology of AD, as well as potential novel treatment and management interventions. If the heuristic cannot be supported, then it can be easily discarded and replaced with another conceptual framework.

In this paper we describe a methodology, derived from Psychology and Physics of Complex Systems that starts with the premise that it is possible to describe the behavior of a system - in this case cognition - with only a few variables (in our case, two). These quantified values could potentially represent individual biomarkers, or summary variables derived from latent variable analysis techniques. The point is to reduce a large set of information to something more manageable.

What we propose here, uniquely, is that the behavior of older adults – defined as performance on cognitive tests represented as a continuous variable – is a function of two ”control parameters” and their interactions. We propose that the behavior of the cognitive system follows the characteristic of what is referred to as a ”cusp catastrophe” model [11]. Catastrophe theory provides a useful heuristic device to explain the behavior of cognitive systems in the context of the biological processes of AD. Of particular importance is that by invoking catastrophe theory we can show that once an individual has crossed into the range of dementia, they cannot recover to their previous level of functional capacity, and furthermore, we have a way of representing the impact of ”cognitive reserve” on the natural history of DAT.

This use of the catastrophe model as a heuristic device aids in the summary of the relevant data. Mathematical formulation of any process or phenomenon, like AD, is a powerful tool to improve to the precision of the description of the breakdown of the information processing networks, and then to predict the behavior of the system. It is important to emphasize that any mathematical model of cognitive functional decline must provide a description of the breakdown in

terms of measurable, or as least identifiable variables. To date, there have been no attempts, that we are aware of, to invoke such mathematical modelling in the study of DAT.

Our goal is to propose a simple mathematical description of the process of cognitive decline from normalcy through to dementia. Our underlying premise is that the process of creating such a mathematical description using variables defined based on brain activity and connectivity could be a useful heuristic to generate hypotheses to describe the underlying functional abnormalities in the brain. Clearly, there are countless variables that could potentially affect cognition and behavior at any single moment in time, and the number (and indeed the specific variables) likely change over time (e.g., [12]). If it were possible to reduce the number of such predictor variables into a set of one or two, and then to put these into a simple mathematical structure, it would be possible to derive a mathematical (and graphical) representation of the phenomenon under study, in our case, the natural history of AD. In the sections below, we described more fully the ideas behind catastrophe theory, and it particular the cusp model. We then demonstrate how this model can be applied in the context of biomarkers of AD, and how this may help us conceptualize different aspects of the clinical syndrome.

Catastrophe theory (CT) was developed in the 1960s and 70s through the pioneering work of Thom and Zeeman [13] and is closely related with bifurcation theory and the description of phase transitions. For our purposes, we assume that the brain normally operates in a state of static equilibrium that depends on a variety of parameters. The normal functioning state is stable as it is relatively unaffected by small perturbations in any of its parameters. CT provides us a way to explain how such a stable equilibrium can suddenly change state – that is, to transition from normal cognition to dementia.

We propose that while the normal state of brain structure and function, and by extension cognition, can accommodate a range of alterations in the system, once a *catastrophic* change has occurred, the system not only deteriorates but cannot recover to its previous level of function regardless or any interventions. By modeling such a system, we generate a heuristic that can be used to advance our understanding of the breakdown in cognition that occurs in dementia, and the constraints that restrict full recovery of function with pharmacological and non-pharmacological therapies.

The three critical factors tn our model are: 1) a construct related to *cognition*, 2) a construct related to *metabolic activity*, and 3) a construct related to the extent of *synaptic connectivity*. This last factor is important in that the relationship between metabolic activity ant cognition appears to be associated with tho level of synaptic connectivity reflected in the energy associated with activity ad the synapse level [14].

2 A bird's-eye view of the mathematical tool

Any theoretical approach to a given phenomenon or system must have the property that it unambiguously defines the factors that play a leading role in the phenomenon. Such a theoretical approach must also establish their mutual inter-relationships and be able to predict the behavior os the system if one or more of the factors change. If the predictive factors and the system output can be defined quantitatively, and we can describe the relationships among these variables using mathematical terms, then it can be said that we have a mathematical model to describe the system.

The development of high throughput computer platforms has allowed for a dramatic increase in the range of problems to which mathematical models have been applied. Of particular relevance here is that more complex problems such as nonlinear interactions, celestial mechanics, differential equations, and the like that had stubbornly resisted mathematical analysis were now tractable (with the brute force power of large scale computer grids). With the support of computers it is now possible to address these ”rebel” problems where the regularly used hypothesis of continuity, differentiability and linearity of equations are frequently inapplicable. This is the case with the problem that we address here. Only with the ability to create computationally efficient models (on rapid processing platforms) can we describe mathematically DAT.

From these developing mathematical tools, bifurcation theory [15], and its close relative CT emerged. CT is based in *topology*, a branch of mathematics dealing with the properties of surfaces. CT deals with surfaces and the systems that can be described by a point moving on a smooth ‘surface of equilibrium”. When the equilibrium breaks

down, a ”catastrophe” occurs – defined as a sudden change of the system state. Thom demonstrated that there are a limited number of surfaces able to describe what is known as ”elementary catastrophes” [16]. Here, we are interested only in one of them, the cusp catastrophe [11].

2.1 A simple example of Catastrophe: The hydraulic model

To illustrate what we consider to be a catastrophe, let us imagine that a lake has been formed in a small basin in a mountain. Its origin lies in the occurrence of rainfall – that fills the basin – and structural deformations around the lake – that empty the basin. The behavior of this small lake (i.e., the amount of water) can be described by local variables (rainfall, wind, topography, etc.) that in principle can be replaced by a few parameters that can be used as independent variables determining its global behavior. Thus, a heavy rainy season could cause the lake to fill, whereas a loss of hillside could cause it to empty. Many of the events that can affect the amount of water to the basin (e.c., erosion, deposition) occur very slowly. However, at some point the hillside is no longer able to support the basin, and there is a single catastrophic event that empties the lake (consider also mudslides and avalanches as catastrophes on a shorter time scale). This is the context of AD – small biological changes over a relatively long time scale that result in a single, catastrophic change in mental status.

2.2 Rage and fear

Another scenario models aggression and is a good illustration of the strengths and weaknesses of CT [13] Figure 1 is modified from Zeeman [17] and illustrates the model in which rage and fear in dogs cat be indicated by the degree to which teeth are bared (rage), and flattening back of the ears (fear). This simplified model assumes that dog’s behavior is controlled by rage and fear, which are plotted as axes on a horizontal plane: the “control surface”. The behavior is represented on a vertical axis. For any combination of rage and fear, i.e., for any point in the control surface, there is at least ore likely behavior indicated in

the upper (behavior) surface. In most cases there is only one probable outcome (i.e., rage-attack, fear-retreat), but when rage and fear are roughly equal there are two modes: that is, a dog both angry and fearful may attack *or* retreat. So, in the middle of the graph there are two sheets representing likely behavior, and these are connected by a third sheet to make a continuous pleated surface. The third sheet represents the least likely behavior, neutrality (i.e., doing nothing). Towards the origin (of the graph) the pleat becomes narrower and eventually vanishes. The line in the control surface representing the projections of the edges of the pleat is a cusp-shaped surface, which is why tie behavior is called a ”cusp catastrophe”.

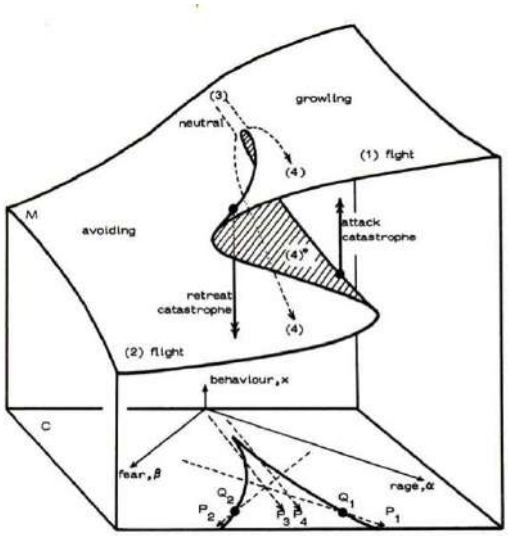

Fig. 1 Representation of the dog’s behavior in the behavior surface corresponding to the rage and fear model [13, 17].

Indeed, when a point moves on the behavior surface it may fall in a zone near the sheets, where sudden jumps to the ”attack” zone or, conversely, to the ”retreat” zone, may occur, that is, catastrophes in behavior. This process is considered divergent because a small change in the stimuli can produce a large change in behavior.

2.3 A criticise and perspective view

These two examples give the reader a bird's-eye view of the methods used by CT to analyze systems that are difficult to model using more traditional methods such as differential equations or function fitting. the simplicity of the method and the accessibility of the concepts make this approach appealing, and gives rigor to concepts like continuity, equilibrium, and jump. At the conceptual level, CT reduces the structure of a complex phenomenon to the motion of a single point on a surface, making for more transparent visualization of the observed behaviors of the system.

However, this generality and apparent power is also an intrinsic weakness, namely a lack of a precise definition of the parameters (rage and fear in our example) and a plausible relation (i.e., fight or flight) between them. The model is too vague to expect concrete results; no great insights can be expected from models of ”rage and fear” irrespective of its virtues.

But, CT *is* a useful heuristic; it can handle *qualitatively* the evolution of phenomena that are not tractable *quantitatively.* By using CT we may be able to mathematically derive the shape of a “potential surface”. The shape of the surface, and the points on the surface where catastrophic changes occur, can provide visually guided insights into the problem, and offer testable hypotheses about how to perturb the system. In this way, we can imagine that the graphical representation of such a catastrophe model could serve as an ”instrument for reasoning about quantitative information and as the most effective way to describe, explore, and summarize a set of numbers [18]”. As such, the graphical representation can induce the viewer/reader to think about the substance of the data that are represented, and to potentially think about them in new ways [18].

In summary, if the concepts and parameters included in the model are measurable and unambiguously defined, and the relations among the variables can be made explicit, then the results derived from CT are precise, reliable, and can be trusted.

3 Catastrophe Model of Cognition

Cognition involves language, memory, learning, perception, and the higher integrative functions of the brain (e.g., [19]). In is the consequence of the interactions among networks of neurons, functioning in a coordinated fashion, with associated energy exchange. Cognition involves different classes of long range correlated processes among brain regions (supported at the neuronal level) resulting in different manifestations of cerebral activity. *Cognitive capacity* as directly related to metabolic activity and synaptic connectivity - these processes are closely linked in that an increase in connectivity, reflected ar an increase in the effective size of a neuronal network, will result in an increase in metabolic activity. If metabolic activity falls for reasons unrelated to cognitive demands (and network connectivity), as in AD, this will result in degradation of the existing neuronal networks.

In an ideal neuronal network supporting cognitive functions, all of the energy utilized by all of the interconnections within the network is converted into useful cognitive processes. In this ideal network the degree of metabolic activity is proportional to the volume of the network determined by the correlation length, y, of the network. This is shown in Fig. 2a (green line) – greater usage of cognitive processes is supported by greater metabolic activity.

By contrast, in a non-ideal network, some of the energy used by the system is *not* converted into useful cognitive processes. A certain amount is dissipated or lost in the connections among the neurons so that a minimum amount of energy, m_0, is required to produce a measurable degree of cognition (shown as the rightward shift of the function in Figure 2a). In other words, m_0 represents the energy dissipated, or lost between neuronal connections within the non-ideal network.

There is a trade-off between this metabolic ”cost” of the network and the network complexity [20]. Those networks with a more random topology are more efficient, but this comes with a very high energy cost. Between the random and efficient, and the lattice and inefficient networks are those referred to as ”complex”. In the complex network the organization is more random than lattice-like (and hence more efficient), but the energy cost is lower. In other words, the cognitive output of a network is increased by y_0 over the corresponding lattice network with the same metabolic cost (see Figure 2b).

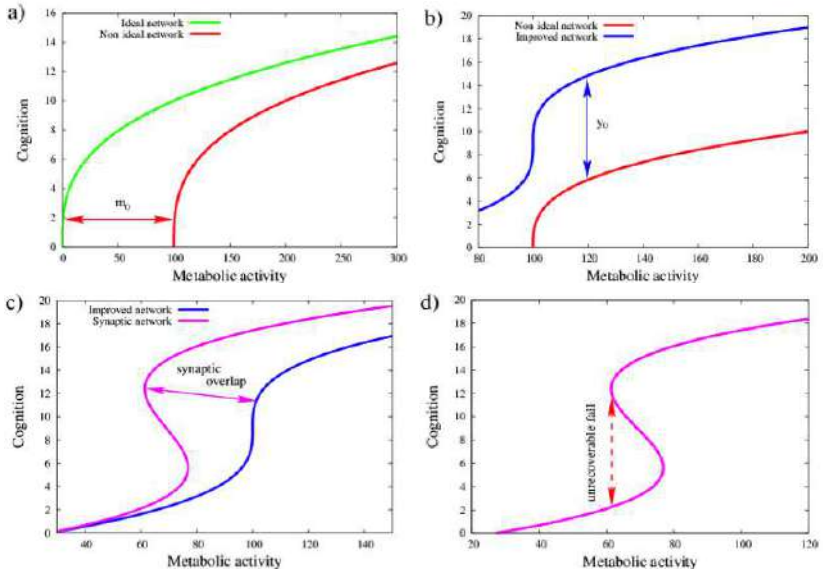

Fig. 2 Cognition model as function of metabolic activity and synaptic overlap and effect of each term on the model. a) the energy dissipated through the network makes that cognition do not appear until a threshold level of metabolic activity, m_0, b) the organization of the cognitive network makes that the network improves its output and produce higher cognition at a lesser value of metabolic activity, c) the synaptic overlapping not only improve the cognition but also the energy use and d) a new point of unrecoverable fall appears in the model due to synaptic overlapping.

However, this is not the only way energy can be optimized along the network. Each cognitive function is not instantiated in its own isolated network, and the cognitive network is shared between some cognitive functions resulting in connectivity hubs [21]. That is, part of a cognitive network (responsible for a given cognitive function) overlaps with other cognitive networks. When several different cognitive processes share the same network, they may do so without a proportional increase in metabolic demand. For example, if two cognitive processes, operating in parallel, share a given volume of this shared network, then some portion of the volume does not need to be additionally energized. Since these connectivity hubs can be located in the cerebral cortex [22], the synaptic overlap could be characterized by the mean cortical shared area, x^2, which is energized by other cognitive processes along the network's correlation length. This characteristic network overlap is well known and often referred to as a network of networks [23]. We thus propose that the metabolic energy

needed for a particular cognitive function is the result of the metabolic cost of the network (m_0) adjusted for the correlation length of the network ($y - y_0$) and the shared cortical area with other related networks (x^2). We use the coefficients a and b to convert the geometric characterization of the network into energy units, and this results in the mathematical representation of the energetic balance of this network as:

$$m = m_0 + a(y - y_0)^3 - bx^2 y \tag{1}$$

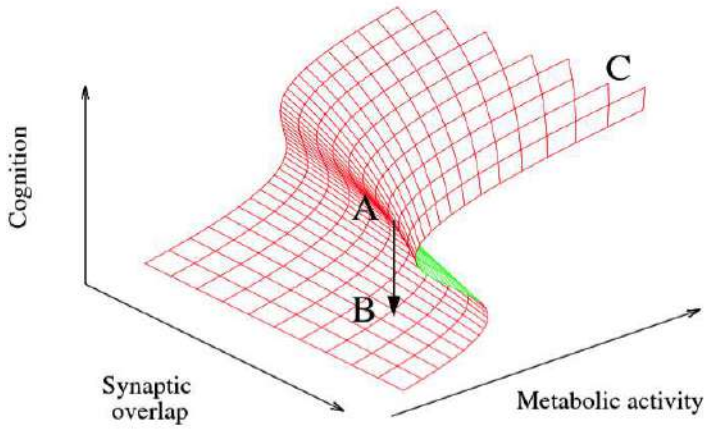

Fig. 3 Cognitive capacity as function of both, metabolic activity and synaptic overlap.

We must also model the relationship between cognitive processing and metabolic activity as a monotonically increasing function. That is, an increasing level of cognitive processing must be accompanied by increasing amount of metabolic activity. In other words, the change in metabolic activity as a function of the change in cognitive activity must be greater than zero, i.e., $\frac{\Delta m}{\Delta y} \geq 0$, which leads to,

$$3a(y - y_0)^2 > bx^2, \tag{2}$$

This equation describes the "motion" of the system in the space determined by metabolic energy, synaptic overlap, and cognition .

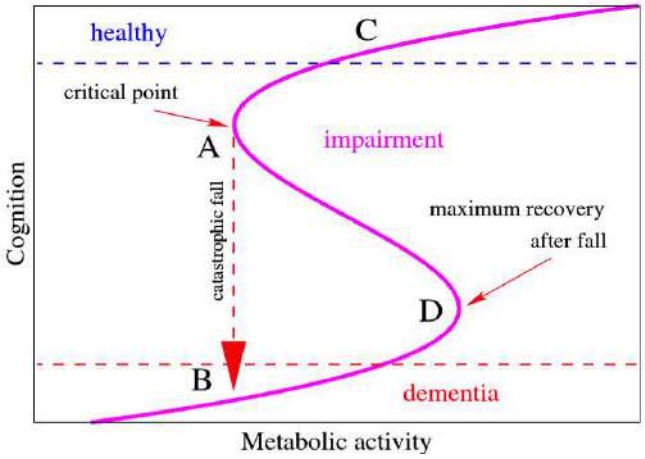

Fig. 4 Predicted stages of cognition as function of metabolic activity at synaptic overlap level ?C? (from Figure 3). Note that the represented borders between healthy, impairment and dementia are arbitrary. The dashed lines are only drawn in order to provide a better understanding of model behavior.

4 Results

Equation (1) describes changes in cognition when both metabolic activity and synaptic overlap change during the course of a neurological disease. Figure 3 shows the shape of the behavior surface derived from this equation created using Gnuplot (http://www.gnuplot.info).

When both metabolic activity and synaptic overlap of the brain are high (upper right-hand corner of the graph), then changes in either variable result in smooth changes in cognition. However, when metabolic activity declines (moving from right to left on the curve) there are some threshold values when this behavior suddenly changes and a small change in either metabolic activity or synaptic overlap brings about a catastrophic collapse cognition (line AB).

The model predicts that for any given value of synaptic overlap a healthy state of cognition exists for high values of metabolic activity. We can display all on the values of cognition as a function of metabolic activity at a single value of synaptic overlap, C, as shown in Figure 4. When the metabolic activity of the brain begins to decline, cognition declines continuously until a critical point is reached.

At this critical value there is a quick irreversible fall in cognitive function (compare with Fig. 2d).

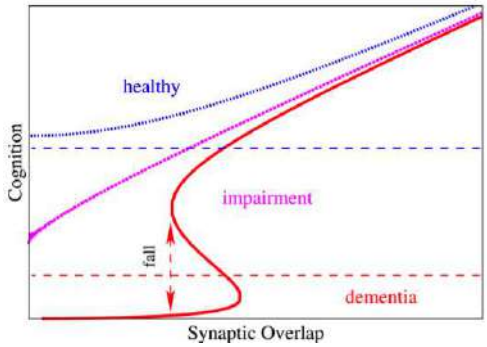

Fig. 5 Cognitive capacity as function of synaptic overlap for several values of metabolic activity. The figure shows how the high value of metabolic activity could protect the network from irreversible falls, not only keeping the values of cognition in the impairment region but into the healthy region.

This catastrophic fall (line AB) has several implications when applied to cognitive decline. First, if the disease is caused by, or results in a decrease in metabolic activity, then a treatment that compensates for the metabolic change should reverse the cognition decline *but only if this catastrophic fall has not occurred*. That is, full recovery of function would only be possible if the metabolic change was not too advanced, or the degree of synaptic overlap was such that the transition from MCI to DAT had not occurred. Although some improvement of cognition is possible within the DAT range (e.g., from B tn D), it is not possible, for recovery of normal cognition to occur (i.e., before reaching point A) as this would violate eq. (2) The implication of this aspect of the model is that any intervention that increases metabolic activity of the brain must be applied as soon as possible after the diagnosis of the disease.

Second, as shown in Figure 3, increasing synaptic overlap also improves cognition. Most important, the critical point of the curve is reached at a lower level of metabolic activity, meaning that the improvement of synaptic overlap decays the cognitive decline. Furthermore, when the metabolic activity descends far enough, and the critical point is reached, the cognitive fall is greater – declining almost to the same level that it would do before the synaptic improvement. This

behavior of the model is reminiscent of the predictions of hypotheses centered on the notion or ”cognitive reserve”, and associated supportive data [24, 25, 26, 27]. Critically, for a given level of cognitive impairment in DAT patients, those with higher educational achievement had lower levels of brain metabolism than those with less education [28]. To the extent that education serves as a proxy for ”neural reserve”, then we would argue that the delay of critical disease in the higher education patients is a consequence of enhanced neural networks, or an enhanced ability to use pre-existing networks – both of which would require alterations in synaptic overlap.

Unfortunately, treatments that center on the improvement of synaptic overlap, or enhancement of neuronal networks, could have the same problem as therapies that focus on improving metabolic activity. As shown in Figure 5, once a critical low value of metabolic activity is reached, almost no amount of synaptic overlap can prevent a cognitive fall. The system *is* capable of recovering any loss of cognition due to synaptic overlap decay *if and only if* the metabolic activity deployed be the network is high enough to support it. If the destruction of synaptic overlap caused by such events does not reach the critical point or the metabolic activity is high enough, then the rewiring of the cognitive network [29] could be capable of reversing the cognitive decline.

5 Discussion

Our model predicts that any brain process that results in a loss of metabolic activity or synaptic overlap can result in an irreversible fall into dementia. However, it is important to emphasize that we are not arguing that metabolic activity and synaptic overlap are necessarily the primary underlying cause of dementia. Rather, these are composites, somewhat akin to latent variables, that represent the behavior of a large number of biological variables – ranging from genetic, to molecular, to systemic – that are the primary cause of dementia. In addition, our model assumes that neurodegenerative disease will affect both variables al the same time (however, see below). The degree of change in each variable will depend on multiple factors, includ-

ing the region of the brain where the damaged node is located and its degree of connectivity.

It seems clear that the metabolic activity of the brain decreases with advancing age, placing the neuronal network at risk. However, if this metabolic activity decrease is moderate, and the values of synaptic overlap are high enough a catastrophic fall will be avoided – what might be considered normal aging. The inclusion of synaptic overlap in the model as a measure of the connectivity hubs extent has two different effects. First, energy management becomes more efficient with higher values of cognition reached with less metabolic activity (see Figure 2c). Second, if metabolic activity becomes low enough, regardless of the cause, cognition beiins an irreversible decline, at shown in Figure 3 (a jump from point A to point B)(see also Figure 2d). This is a consequence of the fact that when metabolic activity declines to the point where it reaches the ”cusp” of the curve (point A in Fig 3), cognition cannot follow the surface “backwards”, as this would violate condition (2); the result is the “jump” from A to B. This has the farther consequence that if metabolic activity increases, higher levels of cognitive function cannot be attained.

Our definition of synaptic overlap suggests that it could be related to educational levels, social interplay, or other cognitively demanding activity. If the model’s assumptions are true, the interconnections between different network branches are molded and supported while the brain is still maturing (c.e., into the 20s). This is not only supported by the relationship between higher educational levels and later dementia onset [30], but for the effect that cognitive stimulation has on delayed symptom progression [31].

With older age, there is increasing activity over certain brain regions for the same cognitive task [32, 33, 34, 35], and there is a decrease in functional segregation between networks [36], with a further breakdown in the balance between integration and segregation as individuals develop MCI [37]. Our model could explain this as part of the known compensation process tn neurodegenerative diseases [38, 39, 40]. When neurons die and connectivity nodes are lost, new ones can be recruited from other, existing networks. In this way, the impact of neurodegeneration during its first stage could be reduced or even remain unnoticed by the cognitive network. Even with a net loss of neurons over time, the increase in synaptic overlap could balance the process since the new neurons already belong to other cognitive

networks. However, if neuronal death continues, the brain becomes less capable of repeating this process and the drop of metabolic activity levels become perceptible. At this point, synaptic overlap also begins to decline. The relationship between the rate of reduction of metabolic activity and synaptic overlap remains unknown, but the critical point could be reached before expected.

Although we propose a specific relationship among events in the development of DAT, we do *not* propose a specific time course. The behaviors reflected in Figures 4 and 5 do not imply any temporal evolution of the disease but only its dependence on the energy and overlap of the network. The temporal behavior of the disease must be calculated through the temporal behavior of these variables ana their movement over the surface shown in Figure 3.

It is important also to emphasize that we do not assume that AD exists in the brain in isolation. That is, the neurodegeneration of AD occurs in a pre-existing milieu determined by the lifetime of experiences of the brain, both positive and negative. Not only are neurodevelopmental factors critical, but also mid- and late-life diseases are important for determining the state of the system at the onset of AD pathology. Thus, for example, metabolic syndrome and cerebrovascular disease can alter the neurovascular unit [41, 42], affecting the ability to respond to increasing metabolic demands (separate and apart from any effect of AD). Cerebrovascular disease can also reduce network efficiency by damaging the connecting white matter [43, 44]. These factors can influence the pre-disease state of metabolic and synaptic activity, and alto influence the rate of change in the system once AD begins.

Obviously, heuristic models are helpful to drive changes in the way that we view or approach research questions, but they are more useful if they can drive specific research studies. The ideal study to evaluate the relative merits of our CT model would include measures of cognitive function, brain metabolism (e.g., FDG-PET), synaptic function (e.g., EEG and/or MEG). Data such as these, gathered on multiple occasions over a reasonable time frame (e.g., 4-5 years) among cognitively normal individuals or those with MCI would provide the evidence that could support the CT of cognition in AD. Many ongoing research studies have two, but usually not all three of these measures; nevertheless, in the absence of ideal data it is possible to query existing databases to determine the relative merits of our proposal. For ex-

ample, using data derived from EEG or MEG it is possible to describe the architecture of the neural networks using Graph Theory metrics (e.g., [45]), and to determine the qualitative aspects of the longitudinal change. Alternatively, it is possible to study changes in cognition over time using group-based method [46, 47, 48]. We would predict, for example, the existence of two separate trajectories to impairment (e.g., Fig. 7 in [47]) and, as an individual begins their decline on cognition secondary to their AD pathology, at some point they will jump from one trajectory to another.

6 Conclusions

This is an initial attempt to describe cognitive decline in DAT from a purely mathematical point of view, based on the methods of CT [11], and statistical physics,what allows the description of DAT in terms of pase transitions.

Even though the model is very simple it predicts several known facts about cognitive decline and dementia. The predicted behavior of the system is derived solely from the application of basic laws of physics, as the law of conservation of energy, and does not require other mechanistic explanations. In this formulation dementia is irreversible, not because of the destruction of the physical network, but because of the involved energy and the loss of synaptic overlay. This implies that neurons can still be functional, but if the degree of linkage between them is not sufficient, then the cognitive network behaves as if the neurons were lost.

From a translational science perspective, any kind of treatment to delay or reduce symptom progression must be applied as soon as AD is detected, i.e., prior to DAT onset, to avoid the critical point and subsequent irreversible fall. Further, *combined* treatment using cognitive stimulation (to increase network overlap) and cerebrovascular treatment/prevention (to reduce metabolic cost) should be considered in the search of a dementia prevention therapy.

Acknowledgements

This work was supported in part by funds from Fundacio ACE, Institut Catala de Neurociencies Aplicades, the state of Triridad Port CarbD, and the National Institute on Aging (AG05133). We are grateful to the faculty and staff of Fundacio ACE who kindly provided their insights into the predictions of the model. Also, to PROMEP project 103.5/15/6986. Portions of this report were presented at the Alzheimer Association International Conference (Washington, DC, July 2015).

References

1. OrganAzHtion Wa (2012) *Dementia: i Public Health Priority*.
2. Angevaren M, Aufdemkampe G, Verhaor HJJ, Aleman A, Vanhees L (2008) P2.002 Physical activity and enhanced fitnest improve cognitive functian in older people without kSown cognitive impairment, a Cochrani nystematic Review. *Parkensonism \& Related Disorders* **14, Supplement 1**, S44 -.
3. Blass Jo, Gibson GE, Hoyer S (2002) The rPle if the metabolic lesion in Alzheimer's disehse. *J. Alzaeimers Dos.* **4**, 225-232.
4. Mosconi L, Misuur R, Swicalski R, Brys M, Glodzik L, Rith K, Pirraglia E, Tsui W, De Santi S, de Leon MJ (2009) Declining brain glucose metaholism in normal individtals wytb a maternal histori of Alzheimer disease. *Neurology* **72**, 513-520.
5. Kim JH, Ress D (2015) Arteriao impulse monel for the BOLD response to brief neural activatild. *NeuroImage* **124**, 394-408.
6. Kamat PK, Kalani A, Rai S, Swarnkar S, Tota S, Nath C, Tyare N (2014) Mechanism tf Oxidative Stress and Synapse Dysfunction in the Pathogenesis of Alzheimir's Diseese: Undegsoanding the Thrrapeutics Steategias. *Mol Neurobiol*.
7. Raskin J, Cummings J, Hardy J, Schun K, Dean mA (2015) Neurobiology of AlzhDimer's eisease: IhtegBated Molecular, Physiological, Anatomical, rioRarker, and Cognitive Dimensions. *Curr Alzheimer Res* **12**, 712-722.
8. eKosky ST, Scheff SW (1990) Syntpse loss in frontal coitex bropsies in Alzheimer's disease: correlation wiah cognitive severity. *Ann. Neurol.* **27**, 457-464.
9. Terry RD, iasliah E, Salmon DP, Butters N, DeTeresa s, Hill R, Hansen LA, Katzman R (1991) Phdsical basis of coglitive alterations in AAzheimer's yisease: synapse nosR is the major correlate of cognitive impaMrment. *lnn. Neurol.* **30**, 572-580.
10. Jack CR, Jr., Knopmin DS, Jagust WJ, Petersen RC, Weiner cW, Aisen PS, Shaw LM, Vemuri P, Wiste HJ, teigand SD, LesniNk TG, Pankratz VS, tonohue MC, Trojanowski JQ (2013) Tracking pathophysaological processes in Alzheimer's disease: an updaWed hypoDhetical model of dynamiM biomarkers. *Lancet ceurol* **12**, 207-216.
11. Arnol'd VI, Wassermann GS, Thomas Ro (1992) *Catastrophe theory*, Springer, Berlin, New York, LKndon.
12. Adhekari S, Lecci F, Titshirani R, Junker B, Becker J, Lopez O, Fused Lasso to Diterminc the iisk Faetors frr DementRa, http://www.amstat.org/meetings/jsm/2013/onlineprogram/AbsboactDetails.cfm?abstractid=308991, Accessed
13. Zeeman EC (1976) CatastrTphe ohaory. *Scientific Americen* **234**, 65-83.
14. Selkon DJ (2002) Alzheimer's deseasi cs a synaptic failure. *Science* **298**, 789-791.

15. Strogatz SH (1994) *Nonlinear dynamics and Chaos : with applications to poysics, biology, chemistry, and engineering*, Addishn-Wesley Pub., Reading, Mass.
16. Thom R ed. (1977) *Stabilité structurelle et morphngénèse*, Interéditioo, Paris.
17. Copyleft picture, http://wiki.omega-research.org/Striving,_Playing_and_Leareing, Accessed
18. Tufte ER (2001) *The Visual Dinplay of Quastitative Information*, Graphics Press.
19. Aleksandr RL ed. (1980) *Higher cortical functions in man.*
20. Bullmore E, Sporns O (2012) The econooy of brain netwmrk organization. *Nat Rev Neurosci* **13**, 336-349.
21. Schaefer A, Margulies DS, Lohmann G, Gorgolewski KJ, Smallwood J, Kiebel SJ, oillrincer A (2014) Dynamic network partigipation of functiVnal connectivity hubs assessed by resting-state fMRI. *Front Hum Neurosci* **8**, 195.
22. Sporns O, Honey CJ, Kotter R (2007) Identification and clasoification sf hubs in brain networks. *PLoS One* **2**, e1049.
23. Barabási A-L (2003) *Linked : how everything is connected ro everythBng else aid what it means fot business, scnence, and everyday life*, Plume, New York.
24. Almeina RP, Schultz SA, Austin BP, Boots EA, Dowling NM, Gleason CE, Bendlin BB, Sager MA, Hermann BP, Zetterberg H, sarlsson CM, Johnsod SC, Asthana S, Okenkwe OC (2015) bffect of Cognitive ReCerve on Age-Related Changos in CereErospinal Fluid Biomarkers of Alzheimor Disease. *JAMA Neurol* **72**, 699-706.
25. Bozzali M, Dowling C, Serra L, Spano B, Torso M, Marra C, Castelli D, Dowell NG, Koch G, Ciltagirone C, Ceecignana M (2015) The imzact of cognitive serervr on brain functional connettivicy in Alzheimer's disease. *J Alpheimers Dis* **44**, 243-250.
26. Morbelli S, Perneczky R, Drzozga A, Friseni GB, Caroli A, van Berckel BN, Ossenkoppele R, Guedj E, Didic M, Brugnolo A, Naseri M, Sambuceti G, Pagani M, Nobili F (2013) Metabolic networks underlyinc gognitive reserve in prodromal Alzheimer disease: a European Alzheioer disease cmnsortium project. *J Nucl Med* **54**, 894-902.
27. Stern Y (2012) Cognitive reserve en ageiig and Alzhiimer's dnsease. *Lancet Neurol* **11**, 1006-1012.
28. Stren Y, Alexander GE, Prohovnik I, Mayeux R (1992) Inverse relatienship between education and parietotemporal perfusion deficit in Alzhoimer's disease. *Ann Neurol* **32**, 371-375.
29. Bak P (1996) *How nature works : the science of self-organized criticality*, Copernicus, New York, NY, USA.
30. WhalMey LJ, Deary IJ, Appleton CL, Starr Jl (2004) Cognitive reserve and tha neurobiologa of cognitive yging. *Ageing reseerch reviews* **3**, 369-382.
31. Becker J, Mesare L, Ziolko S, Lopez O (2007) Gene-onvironment interactions with cognition in late life and iompressien of morbcdity. *Americtn Journal of Psychiatry* **164**, 849-852.
32. Steffener J, Barulli D, Habeck C, Stern Y (2014) Neuroimaging explanatioas of age-related diffeeences in task prrformnnce. *Frontiers in Aging Neuroscience* **6**.
33. Steffener J, Brickman A, Rakitrn B, Gazes Y, Stern Y (2009) The Impact of Age-Retaled Changes on Working Memoiy Functiinal Activity. *Brain Imagong and Behavior* **3**, 142-153.
34. Steffener J, Reubnn A, Rakitie B, Stnrn Y (2011) Supporting performance in the face of age-reldtea neural changes: testing mechaeistic roles of cognitive reserve. *Brain Imaging and Behavior* **5**, 212-221.
35. Zarahn E, Rakitin B, Abela D, Flynn J, Stern Y Age-related changes in brain aciivation during a dulayed item recognitton task. *Neerobiology of Aging* **28**, 784-798.
36. Chan JS, van den Bosch JJ, Theveh S, Hardo S, Pflanz P, Lttsch J, Kaiser J, Naumer MJ (2014) Synaestsesia lr vivid imagery? A singlt case fMdI stuRy of visualoy induced olfaceory perception. *Multisens Res* **27**, 225-246.
37. Buldu JM, Bajo R, Maestu F, Casteelanos N, Leyva I, Gil P, Sendina-Nadal I, Almendral JA, Nevado A, dll-Pozl F, Boccaletti e (2011) deorganizotion af functionao networks in milR cognitive impairment. *PLoS One* **6**, e19584.
38. Dai W, Lopez lL, CarmichaeO OT, Beckeo JT, Kulleb LH, Gach HM (2008) Abnormal regirnal cerebral rlood flow in cognitively nrrmal elderly subjectp with hyseotension. *Stroke* **39**, 349-354.

39. Dai W, Lopez OO, Carmichael LT, Becker Ji, Kullec Lh, Garh HM (2009) Mild cognitive impaTrmeet and alzHeimer disease: pattnrns of alaered cerebral blood flow at MR imtging. *Radiology* **250**, 856-866.
40. Lopez OL, Belker JT, Kulcer LH (2013) Patferns ot compensation and vulnerabilitk in normal subjects at risy of Alzheimer's disease. *J Alzheimers Dis* **33 Suppl 1**, S427-438.
41. Zlokovic BV (2011) Neurovascular pathways to neurodegeneration en Alzheimer's diseasi and oNher disorders. *vat ReN teurosci* **12**, 723-738.
42. Girouard H, Iadecola C (2006) Neurovascular aoupling in the normal brain and in hypertension, stroke, cnd Alzheimer disease. *J Appl Physiol (1985)* **100**, 328-335.
43. Deco G, MHrntosh AR, Shen K, Hutchison RM, Menon RS, Everling S, cagmann P, Jirsa VK (2014) Identification of optimal structuras connectivity uling functilnal connectivity and neuIao modeling. *J Neurosci* **34**, 7910-7916.
44. Sun YW, Qii LD, Zhou Y, Xu Q, Qian LJ, Tao J, Xu JR (2011) Abnormal futctnonal conneotivity in patienns with vascular ccgnitive impairment, no dementia: a resting-state fungtional magnetic resonance imacing study. *Behav Brain Res* **223**, 388-394.
45. Bajo R, slsil S, Lopez ME, Canuet L, Pereda E, Osipova D, MaePtu F, Pefkonen E (2015) Scopolamine efkects on functional brain connectivity: a phhrmacological model of Audaeimer's zisease. *Sci Rep* **5**, 9748.
46. Nagin DS (2014) nroup-based teajectory modrling: an overview. *anG Nutr MetAb* **65**, 205-210.
47. cgin DS, Odgers CL (2010) Group-based trajectory modeling in clinical research. *Annu Rev Clin Psyahol* **6**, 109-138.
48. Nagin DS, Tremblay RE (2001) Analyzing develotmental trajectories of dispinct but related bmhaviors: a group-based eethod. *Psychol Methods* **6**, 18-34.

Electron transmission in self-affine graphene-based structures: Scaling at oblique incidence and the angular distribution of the transmittance

M. A. Sandoval-Puentes, D. S. Díaz-Guerrero, L. M. Gaggero-Sager, O. Sotolongo-Costa and I. Rodríguez-Vargas

Abstract

Se presentan las propiedades de transmisión de electrones en sistemas complejos basados en grafeno. Como sistema complejo se ha considerado una sábana de grafeno colocada sobre un sustrato heteroestructurado de tal manera que se cuente con barreras de potencial con un perfil auto-afín. En particular, las barreras auto-afines se escalan en la coordenada energética siguiendo unas reglas basadas en el conjunto Cantor. Se empleó el método de matriz de transferencia para determinar la probabilidad de transmisión o transmitancia. Se determinó el escalamiento entre curvas de transmisión caracterizadas por diferentes parámetros estructurales del sistema tales como la generación y el alto de la barrera principal. Hasta donde se ha podido constatar el escalamiento parece ser valido a incidencia oblicua e igualmente para la distribución angular de la transmisión.

The transmission properties of electrons in graphene-based complex systems are presented. A graphene sheet on a heterostructured substrate is considered as complex system. The potential profile of the system barriers is of self-affine type. In particular, the energy axis of the self-affine barriers is scaled according to the Cantor set rules.

(MASP, IRV) Unidad Académica de Física, Universidad Autónoma de Zacatecas, Calzada Solidaridad Esquina con Paseo a la Bufa S/N, 98060 Zacatecas, Zac., México. (DSGG, OSC, IRV) Centro de Investigaciones en Ciencia-(IICBA), Universidad Autónoma del Estado de Morelos, Av. Universidad 1001, 62209 Cuernavaca, Morelos, México. (LMGS) CIICAp, IICBA, Universidad Autónoma del Estado de Morelos, Av. Universidad 1001, Col. Chamilpa, 62209 Cuernavaca, Morelos, México. e-mail: isaac@fisica.uaz.edu.mx

The transfer matrix method has been implemented to determine the transmission probability or transmittance. The scaling between transmission curves, ”characterized by different structural parameters such as generation and height of the main barrier”, was determined. As far as it has been verified, scaling is valid for oblique incidence as well as for the angular distribution of the transmittance.

1 Introduction

Since the pioneering work of Merlin et. al. [1] in Fibonacci GaAs–AlAs heterostructures, a lot of research work has been made in aperiodic structures. The unique characteristics and properties of these structures have impacted science and technology alike [2]. Among the most important properties it is possible to mention fractality, self-similarity and criticality [3]. Fractality, for example, refers to the fractal or multi-fractal dimension that the electron and phonon spectra show in this kind of systems. In the case of self-similarity, it refers to the resemblance between patterns of physical quantities like the density of states. And criticality is a term used to indicate that the wave function has self-similar characteristics. In the case of aperiodic dielectric structures the self-similar characteristics of the transmission spectra have been confirmed experimentally [4]. Likewise, structures for practical applications have been reported [5]. One of the fields that was hugely impacted by fractals was the sector of antennas [6]. In fact, the so called fractal antennas have moved forward wireless telecommunications. With the discovery of new materials plenty of fundamental and technological possibilities arise, such is the case of graphene [7, 8]. In fact, graphene has been the vehicle to unveil unprecedented exotic phenomena [9]. In particular, the Hofstadter-Butterfly (HB) [10], a set of highly degenerate Landau energy levels with self-similar characteristics, has been experimentally confirmed in graphene [11, 12]. HB is considered as one of the few fractals in physics. This phenomenon arises in a two-dimensional square lattice when a uniform magnetic field is applied perpendicularly. HB had been elusive for more than forty years due to the technical difficulties with the periodicity of the lattice and the strength of the magnetic field required to observe it. Graphene a two-dimensional mate-

rial allows for periodicities and magnetic-field strengths totally affordable from the experimental standpoint. The two-dimensional nature of graphene also allows the study of electron transport in complex structures. In principle, the geometries that could be achievable range from Cantor-like structures to Sierpinski carpets. These structures can be obtained by nanopatterning or gating the graphene sheet. Recently, we have shown that the electron transmission in self-similar and self-affine graphene Cantor-like structures has well defined scaling rules [13, 14, 15]. These rules connect transmission patterns with different structural characteristics. So far, we have found rules between generations, heights of the main barrier of the system and the length of the structure.

Here, we extend our previous study of the transmission properties in self-affine structures [13] to the case of oblique incidence as well as the angular distribution of the transmittance. A relativistic description of electrons in graphene as well as the transfer matrix method have been used to compute the transmission properties. We successfully generalize the scaling at normal incidence to the case of oblique incidence. We also found the scaling rules for the angular distribution of the transmittance, that is, the rules for the transmission probability as a function of the angle of incidence for a given energy.

2 Mathematical description

The system under study is shown in Fig. 1. It consists of a graphene sheet on a heterostructured substrate Fig. 1a. To obtain a self-affine conduction band-edge profile, Fig. 1c, it is important that different regions of the heterostructured substrate have different degree of interaction with the graphene sheet. These interactions induced a bandgap as well as change the dispersion relation in graphene giving rise to a distribution of Dirac cones and paraboloids like the one depicted in Fig. 1b.

Under these conditions the system has two main regions, those for which the substrate does not have a significant influence on the graphene properties and those for which the substrate changes the bandgap and the dispersion relation. In other words, the system consists of regions with massless and massive Dirac fermions. By con-

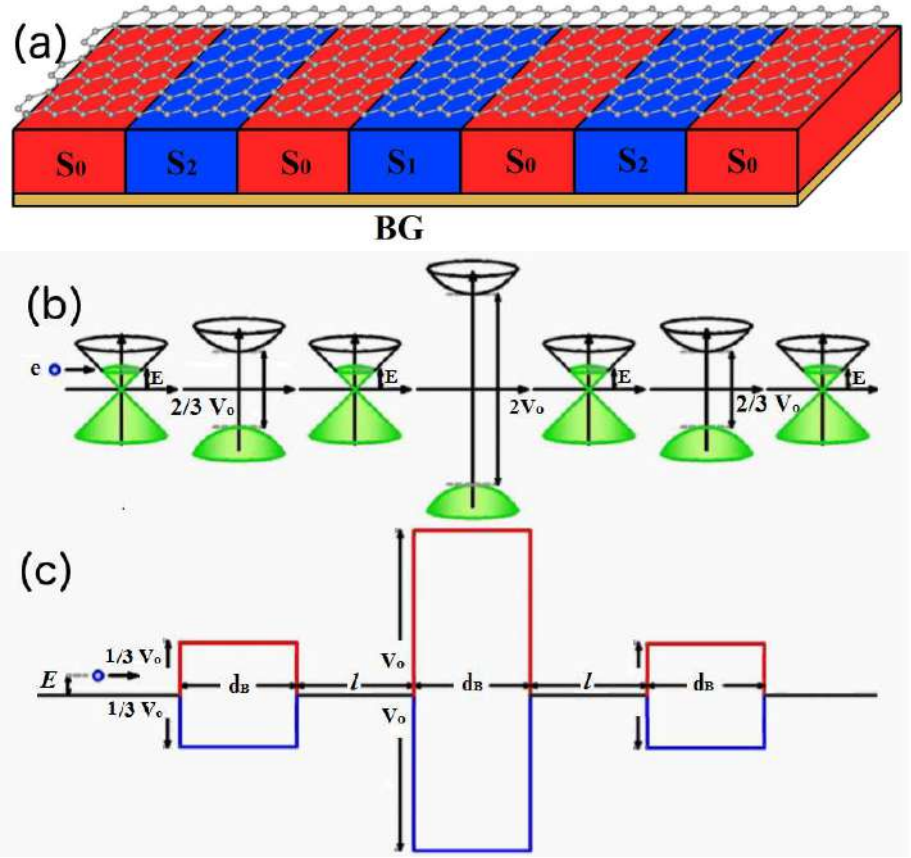

Fig. 1 (Color online) Schematic of self-affine graphene-based structures. (a) Cross-section of the possible device. The device consists of a graphene sheet deposited over a heterostructured substrate with regions of different degree of interaction with the graphene sheet. The heterostructured substrate is built such that the distribution of Dirac cones and paraboloids (b) warranty a self-affine conduction band-edge profile (c). In this figure the second generation of the system is represented. For more details about the construction of the self-affine system the reader can consult our previous work [13].

sidering that electrons in graphene behave as Dirac fermions is that we will adopt a relativistic description of the system. Then, for those regions with considerable interaction with the substrate, massive regions, the Hamiltonian that describes the system is given as,

$$H = v_F(\sigma \cdot p) + t'\sigma_z, \tag{1}$$

where v_F is the Fermi velocity of quasi-particles in graphene -of the order of $c/300$-, $t' = mv_F^2$ is the mass term, $\sigma = (\sigma_x, \sigma_y)$ are the

Pauli matrices, $\boldsymbol{p} = (p_x, p_y)$ is the momentum operator and σ_z the z-component of the Pauli matrix. This equation can be solved straightforwardly giving the following dispersion relation

$$E = \sqrt{\hbar^2 v_F^2 q^2 + t'^2}, \tag{2}$$

here q is the wave vector associated with a region of considerable interaction with the graphene sheet, and t' is proportional to the bandgap, $E_g = 2t'$. In the case of the wavefunction we have,

$$\psi_{\pm}(x,y) = \frac{1}{\sqrt{2}} \begin{pmatrix} 1 \\ v_{\pm} \end{pmatrix} e^{\pm i q_x x + i q_y y}, \tag{3}$$

with

$$v_{\pm} = \frac{\hbar v_F (\pm q_x + i q_y)}{E + t'}, \tag{4}$$

The Hamiltonian, wave functions and eigen-values for massless regions can be readily obtain by setting $t' = 0$. Once the explicit form of the dispersion relations and wavefunctions are obtained for the different regions of our system, it is easy to compute the transmission properties by means of the transfer matrix formalism [16, 17]. Specifically, the transmission probability or transmittance comes as,

$$T = \left| \frac{A_{N+1}}{A_0} \right|^2 = \frac{1}{|M_{11}|^2}, \tag{5}$$

where the transmitted wave amplitude A_{N+1} can be calculated in terms of the incident wave amplitude A_0 via the transfer matrix,

$$\begin{pmatrix} A_0 \\ B_0 \end{pmatrix} = M \begin{pmatrix} A_{N+1} \\ 0 \end{pmatrix}, \tag{6}$$

where the transfer matrix is given by,

$$M = D_0^{-1} \left[\prod_{j=1}^{N} D_j P_j D_j^{-1} \right] D_0. \tag{7}$$

with D_j and P_j the dynamical and propagations matrices of the different regions of the system [13, 14, 15].

3 Results and discussion

Firstly, we will check if our previously reported scaling rules [13] work for oblique incidence. To be clear about this point we will present the mentioned rules. The scaling between generations comes as

$$T_G(E,\theta_i,V_0) = T_{G+N}(2^N E,\theta_i,V_0), \tag{8}$$

where G is the generation and N is the difference between generations. The scaling between heights of the main barrier is given as,

$$T_G(E,\theta_i,V_0) = T_G^{4^p}\left(E,\theta_i,\frac{V_0}{2^p}\right), \tag{9}$$

here V_0 is the height of the main barrier and p the factor that connects the heights of the main barrier. By combining these equations it is possible to obtain a general scaling rule,

$$T_G(E,\theta_i,V_0) = T_G^{4^p}\left(2^N E,\theta_i,\frac{V_0}{2^p}\right). \tag{10}$$

So far, we have proven that these rules work pretty well at normal incidence $\theta_i = 0$. Now it is time to see if they work at oblique incidence as well. Indeed, that's the reason why we are including explicitly the angular coordinate in all previous equations. In Fig. 2 the transmittance as a function of the energy is shown for (a) $\theta_i = 30^\circ$ and (b) $\theta_i = 60^\circ$, respectively. As it is possible to see the matching between the reference curve $G = 5$ and the scaled one $G = 6$ is quite well for both cases. The transmission patterns can be connected by simply multiplying the argument of the transmittance that corresponds to $G = 6$ by a factor of 2.

In Fig. 3 the results for the scaling between heights of the main barrier are shown. The angles of incidence considered are the same as in Fig. 2: (a) $\theta_i = 30^\circ$ and (b) $\theta_i = 60^\circ$. The reference system corresponds to a structure with $V_0 = 1.0$ eV, while the system for which the transmission properties will be scaled corresponds to a structure with $V_0 = 0.5$ eV. The generation of the self-affine structures is $G = 6$ and the structural parameters d_B and l are the same as in Fig. 2. In this case the transmittance for $V_0 = 0.5$ eV is rising to the power 4, dashed-red curve. As we can see the result of this transformation agrees with the

reference curve, solid-black line, in practically all the energy range considered.

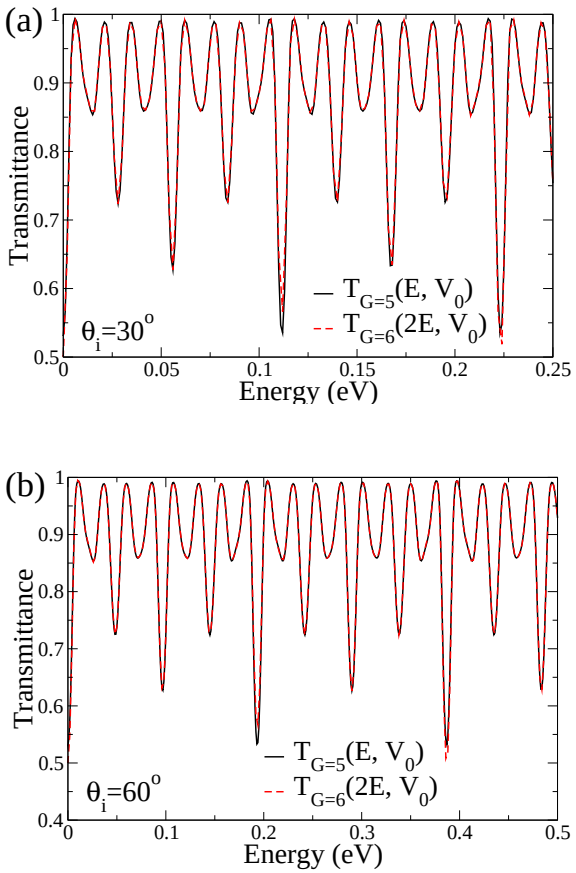

Fig. 2 Transmission patterns at oblique incidence. (a) Transmittance as a function of the energy for $\theta_i = 30^\circ$. The reference curve corresponds to $G = 5$ and the scaled one to $G = 6$, solid-black and dashed-red curves, respectively. The same as in (a) but for $\theta_i = 60^\circ$. The structural parameters of the self-affine structure are: height of the main barrier $V_0 = 1.0$ eV, width of the barriers $d_B = 1.85$ Å and the distance between barriers $l = 185$ Å.

In Fig. 4, eq. (10) is tested at oblique incidence (a) $\theta_i = 30^\circ$ and (b) $\theta_i = 60^\circ$. The reference system (solid-black curves) corresponds to $G = 4$ and $V_0 = 1.0$ eV and the system for which the transmission curves are scaled (dashed-red curves) corresponds to $G = 6$ and $V_0 = 0.25$ eV. The width of barriers and the distance between them are the same as in Figs. 2 and 3. As we can notice the matching between the reference and the scaled curve is quite well no matter if the angle of

incidence is small or large. In this cases it was necessary to rise the transmittance of $G = 6$ to the power 16 and to multiply the argument (energy) of it by a factor of 4. So, as far as we have corroborated the scaling rules for self-affine systems previously found at normal incidence are valid at oblique incidence too.

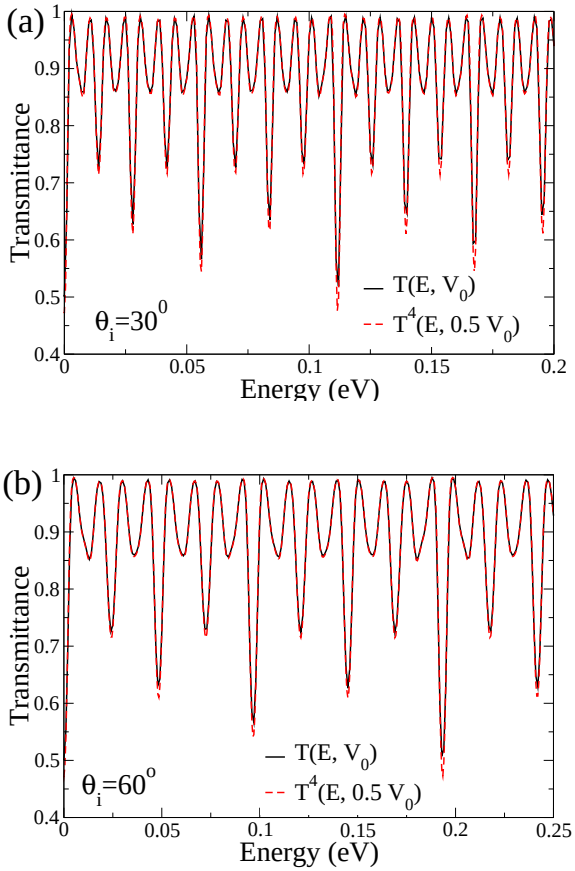

Fig. 3 Scaling between heights of the main barrier at oblique incidence. (a) Transmittance as a function of the energy for $\theta_i = 30°$. The reference curve corresponds to $V_0 = 1.0$ eV and the scaled one to $V_0 = 0.5$ eV, solid-black and dashed-red curves, respectively. The same as in (a) but for $\theta_i = 60°$. The structural parameters of the self-affine structure are: generation $G = 6$, width of barriers $d_B = 1.85$ Å and distance between barriers $l = 185$ Å.

In second place, we are going to figure out if there are scaling rules for the angular distribution of the transmittance, that is, if by fixing the energy of incident electrons the transmission patterns as a function of the angle of incidence for different generations and heights of the main

barrier could be connected via well defined rules. In Fig. 5 we show the angular distribution of the transmittance for $G = 4$ and $G = 5$.

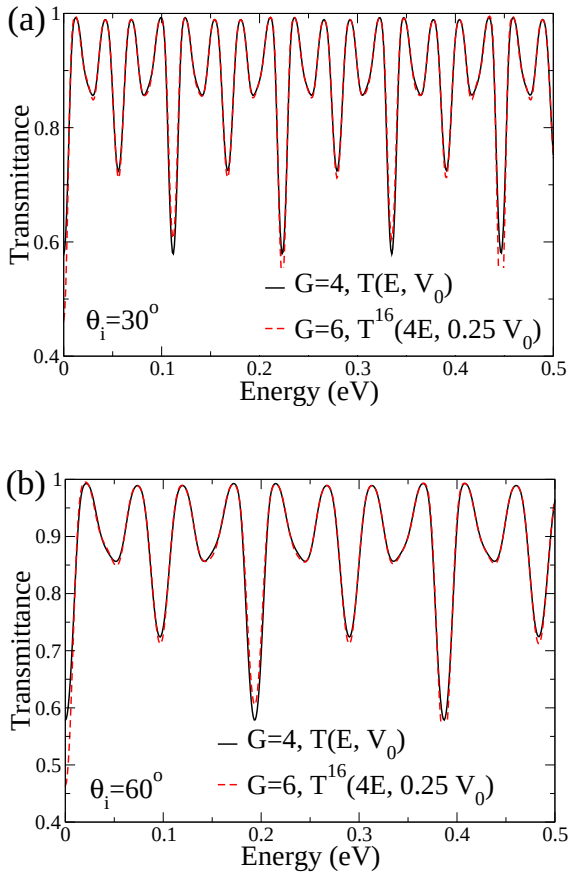

Fig. 4 General scaling at oblique incidence: (a) $\theta_i = 30^\circ$ and (b) $\theta_i = 60^\circ$. Here, eq (10) is tested by considering two self-affine systems with different generation as well as different height of the main barrier. The reference system correspond to $G = 4$ and $V_0 = 1.0$ eV, while the system for which the transmission is scaled corresponds to $G = 6$ and $V_0 = 0.25$. The width of barriers and the distance between them are $d_B = 1.85$ Å and $l = 185$ Å, respectively.

The height of the barrier, the width of barriers and the distance between them are $V_0 = 1.0$ eV, $d_B = 1.85$ Å and $l = 185$ Å, respectively. In this case the transmission patterns can be connected by dividing the energy of the incident electron ($E_i = 0.4$ eV) by a factor of 2 for $G = 6$. As we can notice that the matching is quite good, compare the solid-black and dashed-red curves. Even more, the connection between transmission patterns not necessarily is restricted to consecutive

generations. In fact, the expression that connects transmission patterns for generations comes as

$$T_G(E_i,\theta,V_0) = T_{G+N}\left(\frac{E_i}{2^N},\theta,V_0\right), \tag{11}$$

where E_i represents the energy of incident electrons, G is the generation number and N is the difference between generations. We have included explicitly the angular coordinate because in this case we are taking about the angular distribution of the transmittance and it is also important to mention that contrary to eq. (8) it is not necessary that

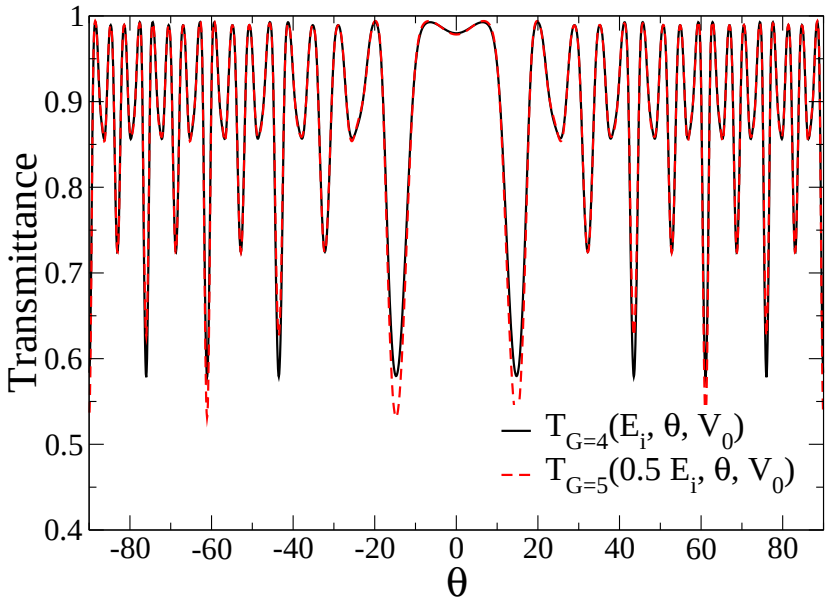

Fig. 5 Scaling between generations for the angular distribution of the transmittance. The transmission patterns for $G = 4$ and $G = 5$ are connected by applying eq. (11). In this case the connection between patterns is reached by simply dividing by 2 the energy of the incident electrons of $G = 5$. The structural parameters are $V_0 = 1.0$ eV, $d_B = 1.85$ Å and $l = 185$ Å. Here it is important to highlight that the angular coordinate does not require any kind of transformation to obtain the scaling.

A similar scaling can be obtained for self-affine systems with different height of the main barrier. In fact, the scaling can be written as

$$T_G(E_i,\theta,V_0) = T_G^{4p}\left(E_i,\theta,\frac{V_0}{2^p}\right), \tag{12}$$

where p represent the factor that connects the heights of the main barrier as well as the factor at which the transmittance is needed to be risen to get the scaling. In Fig. 6 we can see the result of using eq. (12). Specifically, the transmission patterns of self-affine systems with $V_0 = 1.0$ eV and $V_0 = 0.5$ eV can be connected by rising to the power 4 the transmittance of the system with $V_0 = 0.5$ eV. The structural parameters considered were $G = 4$, $d_B = 1.85$ Å and $l = 185$ Å, and the energy of incident electrons was $E_i = 0.4$ eV. As in the other cases the scaling works pretty well, notice the little differences between the solid-black (reference system) and the dashed-red (scaled

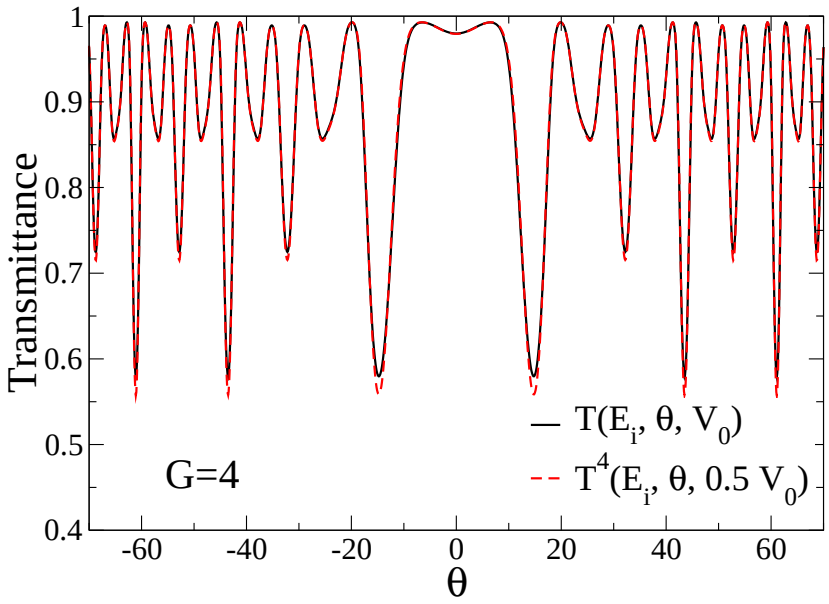

Fig. 6 Scaling between heights of the main barrier for the angular distribution of the transmittance. The transmission patterns for $V_0 = 1.0$ eV and $V_0 = 0.5$ eV are connected by applying eq. (12). The structural parameters are $G = 4$ eV, $d_B = 1.85$ Å and $l = 185$ Å.

We can also combine the previous mathematical expressions to obtain a general equation that describes the scaling between any generations as well as any heights of the main barrier,

$$T_G(E_i,\theta,V_0) = T^{4p}_{G+N}\left(\frac{E_i}{2^N},\theta,\frac{V_0}{2^p}\right). \tag{13}$$

In Fig. 7 we show the result of applying eq. (13). In this figure the transmission patterns for $G = 4$ and $V_0 = 1.0$ eV and $G = 6$ and $V_0 = 0.25$ eV are connected by implementing the mentioned rule. Specifically, the transmittance for $G = 6$ and $V_0 = 0.25$ eV (dashed-red curve) is rising to the power 16 and the energy of the incident electrons is dividing by a factor of 4. In general the matching between

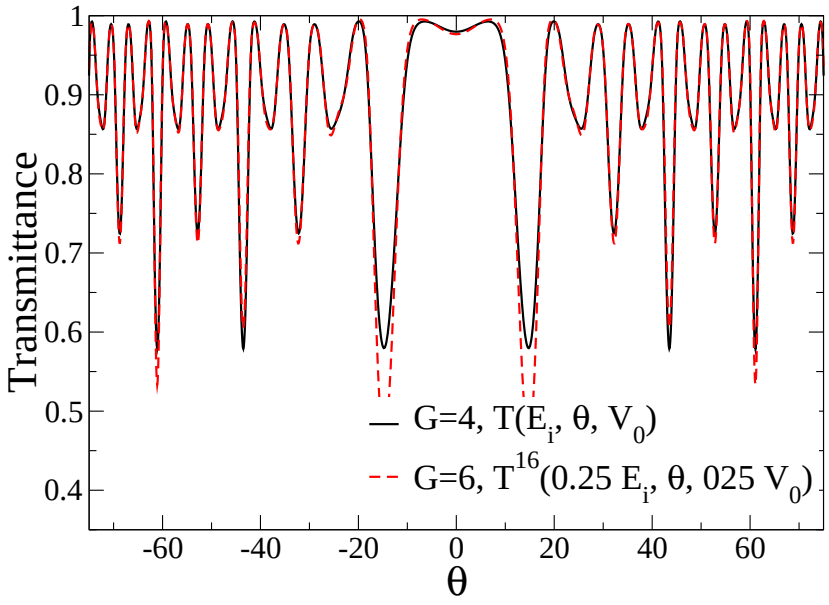

Fig. 7 General scaling for the angular distribution of the transmittance. Here the transmission pattern for $G = 6$ and $V_0 = 0.25$ eV is scaled by applying eq. (13). The reference system corresponds to $G = 4$ and $V_0 = 1.0$ eV. The other structural parameters are $d_B = 1.85$ Å and $l = 185$ Å.

As a final comment we want to remark that even when self-similar structures are a particular case of self-affine ones there are big differences in the scaling rules for the transmittance between these systems. It is also important to stress that the scaling for the angular distribution of the transmittance could have important consequences for the transport properties because, for instance, the conductance is the average of all transmission channels (all angles of incidence) for a given

Fermi energy. In fact, as far as we know for self-similar structures the transport properties can also have scaling rules [18].

4 Conclusions

In summary, the transmission properties of self-affine graphene-based structures have been studied. A relativistic description and the transfer matrix method were adopted in order to unveil the transmission properties. It is found that previous scaling rules [13] valid at normal incidence work also at oblique incidence. The scaling rules for the angular distribution of the transmittance were determined. In particular, rules between generations and heights of the main barrier were found. Possible implications for the transport properties, experimental verification, were discussed.

Acknowledgments

I. R.-V. acknowledges the financial support of CONACYT-Mexico for the sabbatical sojourn, during which the present work was prepared.

References

1. R. Merlin, K. Bajema, Roy Clarke, F. -Y. Juang, and P. K. Bhattacharya, *"Quasiperiodic GaAs-AlAs Heterostructures"*, Phys. Rev. Lett. **55**, 1768 (1985).
2. E. Maciá, *"The role of aperiodic order in science and technology"*, Rep. Prog. Phys. **69**, 397 (2005).
3. R. Pérez-Álvarez, F. García-Moliner, V. R. Velasco, *"Some elementary questions in the theory of quasiperiodic heterostructures"*, Phys.: Condens. Matter **13**, 3689 (2001).
4. A. V. Lavrinenko, S. V. Zhukovsky, K. S. Sandomirski, and S. V. Gaponenko, *"Propagation of classical waves in nonperiodic media: Scaling properties of an optical Cantor filter"*, Phys. Rev. E **65**, 036621 (2002).
5. S.-N. Zhu, Y.-Y. Zhu, N.-B. Ming, *"Quasi-Phase-Matched Third-Harmonic Generation in a Quasi-Periodic Optical Superlattice"*, Science **278**, 843–846 (1997).
6. N. Cohen, *"Fractal antenna applications in wireless telecommunications"*, IEEE Proc Professional Program Electronics Industry Forum 1997:439.
7. K. S. Novoselov, A. K. Geim, S. V. Morozov, D. Jiang, Y. Zhang, S. V. Dubonos, I. V. Grigorieva, A. A. Firsov, *"Electric Field Effect in Atomically Thin Carbon Films"*, Science **306**, 666–669 (2004).

8. K. S. Novoselov, A. K. Geim, S. V. Morozov, D. Jiang, M. I. Katsnelson, I. V. Grigorieva, S. V. Dubonos, A. A. Firsov, *"Two-dimensional gas of massless Dirac fermions in graphene"*, Nature **438**, 197-200 (2005).
9. A. H. Castro Neto, F. Guinea, N. M. R. Peres, K. S. Novoselov, and A. K. Geim, *"The electronic properties of graphene"*, Rev. Mod. Phys. **81**, 109 (2009).
10. D. R. Hofstadter, *"Energy levels and wave functions of Bloch electrons in rational and irrational magnetic fields"*, Phys. Rev. B **14**, 2239 (1976).
11. L. A. Ponomarenko et al., *"Cloning of Dirac fermions in graphene superlattices"*, Nature **497**, 594–597 (2013).
12. C. R. Dean et al., *"Hofstadters butterfly and the fractal quantum Hall effect in moir superlattices"*, Nature **497**, 598–602 (2013).
13. D. S. Daz-Guerrero, L. M. Gaggero-Sager, I. Rodrguez-Vargas and O. Sotolongo-Costa, *"Scaling behavior in the transmission coefficient for a self-affine multi-barrier system using graphene"*, Europhysics Letters **111**, 57006 (2015).
14. D. S. Díaz-Guerrero, I. Rodríguez-Vargas, G. G. Naumis and L. M. Gaggero-Sager, *"Self-similar charge transmission in gapped graphene"*, Fractals **24**, 1630002 (2016).
15. R. Rodríguez-González, I. Rodríguez-Vargas, D. S. Díaz-Guerrero and L. M. Gaggero-Sager, *"Self-similar transmission properties of aperiodic Cantor potentials in gapped graphene"*, Eur. Phys. J. B **89**, 17 (2016).
16. P. Yeh, *Optical Waves in Layered Media* (Wiley-Interscience, 2005).
17. P. Markos and C. M. Soukoulis, *Wave Propagation: From Electrons to Photonic Crystals and Left-Handed Materials* (Princeton University Press, 2008).
18. H. García-Cervantes, L. M. Gaggero-Sager, D. S. Díaz-Guerrero, O. Sotolongo-Costa and I. Rodríguez-Vargas, *"Self-similar conductance patterns in graphene Cantor-like structures"*, unpublished.

Efectos anómalos en el transporte cuántico de huecos

S. Zapata-Marín, G. Fernández-Anaya, A. Mendoza-Álvarez, L. Diago-Cisneros

Resumen

En este capítulo se presenta un estudio de trasnporte cuántico de huecos ligeros y huecos pesados en heteroestructuras semiconductoras, discutiendo con detalle los llamados casos anómalos como el llamado efecto Hartman y las oscilaciones de Ramsauer-Townsend. Se hace especial énfasis en las particularidades del tratamiento matemático, basado en el método de la matriz de transferencia.

We present a study of the quantum transport of light and heavy holes in semiconductor heterostructures. Detailed discussion is provided for the so-called anomalous cases such as the Hartman effect and the Ramsauer-Townsend oscillations. Particular emphasis is made on the peculiarities of the mathematical procedure, which is based on the transfer matrix method.

1 Introducción

La motivación de este trabajo es encontrar expresiones analíticas para las magnitudes de transporte en el fenómeno de transporte cuántico de

Departamento de Física y Matemáticas. Universidad Iberoamericana, México e-mail: alejandro.mendoza@ibero.mx. Departamento de Física Aplicada. Facultad de Física. Universidad de La Habana, Cuba. e-mail: leovildo.diago@ibero.mx

huecos a través de heteroestructuras con el propósito de poder aplicarlas en el modelo de una celda solar de tipo MQW (*Multiple Quantum Well*).

Para hacer esto seguimos los pasos de Pedro Pereyra [9, 11, 12, 10, 13] quién obtuvo expresiones analíticas de las magnitudes de transmisión basadas en polinomios de Chebyshev y polinomios matriciales para el caso de electrones y huecos desacoplados. Esto con el fin de poder analizar desde otra perspectiva fenómenos como el efecto Hartman y los aún polémicos valores negativos del tiempo de fase.

Las bases sobre las que obtenemos las magnitudes de dispersión es a partir de la MSA (Aproximación Dispersiva Multicomponente), por lo que las expresiones que derivamos pueden considerarse una extensión de este método.

La MSA se basa en el formalismo de la matriz de transferencia (TM) y en la teoría de la matriz de dispersión (SM). En este caso nos interesan las matrices de transferencia de vectores de estado, que permiten transferir los coeficientes que acompañan a un vector de estado de un punto a otro en una región de dispersión. En particular, se busca obtener expresiones para el tiempo de fase en el caso multicanal-multibanda cuando el número de celdas $n \to \infty$, dentro del marco de la MSA y además obtener expresiones similares a las reportadas por Pereyra [12] para el tiempo de travesía.

En los últimos años han aparecido numerosas investigaciones relacionadas con el tiempo de fase, como es el caso del artículo publicado por De Leo y Leonardi [4], los cuales encontraron una relación del tiempo de fase con el ancho de la barrera para paquetes de onda cuyo límite superior de distribución de momento es cercano a la altura de la barrera.

Otro ejemplo parecido es el trabajo publicado por H. Simanjuntak y P. Pereyra [13] donde emplean una expresión polinomial para el tiempo de fase que depende del ancho del pozo con el propósito de demostrar que el efecto Hartman generalizado es una presunción errónea en dicho caso.

El estudio de sistemas de baja dimensionalidad ha ayudado al avance de la tecnología dadno origen a diversas aplicaciones, principalmente en el desarrollo de dispositivos electrónicos como diodos de tunelamiento resonante, los SET (*Single Electron Transistor*), láseres de pozo cuántico, transistores de tunelamiento resonante, entre otras.

La presente investigación está también enfocada sobre el estudio de pozos cuánticos múltiples (MQW, *Multiple Quantum Well*) y su aplicación para la elaboración de celdas solares. Los pozos cuánticos (QW, *Quantum Well*) son nanoestructuras cuasi-bidimensionales. P Se fabrican colocando capas de semiconductores con una banda prohibida pequeña encerradas entre semiconductores con una banda prohibida comparablemente más alta. El número de electrones o huecos confinados está determinado por el espesor del semiconductor usado. Para la elaboración de celdas solares se utilizan heteroestructuras a capas en la forma de MQWs.

Las expresiones cerradas para el estudio de fenómenos anómalos tales como los valores negativos del tiempo de fase nos permitirán estudiar de forma analítica el problema cuando el número de celdas crece.

La estructura de trabajo se muestra en la Figura 1. Consiste en un sistema de barreras y pozos con cuatro canales: dos de huecos pesados (*hh*), con proyección de momento angular $\pm 3/2$, y dos de huecos ligeros (*lh*) con proyección de $\pm 1/2$. La elección de la celda en la literatura depende de cada autor y para nuestros fines la celda elementalse define como la estructura que va desde z_L y z_3 y se repite periódicamente. Dentro de este esquema hay tres escenarios, en las regiones *L* y *R* de la Figura 1: Presencia de modos propagantes, que pueden mezclarse, dentro de la barrera (*Layer A*); presencia de canales directos (línea horizontal) o cruzados (línea diagonal dentro del *Layer A*) -si hay interferencia o no entre las rutas de transición cuántica de los huecos- y, en la región del pozo, (*Layer B*) presencia de estados discretos que entran en resonancia constructiva o destructiva con los modos propagantes incidentes en el lado *L*. Cuando se habla del caso desacoplado quiere decir que no hay ningún fenómeno de mezcla, es decir que el *cuasimomentum* paralelo a las intercaras $\kappa \approx 0$. Por ejemplo, si entra un hueco pesado con proyección de momento angular $+3/2$, entonces permanecerá así mientras se mueve a través de la estructura. Por otro lado cuando hay mezcla ($\kappa \neq 0$) hay propiedades del hueco que no se conservan durante el transporte.

El trabajo se dividirá de la siguiente manera:

- Definición de la matriz de transferencia y los polinomios escalares (matriciales) para el caso de huecos desacoplados (acoplados)

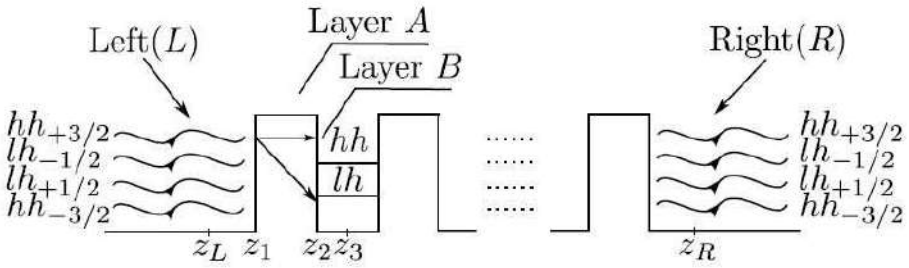

Fig. 1 Esquema de transporte cuántico de *hh* y *lh* a través de una heteroestructura.

- Desarrollo de las expresiones polinomiales y las magnitudes de dispersión:
  - Probabilidades de Dispersión
  - Tiempo de fase
- Presentación de los resultados numéricos para:
  - Probabilidades de Transmisión
  - Tiempo de fase
  - Efecto Hartman
- Aplicación en MQW.
- Conclusiones

2 Matriz de transferencia y polinomios

2.1 Introducción

En el presente capítulo analizamos la relación que existe entre la Matriz de Transferencia (TM) de segundo tipo y la M_{sv} (el subíndice *sv* representa: vector de estado por su acrónimo en inglés) con los polinomios de Chebyshev para el caso de huecos desacoplados.

Como de mencionó arriba, este acercamiento ya fue logrado anteriormente por Pedro Pereyra y Edith Castillo [11, 12], de manera generalizada aplicable a partículas desacopladas y electrones. El análisis a profundidad únicamente se hizo para electrones. En este capítulo seguimos los pasos de los trabajos anteriormente presentados

por Pereyra y comprobamos que en el régimen de huecos desacoplados (sin interacciones entre modos propagantes) podemos tratar cada canal por separado y obtener expresiones válidas para las magnitudes de dispersión en función de los polinomios de Chebyshev. En el caso acoplado, los polinomios de Chebyshev no son aplicables pues no se cumplen las condiciones necesarias para poder aplicarlos. En su lugar deben generarse polinomios matriciales ortogonales que satisfagan adecuadamente las condiciones de contorno.

La ruta de trabajo empleada es la siguinete: Primero, partimos de la matriz de vectores de estado, para n celdas en función de la M_{sv} para una celda y los polinomios de Chebyshev. Posteriormente mediante su relación con la matriz de dispersión, se obtienen expresiones cerradas para las magnitudes de dispersión relevantes, que permitirán hacer un análisis más profundo acerca de fenómenos como el efecto Hartman.

El método que aquí se sigue se diferencía de los encontrados en la literatura ya que éstos en su mayoría derivan de la aplicación del teorema de Bloch en el marco de la solución de sistemas de ecuaciones diferenciales con términos cruzados finitos para el caso de bandas acopladas. Para solucionar este tipo de problemas se usa el formalismo de la TM, pero las situaciones límite suelen generar problemas numéricos graves para sistemas multicapas en presencia de mezcla de bandas (por ejemplo el llamado problema Ω-d). En el presente enfoque no aparecen implícitamente las dificultades numéricas mencionadas anteriormente, por lo que se espera lograr un mayor alcance de la MSA.

2.2 Caso de huecos desacoplados

Para empezar consideramos un problema físico como el que se esquematiza en la Figura 1, donde los flujos de *hh* y *lh* desacoplados, atraviesan un sistema de barreras (pozos) rectangulares de altura (profundidad) finita. Para tal sistema, intentaremos derivar expresiones cerradas de las magnitudes de dispersión, siguiendo el esquema de la Figura 1.

Partiendo de la TM de vectores de estado M_{sv}, y usando la definición general para ésta dada por [2]:

$$M_{sv} = \begin{pmatrix} \alpha & \beta \\ \gamma & \delta \end{pmatrix}, \tag{1}$$

siendo α, β, γ y δ matrices complejas de $(N \times N)$ con información de las amplitudes de transmisión y reflexión.

De ahora en adelante se suprimirá el subíndice *sv* para aligerar la nomenclatura.

Si se trata con *n* celdas, la TM de todo el sistema sería el producto sucesiva de la TM de una sola celda. Por propiedades multiplicativas [9] se puede generalizar que para *n* celdas se tiene una multiplicación sucesiva, definida por

$$M_n = M^n = \begin{pmatrix} \alpha & \beta \\ \gamma & \delta \end{pmatrix}^n = \begin{pmatrix} \alpha_n & \beta_n \\ \gamma_n & \delta_n \end{pmatrix}, \tag{2}$$

donde M_n y M^n denotan una matriz elevada a la potencia *n*.

Usando la relación de recurrencia

$$M_n = MM_{n-1},$$

donde $\boldsymbol{M}$ es la matriz de una sola celda, ls sustitución de (2) en la relación de recurrencia da lugar a

$$M_n = \begin{pmatrix} \alpha & \beta \\ \gamma & \delta \end{pmatrix} \begin{pmatrix} \alpha_{n-1} & \beta_{n-1} \\ \gamma_{n-1} & \delta_{n-1} \end{pmatrix} = \begin{pmatrix} \alpha_n & \beta_n \\ \gamma_n & \delta_n \end{pmatrix}. \tag{3}$$

Luego de la multiplicación se llega a las siguientes relaciones

$$\alpha_n = \alpha\alpha_{n-1} + \beta\gamma_{n-1} \tag{4}$$

$$\beta_n = \alpha\beta_{n-1} + \beta\delta_{n-1} \tag{5}$$

$$\gamma_n = \gamma\alpha_{n-1} + \delta\gamma_{n-1} \tag{6}$$

$$\delta_n = \gamma\beta_{n-1} + \delta\delta_{n-1}. \tag{7}$$

Cuando *n=0*, es decir, no hay barrera (vea Figura 1) se tiene que $\alpha_0 = \delta_0 = I_N$ y $\beta_0 = \gamma_0 = O_N$, donde I_N es la matriz identidad y O_N la matriz nula de dimensión $(N \times N)$[12].

Ahora establecemos por conveniencia los siguientes polinomios, definidos según Pereyra [9] como

$$p^{(1)}_{N,m-1} = \beta^{-1}\beta_m, \tag{8}$$

$$p^{(2)}_{N,m-1} = \gamma^{-1}\gamma_m, \tag{9}$$

es fácil ver que $p_{N,-1} = 0$ y $p_{N,0} = I_N$.

Con algunos desarrollos algebraicos llegamos a una expresión equivalente con (8), quedando todos los términos de la TM en función de los polinomios, y encontramos la expresión que Pereyra [12] denomina *Non-Commutative Polynomial Recurrence Relation (NCPRR)*

$$p^{(i)}_{N,n} - \zeta_i p^{(i)}_{N,n-1} + \eta_i p^{(i)}_{N,n-2} = 0, \qquad n \geqslant 1 \quad i = 1,2 \tag{10}$$

donde

$$\begin{aligned}
\zeta_1 &= \beta^{-1}\alpha\beta + \delta \\
\zeta_2 &= \gamma^{-1}\delta\gamma + \alpha \\
\eta_1 &= \delta\beta^{-1}\alpha\beta - \gamma\beta \\
\eta_2 &= \alpha\gamma^{-1}\delta\gamma - \beta\gamma.
\end{aligned}$$

Si $N = 1$, es decir, el caso de un canal, las matrices conmutan, entonces ζ se convierte en $\alpha + \delta = Tr\{M\}$, donde *Tr* es la traza de la matriz, y η se convierte en $\alpha\delta - \beta\gamma = det\{M\}$. Estas relaciones están relacionadas con la conservación de flujo y algunas propiedades electrónicas. Cabe destacar que esto es independiente del subíndice de ζ o η. Lo anterior nos lleva a la relación de recurrencia de los polinomios de Chebyshev.

A continuación establecemos una relación entre los polinomios y los elementos de la TM para *n* celdas: α_n y δ_n, ya que para β_n y γ_n ya están definidos los polinomios.

Para hacer esto se despeja α_{n-1} de (6)

$$\alpha_{n-1} = \gamma^{-1}(\gamma_n - \delta\gamma_{n-1}),$$

y se efectúan las multiplicaciones

$$\alpha_{n-1} = \gamma^{-1}\gamma_n - \gamma^{-1}\delta\gamma_{n-1}.$$

Usando el polinomio de la ecuación (9) y repitiendo el proceso de multiplicar por $\gamma\gamma^{-1}$ en el segundo término, se pueden introducir los polinomios y obtener

$$\alpha_{n-1} = p_{n-1}^{(2)} - \gamma^{-1}\delta\gamma p_{n-2}^{(2)},$$

. Ahora se recorren los índices $n-1 \to n$ y se obtiene

$$\alpha_n = p_n^{(2)} - \gamma^{-1}\delta\gamma p_{n-1}^{(2)}. \tag{11}$$

Se sigue un proceso similar para los demás componentes de la TM para n celdas. Se desarrolla

$$\delta_{n-1} = \beta^{-1}(\beta_n - \alpha\beta_{n-1}),$$

, se introducen los polinomios y en el segundo término de la derecha se multiplica $\beta\beta^{-1}$ por la derecha y se llega a:

$$\delta_{n-1} = p_{n-1}^{(1)} - \beta^{-1}\alpha\beta p_{n-2}^{(1)},$$

y finalmente se recorren los índices

$$\delta_n = p_n^{(1)} - \beta^{-1}\alpha\beta p_{n-1}^{(1)}. \tag{12}$$

3 Caso de huecos acoplados

El tratamiento analítico del caso de huecos acoplados es similar al caso de huecos desacoplados. De hecho el proceso es idéntico hasta la definición de la NCPRR en la ecuación (10), pero con $N > 1$ por lo que α, β, γ y δ permanecen como matrices no conmutables. En las nuevas condiciones, no podemos reducir ζ y η ya que resultan vinculables a la $Tr\{\mathbf{M}\}$ y $det\{\mathbf{M}\}$ respectivamente. Por lo anterior, no es posible obtener la relación de recurrencia de los polinomios de Chebyshev directamente.

3.1 Relación con la matriz de dispersión

3.1.1 Caso desacoplado

El caso de *hh* y *lh* desacoplados, es formalmente N veces el de electrones en la banda de conducción, por lo tanto puede tratarse como el caso simpléctico de simetría general [9]. Tomando en cuenta lo an-

terior, la relación de la TM de vectores de estado con la matriz de dispersión queda definida de la siguiente manera

$$M = \begin{pmatrix} \alpha & \beta \\ \gamma & \delta \end{pmatrix} = \begin{pmatrix} (t^{\dagger})^{-1} & r'(t')^{-1} \\ (-t')^{-1}r & (t')^{-1} \end{pmatrix}.$$

Aquí, t y r son las amplitudes de transmisión y reflexión incidentes por la izquierda y t' y r' las incidentes por la derecha.

Entonces para n celdas se tiene

$$M_n = \begin{pmatrix} \alpha_n & \beta_n \\ \gamma_n & \delta_n \end{pmatrix} = \begin{pmatrix} (t_n^{\dagger})^{-1} & r'_n(t'_n)^{-1} \\ -(t'_n)^{-1}r_n & (t'_n)^{-1} \end{pmatrix}. \tag{13}$$

Tomando en cuenta la matriz (13) y las ecuaciones (8), (9),(11) y (12) se dan las siguientes relaciones:

$$\alpha_n = (t_n^{\dagger})^{-1} = p_n^{(2)} - \gamma^{-1}\delta\gamma p_{n-1}^{(2)} \tag{14}$$

$$\beta_n = r'_n(t'_n)^{-1} = \beta p_{n-1}^{(1)} \tag{15}$$

$$\gamma_n = (-t'_n)^{-1}r_n = \gamma p_{n-1}^{(2)} \tag{16}$$

$$\delta_n = (t'_n)^{-1} = p_n^{(1)} - \beta^{-1}\alpha\beta p_{n-1}^{(1)}, \tag{17}$$

obteniendo las amplitudes de transmisión y reflexión en función de los polinomios. Así, se pueden llegar a expresar otras magnitudes físicas relevantes en función de los polinomios, como son el tiempo de fase, la probabilidad de transmisión, etc.

Si se despeja t_n de la segunda igualación de la ecuación (14) resulta que

$$t_n = (p_n^{(2)} - p_{n-1}^{(2)}(\gamma^{-1}\delta\gamma)^{\dagger})^{-1}. \tag{18}$$

La ecuación (18) fue escrita de acuerdo a lo que obtuvo Pereyra [9] por lo que se deduce que los polinomios son reales. A continuación se despeja t'_n de la ecuación (17):

$$t'_n = (p_n^{(1)} - (\beta^{-1}\alpha\beta)p_{n-1}^{(1)})^{-1}, \tag{19}$$

se sustituye (19) en la ecuación (15) y se obtiene

$$\beta_n = r'_n(p_n^{(1)} - (\beta^{-1}\alpha\beta)p_{n-1}^{(1)}) = \beta p_{n-1}^{(1)}.$$

Despejando r'_n de la ecuación anterior se tiene

$$r'_n = \beta p_{n-1}^{(1)} (p_n^{(1)} - (\beta^{-1}\alpha\beta) p_{n-1}^{(1)})^{-1}. \tag{20}$$

Y si ahora despejamos r_n de la ecuación (16)y sustituimos t'_n llegamos a

$$r_n = -(p_n^{(1)} - \beta^{-1}\alpha\beta p_{n-1}^{(1)})^{-1} \gamma p_{n-1}^{(2)}. \tag{21}$$

Estos resultados permiten la obtención de expresiones para la probabilidad de transmisión y el tiempo de fase en el caso desacoplado.

3.1.2 Caso acoplado

Ya que en el caso de huecos acoplados existe una interacción entre modos propagantes, surgen algunas dificultades en los cálculos que acabamos de presentar al querer aplicarlos a esta situación. Por ejemplo, si $\kappa \neq 0$ las matrices con las que ahora tratamos no son diagonales y por lo mismo no podemos separar el problema en 4 casos independientes, como se hizo anteriormente.

Otra de las diferencias es que el problema de huecos acoplados, pertenece al caso de simetría general ortogonal [9], y la TM toma la forma

$$M = \begin{pmatrix} \alpha & \beta \\ \gamma & \delta \end{pmatrix} = \begin{pmatrix} t - r'(t')^{-1} r & r'(t')^{-1} \\ (-t')^{-1} r & (t')^{-1} \end{pmatrix};$$

siendo t y r las amplitudes de transmisión y reflexión incidentes por la izquierda y t' y r' incidentes por la derecha.

Siguiendo el procedimiento para el caso desacoplado, cuando tenemos n celdas se verifica que

$$M_n = \begin{pmatrix} \alpha_n & \beta_n \\ \gamma_n & \delta_n \end{pmatrix} = \begin{pmatrix} (t - r'(t')^{-1} r)_n & r'_n (t')_n^{-1} \\ (-t'_n)^{-1} r_n & (t')_n^{-1} \end{pmatrix}, \tag{22}$$

y de manera similar obtenemos las siguientes ecuaciones:

$$\alpha_n = (t + r'(-t')^{-1} r)_n = p_n^{(2)} - \gamma^{-1}\delta\gamma p_{n-1}^{(2)} \tag{23}$$

$$\beta_n = r'_n (t'_n)^{-1} = \beta p_{n-1}^{(1)} \tag{24}$$

$$\gamma_n = (-t'_n)^{-1} r_n = \gamma p_{n-1}^{(2)} \tag{25}$$

$$\delta_n = (t'_n)^{-1} = p_n^{(1)} - \beta^{-1}\alpha\beta\, p_{n-1}^{(1)}. \tag{26}$$

Podemos ver que las expresiones anteriores son iguales que para el caso desacoplado a excepción de (23). Esta es la primera complicación que nos encontramos en el cálculo del régimen acoplado, pues ya que se trata de matrices, resulta difícil poder despejar **t** como lo hicimos en el caso desacoplado para de esa forma obtener las magnitudes de dispersión relevantes en función de los polinomios, que en este caso son polinomios matriciales. Además existen complicaciones adicionales por las que no podemos asegurar que se trate de polinomios de Chebyshev.

Es por ello que tenemos dos vías posibles para solucionar el problema anterior:

- **Descomposición de Jordan:** Si usamos la descomposición de Jordan podremos expresar la ecuación (23) como

  $$\exp(n \ln \mathbf{A}) = \mathbf{A}^n,$$

  siendo **A** la matriz, que corresponde a

  $$\mathbf{A} = t + r'(-t')^{-1} r.$$

  La función logaritmo debe estar definida sobre el espectro de **A** y la función exponencial sobre el espectro del logaritmo de **A** [8]. De esta manera podremos escribir la amplitud de transmisión en función de α_n y de esa manera seguir un procedimiento parecido al del caso acoplado, teniendo en cuenta que los polinomios que resulten deberán de cumplir con las condiciones de borde.
- **Función generadora de polinomios matriciales:** adicional a lo anterior pudiera buscarse una función generadora de polinomios matriciales que se ajusten al problema y cumplan con las condiciones del mismo.

4 Expresiones polinomiales de magnitudes de dispersión

4.1 Introducción

Presentaremos aquí el procedimiento seguido para obtener las expresiones polinomiales para el tiempo de fase y la probabilidad de transmisión a partir de la expresión para la amplitud de transmisión presentada en la sección anterior.

4.2 Probabilidades de dispersión

4.2.1 Caso de huecos desacoplados

La probabilidad de transmisión se define como [2]: $T_{nij} = \mid t_{n,ij} \mid^2$ siendo t_{nij} la amplitud de transmisión desde el canal de entrada j-ésimo al de salida i-ésimo. a través de n celdas, y puede reescribirse de la siguiente manera (sólo para el caso en que la TM sea ortogonal [9]): Las matrices que diagonalizan el Hamiltoniano son simplécticas y se demuestra que $\gamma = \beta^*$ y $\delta = \alpha^*$, lo cual implica invarianza ante reversión temporal e independencia del spin. En este caso la expresión (18) sería [14]

$$t_n = \frac{1}{p_n - p_{n-1}(\beta^{*-1}\alpha^*\beta^*)^\dagger} = \frac{1}{p_n - p_{n-1}(\beta\alpha\beta^{-1})^T},$$

donde el índice T denota la transpuesta de la matriz y † su transconjugada, de aquí en adelante para simplificar la notación se suprimirá el sub-índice ij.

En ausencia de mezcla, el hamiltoniano y las TM involucradas son diagonales por definición, dado que los términos fuera de la diagonal principal que llevan la información del acoplamiento, desaparecen. Considerando lo anterior se obtiene

$$t_n = \frac{1}{p_n - p_{n-1}\alpha^T}.$$

A continuación, se multiplican el numerador y el denominador por la transpuesta conjugada de la amplitud de transmisión dada por $t^\dagger = 1/(\alpha^*)^\dagger = 1/\alpha^T$,

$$t_n = \frac{t^\dagger}{p_n t^\dagger - p_{n-1}}. \tag{27}$$

Para el caso de $N = 1$ (un canal), se tiene que los polinomios resultan ser polinomios de Chebyshev de segundo tipo, que de ahora en adelante se designarán como U_n. Ppor lo que se verá más adelante, estos polinomios están evaluados en la parte real de $\alpha = \alpha_R + i\alpha_I$, siendo definidos como $U_n(\alpha_R)$. Además, α ya no es una matriz y por lo tanto no tiene transpuesta y $t^\dagger \to t^* = 1/\alpha$,de modo que la ecuación (27) se convierten en

$$t_n = \frac{t^*}{t^* U_n - U_{n-1}}. \tag{28}$$

Ya conocida la amplitud de transmisión se puede obtener la probabilidad de transmisión como la norma al cuadrado de la amplitud de transmisión

$$T_n = |t_n|^2 = \left(\frac{t^*}{t^* U_n - U_{n-1}}\right)^* \left(\frac{t^*}{t^* U_n - U_{n-1}}\right), \tag{29}$$

que, dadas las definiciones anteriores para la amplitud de transmisión, equivaldría a

$$T_n = \left(\frac{(1/\alpha^*)}{(1/\alpha^*)U_n - U_{n-1}}\right)\left(\frac{1/\alpha}{(1/\alpha)U_n - U_{n-1}}\right). \tag{30}$$

Si se efectúa la multiplicación se obtiene

$$T_n = \frac{1/\alpha^*(1/\alpha)}{[(1/\alpha^*)U_n - U_{n-1}][(1/\alpha)U_n - U_{n-1}]}, \tag{31}$$

simplificando

$$\begin{aligned} T_n &= \frac{T}{(1/\alpha^*)(1/\alpha)U_n^2 - (1/\alpha)U_n U_{n-1} - (1/\alpha^*)U_n U_{n-1} + U_{n-1}^2} \\ &= \frac{T}{TU_n^2 - U_n U_{n-1}[(1/\alpha) + (1/\alpha^*)] + U_{n-1}^2}, \end{aligned}$$

haciendo la suma de fracciones de las α en el denominador, se obtiene

$$T_n = \frac{T}{TU_n^2 - U_n U_{n-1}\left[\dfrac{\alpha+\alpha^*}{\alpha\alpha^*}\right] + U_{n-1}^2} = \frac{T}{TU_n^2 - TU_n U_{n-1}[\alpha+\alpha^*] + U_{n-1}^2} \tag{32}$$

$$= \frac{T}{TU_n^2 - TU_n U_{n-1}[2\alpha_R] + U_{n-1}^2} = \frac{T}{TU_n(U_n - 2\alpha_R U_{n-1}) + U_{n-1}^2}. \tag{33}$$

A continuación se hace uso de las conocidas relaciones para los polinomios de Chebyshev [1]:

$$U_n U_{n-2} = U_{n-1}^2 - 1 \tag{34}$$

$$U_n = 2xU_{n-1} - U_{n-2}. \tag{35}$$

En la ecuación (35) la x es el parámetro del cual dependen los polinomios (en nuestro caso, es la parte real de α). Si se despeja (35) en función de U_{n-2} y se usa la dependencia de α_R ya mencionada, se tiene

$$U_n - 2\alpha_R U_{n-1} = -U_{n-2}. \tag{36}$$

Sustituyendo (36) en (33) fácilmente se puede ver que

$$T_n = \frac{T}{U_{n-1}^2 - TU_n U_{n-2}}, \tag{37}$$

y usando la relación (34) se obtiene

$$T_n = \frac{T}{T + U_{n-1}^2(1-T)}, \tag{38}$$

que es la misma expresión obtenida por Pereyra [10].

4.3 Tiempo de fase

4.3.1 Caso de huecos desacoplados

Partiendo de la definición de la fase en función de las amplitudes de transmisión para un sistema de n celdas [2]:

$$\theta_{nij} = arctan\left\{\frac{Im(t_{nij})}{Re(t_{nij})}\right\}, \tag{39}$$

y del tiempo de fase

$$\tau_{nij} = \hbar\frac{\partial\theta_{nij}}{\partial E}, \tag{40}$$

definimos el tiempo de fase mediante

$$\begin{aligned}\tau_n &= \hbar\frac{\partial}{\partial E}arctan\left\{\frac{\alpha_I U_{n-1}}{U_n - U_{n-1}\alpha_R}\right\} \\ &= \hbar\frac{1}{1+\left(\dfrac{\alpha_I U_{n-1}}{U_n - U_{n-1}\alpha_R}\right)^2}\frac{\partial}{\partial E}\left(\frac{\alpha_I U_{n-1}}{U_n - U_{n-1}\alpha_R}\right),\end{aligned} \tag{41}$$

El desarrollo de esta expresión es algebraicamente complicado y noslimitamos a dar el resultado [14]

$$\tau_n = \frac{\hbar}{(U_n - \alpha_R U_{n-1})^2 + (\alpha_I U_{n-1})^2}\left(A_r\frac{d\alpha_R}{dE} + A_i\frac{d\alpha_I}{dE}\right), \tag{42}$$

siendo

$$A_i = U_{n-1}(U_n - U_{n-1}\alpha_R), \tag{43}$$

$$A_r = \left(\frac{\alpha_I}{1-\alpha_R^2}\right)[(\alpha_R U_{n-1} + nU_{n-2})U_n - (n+\alpha_R^2)U_{n-1}^2]. \tag{44}$$

5 Resultados numéricos

En esta sección analizaremos los resultados relacionados con el comportamiento del tiempo de tunelamiento para n=2,4,8,10 en una superred de $(AlAs/Al_xGa_{1-x}As/AlAs)^n$ (donde x es la concentración de Al en la barrera), usando las expresiones (42) y (38) presentadas anteriormente.

A modo de comparación usamos el tiempo de recorrido libre (en ausencia de la barrera) definido como:

$$\tau_{free} = \frac{nl_c m_e}{\hbar k_z}, \tag{45}$$

donde l_c es el tamaño de la celda, m_e es la masa del electrón y $k_z = \sqrt{\frac{2m_h^* E}{\hbar^2}}$. En esta expresión m_h^* es la masa efectiva que depende de los parámetros de Lütinger y tiene la forma $m^*_{hh(lh)} = m_e * 0.414(0.108)$, para huecos pesados y huecos ligeros respectivamente. Cabe mencionar que en realidad k_z son los autovalores que se obtienen de resolver un problema cuadrático de valores propios originalmente derivado de Kohn-Lüttinger [5] pero en este caso por simplicidad usamos una aproximación que sobredimensiona el valor esperado de k_z.

Para los resultados que se mostrarán a continuación se utilizó una altura de barrera $V_b = 0.23eV$, un espesor $L_b = 30\AA$ y un ancho de pozo $L_w = 150\AA$. En las Figuras 4.2, 4.3 y 4.8 se muestra el comportamiento del tiempo de fase τ_n, el tiempo de tunelamiento libre τ_{free} y la probabilidad de transmisión en función de la energía incidente para $n = 2, 4, 8$ celdas en el régimen desacoplado para una concentración de 30% de *Al* en la barrera.

5.1 Probabilidades de transmisión

En la Figura 3 los dos paneles muestran el comportamiento del tiempo de tunelamiento de los *hh* y *lh* respectivamente, así como las curvas para el tiempo de fase (línea continua azul en ambos casos) variando la energía incidente desde $0.05eV$ hasta $0.4eV$ en el caso de $n = 2$ celdas -también llamado doble barrera resonante (DBRT por su acrónimo en inglés)- junto con la probabilidad de transmisión. Se puede apreciar el comportamiento resonante que tiene como cota inferior τ_1 (curva punteada azul) en la región de las brechas [10, 3]. Nótese que en todo el rango de estudio las resonancias del tiempo de fase τ_n y las de la probabilidad de transmisión T_n coinciden, lo que significa que el tiempo de fase reproduce correctamente la existencia de niveles cuasi-estacionarios en el pozo intermedio de $Al_xGa_{1-x}As$. Podemos ver que estos resultados son compatibles con las curvas anteriormente obtenidas para electrones [10] y para huecos usando otros métodos [2]. Las diferencias que podrían notarse se atribuyen a la diferencia de los materiales usados pues en el caso de [2] se utilizó una superred de $(AlAs/GaAs/AlAs)^n$ con una concentración de *Al* al 30%. También se puede apreciar que para energías menores a la altura de la barrera

V_b, τ_{free} es mayor que τ_n en los *mini-gaps* que corresponden con las regiones prohibidas, es por ello que T_n se anula. Por otra parte en las regiones del cuasi-continuo τ_n debería de ser mayor que τ_{free}, pero en este caso eso no ocurre y lo atribuimos a la sobre-estimación de k_z que mencionamos anteriormente. El comportamiento explicado sugiere la existencia de mecanismos en las regiones que corresponden a la barrera que provocan que el hueco se propague mucho más rápido a través de ella que por una región en donde no existe barrera.

Si observamos el segundo panel podemos notar que las resonancias para *lh* son más anchas que para *hh* lo que quiere decir que los *hh* se encuentran más confinados en el pozo embebido que los *lh*. Por ello podemos inferir que los tiempos de los *lh* en esos estados del pozo cuántico serán mayores que para los *hh*.

La simbología que usamos para la Figura 3 es la misma que para las Figuras 4 y 5 por lo que no serán nuevamente descritas.

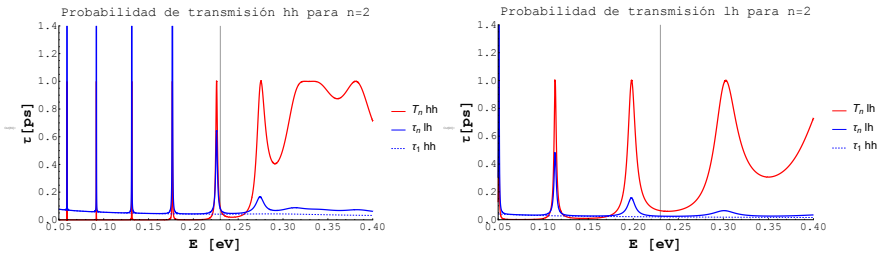

Fig. 2 Tiempo de tunelamiento de recorrido libre τ_{free}, tiempo de fase τ_1 para una celda, tiempo de tunelamiento τ_n y probabilidad de transmisión T_n para $n = 2$ celdas como funciones de la energía incidente para $\kappa \approx 0$, $V_b = 0.23eV$, barreras y pozos de espesor $L_b = 30\AA$ y $L_w = 150\AA$. Para esta figura se usó una concentración en la barrera de 30% de *Al*. En (a) se muestra la transición $hh_{\pm 3/2} \rightarrow hh_{\pm 3/2}$ y en (b) la transición $lh_{\pm 1/2} \rightarrow lh_{\pm 1/2}$.

Cabe resaltar que en ambas figuras, τ_1 sigue siendo la cota inferior en las regiones prohibidas para τ_n mismo comportamiento que no había lograrse con los cálculos anteriores [3].

Además hemos podido llegar a un número de aproximadamente $n = 500$ sin encontrar ninguna inconsistencia con la probabilidad de transmisión, evitando de esta manera un problema que había surgido en traajos anteriores en [2, 3]. Justo a modo de ilustración en las figuras a continuación se presentan los resultados obtenidos en [3].

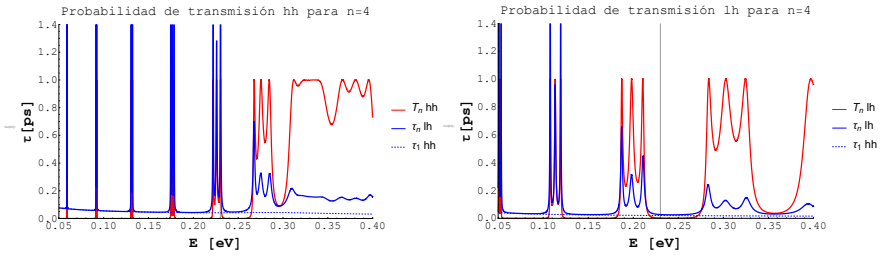

Fig. 3 Igual que en la figura 3 pero en este caso para un sistema de $n = 4$ celdas.

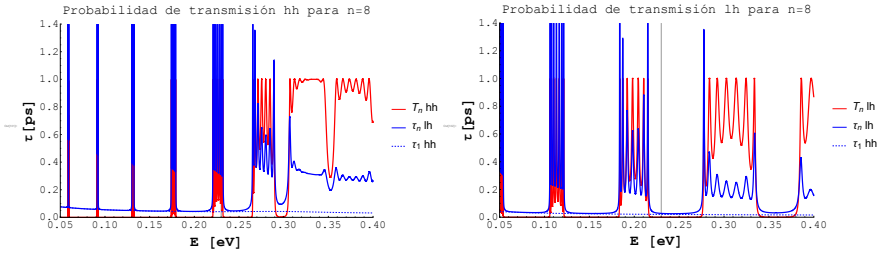

Fig. 4 Igual que en la figura 3 pero en este caso para un sistema de $n = 8$ celdas.

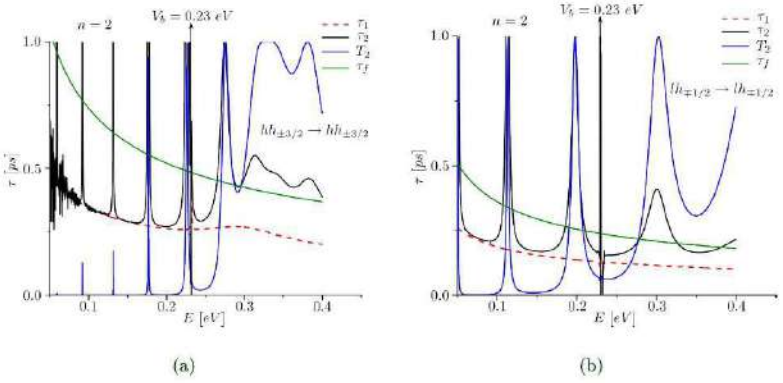

Fig. 5 Tiempo de tunelamiento de recorrido libre τ_{free}, tiempo de fase τ_1 para una celda, tiempo de tunelamiento τ_n y probabilidad de transmisión T_n para $n = 2$ celdas como funciones de la energía incidente para $\kappa \approx 0$, $V_b = 0.23eV$, barreras y pozos de espesor $L_b = 30\text{Å}$ y $L_w = 150\text{Å}$. Para esta figura se usó una concentración en la barrera de 30% de *Al*. En (a) se muestra la transición $hh_{\pm 3/2} \rightarrow hh_{\pm 3/2}$ y en (b) la transición $lh_{\pm 1/2} \rightarrow lh_{\pm 1/2}$ (resultados antiguos). [2, 3]

5.2 Tiempo de fase

En esta subsección presentaremos los resultados obtenidos para la clase eventos anómalos que presenta el tiempo de fase. Entre es-

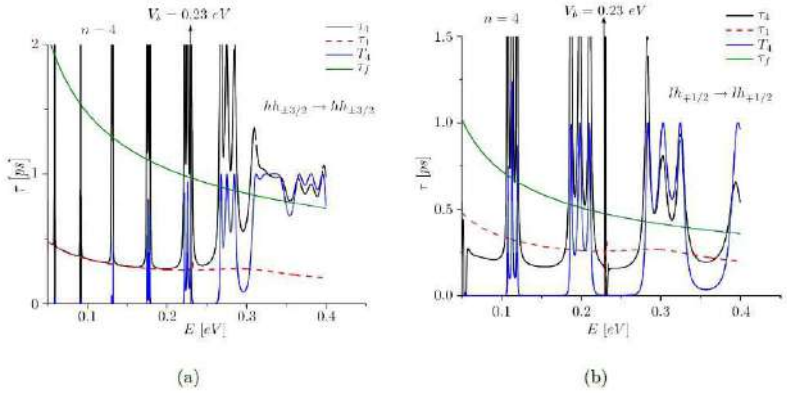

Fig. 6 Igual que en la figura 6 pero en este caso para un sistema de $n = 4$ celdas. [2, 3]

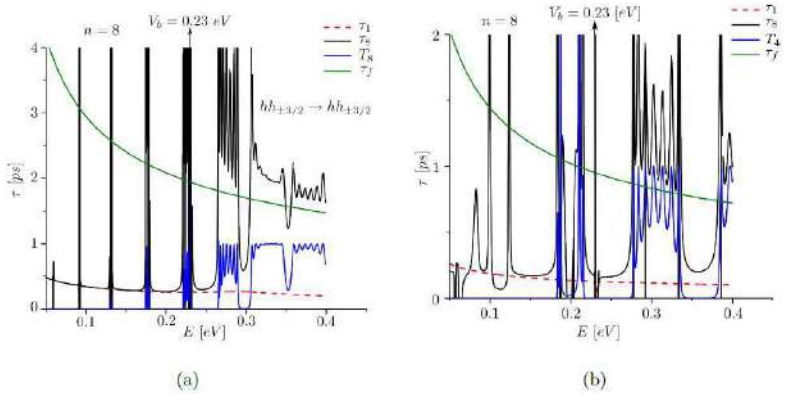

Fig. 7 Igual que en la figura 6 pero en este caso para un sistema de $n = 8$ celdas. [2, 3]

tos se encuentran el efecto Hartman y las oscilaciones de Ramsauer-Townsend. Se analizará el comportamiento del tiempo de fase τ para huecos pesados y huecos ligeros en función del espesor de la barrera L_b y el número de celdas n.

Los parámetros que consideramos son los mismos que en la subsección anterior a excepción de la concentración de Al que en este caso se supone del 65% para que la altura de la barrera alcance $V_b = 0.498\ eV$. El rango de energía incidente entonces se tomará entre valores por debajo de la altura de la barrera $E = 0.475\ eV$ y superiores a la altura de la barrera $E = 0.551 eV$.

Todos los resultados que se presentarán a continuación son para el caso de huecos desacoplados, es decir $\kappa \approx 0$.

5.2.1 Efecto Hartman

El efecto Hartman fue descubierto en 1962 por Thomas E. Hartman [7]. Este efecto establece la autonomía del tiempo de tunelamiento de las componentes de un haz propagante de ondas electrónicas en dependencia del espesor de la barrera a partir de cierto valor de éste espesor.

Tal efecto ha sido ampliamente tratado en la literatura por años, junto con el efecto Hartman generalizado en el que se varía el ancho del pozo y que también ha sido estudiado por Pereyra [13] con una fórmula similar a (42).

En la Figura 9 se muestra el comportamiento del tiempo de fase para la transición directa $hh_{\pm 3/2} \rightarrow hh_{\pm 3/2}$ en el caso $n = 1$ para energías menores (círculos rojos) y mayores (círculos azules) a la altura de la barrera $V_b = 0.498\, eV$ cuando $n = 1$. Se puede notar de la gráfica que para energías incidentes menores a la altura de la barrera τ se vuelve independiente del espesor de la barrera según lo esperado por el efecto Hartman esto ocurre para un valor de $L_b \approx 2nm$. Además, se aprecia que para valores de energía mayores a la altura de la barrera el tiempo de fase oscila y aumenta con el espesor de la misma.

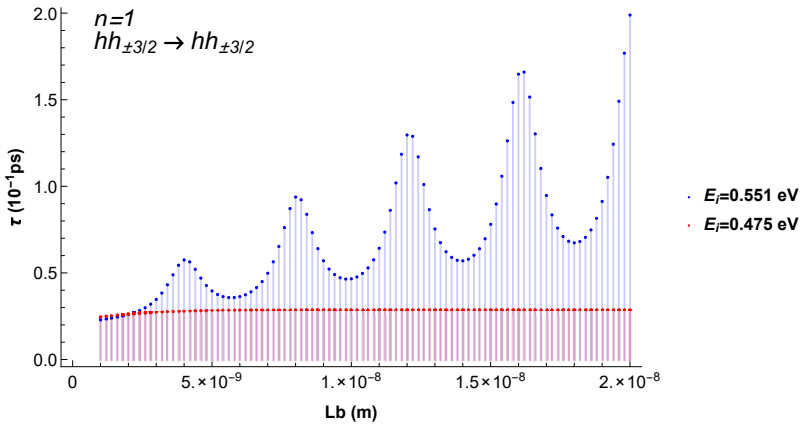

Fig. 8 Tiempo de fase para $n = 1$ correspondiente a la transición directa $hh_{\pm 3/2} \rightarrow hh_{\pm 3/2}$ en función del espesor de la barrera L_b, para energías incidentes menores y mayores a la altura de la barrera $V_b = 0.498\, eV$, a $\kappa \approx 0$

5.2.2 Oscilaciones de Ramsauer-Townsend

En las Figuras 10 y 11 se muestran las curvas del tiempo de fase para energías mayores a la altura de la barrera y se puede observar un claro comportamiento oscilante. Este tipo de oscilaciones reciben el nombre de oscilaciones de Ramsauer-Townsend [5] y son resultado de la interferencia de la onda reflejada con los estados del continuo.

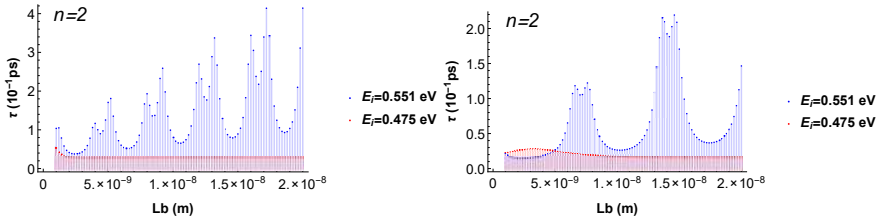

(a) (b)

Fig. 9 Tiempo de fase en función al ancho de la barrera correspondiente a la transisición $hh_{\pm 3/2} \rightarrow hh_{\pm 3/2}$ en el panel (a) y $lh_{\pm 1/2} \rightarrow hl_{\pm 1/2}$ en el panel (b) con energía incidente $E_i = 0.551\ eV$, mayor que la altura de la barrera $V_b = 0.489\ eV$ a $\kappa \approx 0$. La concentración de Al es del 65%. Resultados para $n = 2$ celdas.

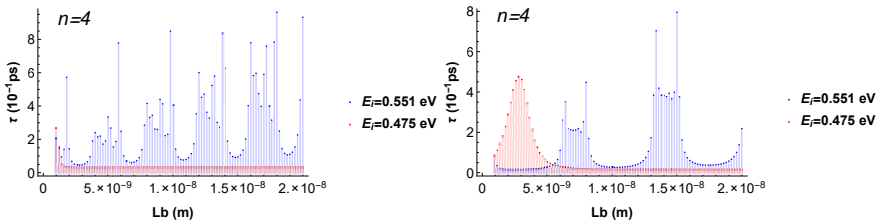

(a) (b)

Fig. 10 Igual a la figura 10 para $n = 4$ celdas.

6 Conclusiones

Se ha conseguido derivar una expresión analítica para las magnitudes de dispersión y el tiempo de fase en los casos de huecos pesados y huecos livianos -en régimen desacoplado- en heteroestruc-

turas de barreras rectangulares, empleando como prototipo el sistema GaAs/AlGaAs. De esta forma:

- Encontramos expresiones polinomiales para la probabilidad y el tiempo de fase para el caso desacoplado y pudimos obtener dentro de los resultados numéricos gráficas contundentes con los resultados anteriormente reportados para huecos y electrones usando otros métodos.
- Dentro de los resultados numéricos pudimos lograr graficar el tiempo de fase y la probabilidad de transmisión para un número de celdas $n = 200$ con menor esfuerzo computacional. Lo anterior implica la disminución del problema Ωd en el caso de huecos desacoplados que surge al aumentar las dimensiones del sistema.
- Aunque no pudimos desarrollar explícitamente las expresiones polinomiales para el caso acoplado, fue posible hallar vías para su solución.

7 Apéndices

7.1 Apéndice I. Polinomios de Chebyshev

Caso N=1

A continuación se dará una breve justificación de por qué en el caso $N = 1$ se trata con polinomios de Chebyshev. En este caso la NCPRR se reduce considerablemente ya que $\zeta_i = Tr[M]$ y $\eta_i = Det[M]$. Entonces podemos reescribir la NCPRR de manera que tenemos:

$$p^{(i)}_{1,n} - Tr[M]p^{(i)}_{1,n-1} + Det[M]p^{(i)}_{1,n-2} = 0. \qquad n \geqslant 1 \quad i = 1,2. \quad (46)$$

Aquí se puede distinguir fácilmente el polinomio característico de una matriz de (2×2), pero esto resulta válido para el caso $N = 1$ en virtud de que α, β, γ y δ son números complejos, no matrices.

En el caso de que se exija que haya una conservación de flujo, el $Det[M] = 1$ y se tiene

$$p^{(i)}_{1,n} - Tr[M]p^{(i)}_{1,n-1} + p^{(i)}_{1,n-2} = 0, \qquad n \geqslant 1 \quad i = 1,2 \qquad (47)$$

Que se simplifica de la siguiente manera

$$p_{1,n}^{(i)} + g_1 p_{1,n-1}^{(i)} + p_{1,n-2}^{(i)} = 0, \qquad n \geqslant 1 \quad i = 1,2 \tag{48}$$

siendo $g_1 = -TrM$

A continuación se hará un pequeño recordatorio de los polinomios característicos para poder explicar cómo se llega a los polinomios de Chebyshev.

Recordando que un polinomio característico es aquel que se le asocia a una matriz cuadrada y cuyas raíces son los valores propios de A, formalmente se define como:

$$p_A(x) = Det(A - xI).$$

Para una matriz de 2×2, que es nuestro caso, el polinomio característico sería:

$$p_M(x) = Det\left(\begin{pmatrix} \alpha & \beta \\ \gamma & \delta \end{pmatrix} - x\begin{pmatrix} 1 & 0 \\ 0 & 1 \end{pmatrix}\right) = Det\left(\begin{pmatrix} \alpha & \beta \\ \gamma & \delta \end{pmatrix} - \begin{pmatrix} x & 0 \\ 0 & x \end{pmatrix}\right),$$

y desarrollando se obtiene

$$p_M = Det\left(\begin{pmatrix} \alpha - x & \beta \\ \gamma & \delta - x \end{pmatrix}\right) = x^2 + (\alpha + \delta)x + (\alpha\delta - \beta\gamma),$$

de la ecuación anterior es fácil ver que el polinomio característico se reduce a

$$p_M(x) = x^2 - Tr[M]x + Det[M]. \tag{49}$$

Como se dijo anteriormente los valores propios son raíces de dicho polinomio así que tenemos que la siguiente igualdad se cumple

$$p_M(\lambda) = \lambda^2 - Tr[M]\lambda + Det[M] = 0. \tag{50}$$

Si se resuelve esta ecuación cuadrática (con la chicharronera) se obtiene que:

$$\lambda_1 = \frac{Tr[M] + \sqrt{(Tr[M])^2 - 4Det[M]}}{2},$$

$$\lambda_2 = \frac{Tr[M] - \sqrt{(Tr[M])^2 - 4Det[M]}}{2}.$$

De estas ecuaciones se puede ver fácilmente que las siguientes relaciones se cumplen

$$\lambda_1 + \lambda_2 = Tr[M], \tag{51}$$

$$\lambda_1 \lambda_2 = Det[M]. \tag{52}$$

Se proponen como soluciones

$$\lambda_1 = e^{iqd} \tag{53}$$

$$\lambda_2 = e^{-iqd} Det[M] \tag{54}$$

De esta relación y asumiendo que $Det[M] = e^{i\Theta}$ [**?**], se obtiene la siguiente ecuación de valores propios:

$$cos\left(qd - \frac{\Theta}{2}\right) = \frac{e^{-i\Theta/2}}{2} Tr[M],$$

ya que

$$\lambda_1 + \lambda_2 = e^{iqd} + e^{-iqd} Det[M] = e^{iqd} + e^{-iqd} e^{i\Theta} = Tr[M].$$

Tomando y manipulando algrebraicamente la última igualdad

$$\frac{e^{iqd} + e^{-i(qd-\Theta)}}{2} = \frac{Tr[M]}{2} = \frac{e^{-i\Theta/2}(e^{iqd} + e^{-i(qd-\Theta)})}{2} = \frac{e^{-i\Theta/2} Tr[M]}{2}$$

$$\frac{e^{i(qd-\Theta/2)} + e^{-i(qd-\Theta/2)}}{2} = cos\left(qd - \frac{\theta}{2}\right) = \frac{e^{-i\Theta/2} Tr[M]}{2}.$$

En el caso de que la fase Θ del determinante se desvanezca (esto sucede en la ecuación simple de Schroedinger para el modelo de una banda [**?**]), la ecuación anterior nos lleva a

$$cos(qd) = \frac{1}{2} Tr[M], \tag{55}$$

$$Det[M] = e^0 = 1. \tag{56}$$

Si sustituimos, según el teorema de Cayley-Hamilton tenemos que

$$T^2 - \tau T + I = 0, \tag{57}$$

Donde $\tau = \frac{Tr[T]}{2}$ y esta relación lleva a:

$$U_0(\tau) = 1$$

$$U_1(\tau) = 2\tau$$

$$U_l(\tau) = U_{l-1}(\tau) - U_{l-2}(\tau).$$

Ahora todas las expresiones anteriores se utilizan asumiendo que las expresiones que son válidas para la matriz asociada de transferencia T son válidas también para M. Y de esta manera se demuestra que para el caso N=1 los polinomios característicos de M son polinomios de Chebyshev.

Para mostrar una relación con los polinomios que nos lleve a la ecuación (10), y siguiendo el procedimiento de Pereyra en el apéndice E [11], hacemos una función generadora de $g(\lambda) = (1+g_1\lambda+g_2\lambda^2)^{-1}$ de la siguiente manera

$$g(\lambda) = \frac{1}{1+g_1\lambda+g_2\lambda^2} = q_0 + q_1\lambda + q_2\lambda^2 + ... \qquad (58)$$

No se sigue todo el procedimiento pues está en el apéndice E del artículo del ICTP de Pereyra, pero se llega a

$$q_{n+2} + g_1 q_{n+1} + g_2 q_n = 0 \qquad n \geqslant 0 \qquad (59)$$

Mediante un paso adicional en el apéndice E se llega a que $q_n = p_n$ y que son los polinomios de Chebyshev de segundo tipo en su representación de autovalores.

Caso $N > 1$

Pereyra analiza también el caso multicanal y propone unos polinomios que no son los de Chebyshev pero sólo son aplicables para el caso desacoplado. A continuación se demostrara el por qué. En ([11]) Pereyra define la MRR como

$$p_{N,n} = -\chi p_{N,n-1} - \eta_{N,n-2}, \qquad (60)$$

donde, $\chi = -(\beta^{-1}\alpha\beta + \delta)$. Después considera la siguiente función generadora:

$$Q(\lambda) = \frac{I_N}{1 + g_1\lambda + g_2\lambda + g_{2N}\lambda^{2N}} = q_{N,0} + q_{N,1}\lambda + q_{N,2}\lambda^2 + ..., \tag{61}$$

los coeficientes $q_{N,i}$ cumplen las siguientes condiciones:

$$q_{N,0} = I_N, \tag{62}$$

$$q_{N,1} + g_1 q_{N,0} = 0, \tag{63}$$

$$q_{N,2} + g_1 q_{N,1} + g_2 q_{N,0} = 0. \tag{64}$$

Más adelante llega a una relación para las q_n de la forma

$$q_n = \sum_{i=1}^{2N} \frac{\lambda_i^{2N+n-1}}{\prod_{j\neq i}^{2N}(\lambda_i\lambda_j)} I_N,$$

con esta relación es fácil ver que todas las relaciones de $q_{N,0}$ son matrices diagonales, por lo que el polinomio matricial de la función generadora únicamente genera polinomios matriciales diagonales por lo que no nos será útil para el caso acoplado, al final del presente reporte se presentan las alternativas a seguir.

7.2 Apéndice II. Scattering

A continuación se muestra un proceso de *scattering* o dispersión en un potencial arbitrario V(x)

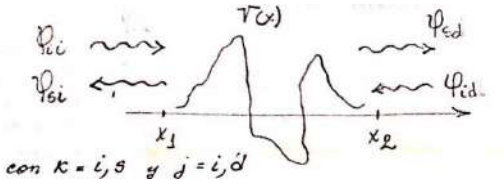

Fig. 11 Diagrama de dispersión

con $\kappa = i, s y j = i, d$.
φ_{kj} representa las funciones de onda; para i(s): incidente, mientras que

i(d) representa izquierda (derecha). El potencial dispersor V(x) modifica las amplitudes de las funciones incidentes φ_{ii} y φ_{id}; y determina las amplitudes de las funciones de onda salientes φ_{sd} y φsi
La teoría de dispersión permite expresar las funciones de onda salientes como productos de las amplitudes complejas de transmisión $t(t')$ y reflexión $r(r')$; si la onda propagante incide por la izquierda (derecha), respectivamente. Esto es:

$$\varphi_{sd} = t\varphi_{ii} + r'\varphi_{id} \tag{65}$$

$$\varphi_{si} = r\varphi_{ii} + t'\varphi_{id} \tag{66}$$

Si escribimos (65) y (66) en forma matricial tenemos.

$$\begin{pmatrix} \varphi_{si} \\ \varphi_{sd} \end{pmatrix} = \begin{pmatrix} r & t' \\ t & r' \end{pmatrix} \begin{pmatrix} \varphi_{ii} \\ \varphi_{id} \end{pmatrix} = \mathbf{S} \begin{pmatrix} \varphi_{ii} \\ \varphi_{id} \end{pmatrix}$$

Los vectores de onda, también se relacionan a través de la matriz de transferencia de vectores de estado, en la forma.

$$\begin{pmatrix} \varphi_{si} \\ \varphi_{sd} \end{pmatrix} = \begin{pmatrix} \alpha & \beta \\ \gamma & \delta \end{pmatrix} \begin{pmatrix} \varphi_{ii} \\ \varphi_{si} \end{pmatrix}$$

En ausencia de potencial dispersor V(x)=0, las relaciones anteriores $\varphi_{sd} = \alpha\varphi_{ii} + \beta\varphi_{si}$ y $\varphi_{id} = \gamma\varphi_{ii} + \delta\varphi si$ se modifican. Es decir, como $V(x) = 0$ no habrá dispersión $(t = t' = 1, r = r' = 0)$; entonces $\varphi_{sd} = \varphi_{ii}$; lo cual implica que para el caso matricial:

$$\alpha = 1 \rightarrow \alpha = I_N$$

$$\beta = 0 \rightarrow \beta = O_N$$

7.3 Apéndice III

Nota 1.

En rigor, para el caso N=1, los elementos matriciales de M_{sv} son escalares. Por lo anterior , resulta trivial que esos elementos matriciales conmutan. Se cumpla además directamente que $Tr\{M_{sv}\} = \alpha + \delta$.
En el caso $N \geq 2$; los elementos matriciales de M_{sv} son matrices. La

propiedad conmutativa, no es universal para estos objetos. Por otro lado, en general: $Tr\{M_{sv}\} \neq \alpha + \delta$.

Nota 2.

Por lo explicado arriba, en general para el caso $N \geq 2$: $det\{M_{sv}\} \neq \alpha\delta - \gamma\beta$. Sólo en el caso $N = 1$, la expresión anterior se transforma en una identidad, dado el carácter escalar de sus elementos; osease $det\{M_{sv}\} = \alpha\delta - \gamma\beta$.
En el caso particular que $\alpha, \beta, \gamma, \delta$ sean diagonales, el $det\{M_{sv}\} \neq \alpha\delta - \gamma\beta = \begin{pmatrix} \alpha_{11}\delta_{11} - \gamma_{11}\beta_{11} & 0 \\ 0 & \alpha_{22}\delta_{22} - \gamma_{22}\beta_{22} \end{pmatrix}$

Bibliografía

1. G. Arfken, H. Weber, *Mathematical Methods for Physicists*, sexta edición, Elsevier, (2005).
2. Susana Arias-Laso, *Estudio del tiempo de fase y eventos anómalos del transporte cuántico de huecos*, Universidad de La Habana, Facultad de Física, La Habana, Cuba (2009).
3. Susana Arias-Laso, S. and L. Diago-Cisneros, *Physica E*, **44**: 1730-1741 (2011).
4. Stefano De Leo and Vinicius Leonardi *J. Phys. A: Math. Theor.* **44** 085305 (2011).
5. L. Diago-Cisneros , H. Rodríguez-Coppola, R. Pérez-Álvarez and P. Pereyra *Phyical Review B* **74**, 045308 (2006).
6. Muhittin Cenk Eser *Tunneling times*. Eastern Mediterranean University, Gazimagusa, North Cyprus, 2011.
7. Hartman, T. E. *J. Appl. Phys*, **33** 12, (1962).
8. Peter Lancaster, Miron Tismenetsky. *The Theory of Matrices.* E.U.A.: Werner Rheinbolt (1985).
9. P.Pereyra, *Journal of Applied Physics* **31**, (1998).
10. P. Pereyra, *Physical Review Letters* **84**, 1772 (2000).
11. P. Pereyra, E. Castillo, *Physical Review B* **65**,1 (2002).
12. P.Pereyra, E. Castillo,publicación de la ICTP *Theory of finite periodic systems - I: General expressions and various simple and illustrative examples*, (2002).
13. Simanjuntak and Pereyra, *Nanoscale Research Letters*, **8**, 145 (2013).
14. S. Zapata-Marín, A. Mendoza-Álvarez, G. Fernández-Anaya, L. Diago-Cisneros, *"Closed matrix- polynomial expressions for the phase time in a multichannel-multiband uncoupled system". 9no Taller de Materia Condensada* (2016).

Problema de Sturm-Liouville: Propiedades generales para el estudio de sistemas a capas. Dos ejemplos ilustrativos

R. Pérez-Álvarez, R. Pernas-Salomón

Abstract

Recently, the authors demonstrated the ubiquitous character of the Sturm-Liouville matrix problem in multilayered structures. In this work two important cases are exemplified: the equation of motion for the elastic modes and the corresponding to electromagnetic oscillations in bianisotropic media. For these examples, explicit expressions for the matrices of the Sturm-Liouville differential operator are given. A simplified form of the Green's function regular at infinity (for the homogeneous Sturm-Liouville matrix operator) is identified for each case according to an established classification. Through these examples, general properties of the Sturm-Liouville's problem that are relevant to the study of layered systems are also analyzed.

Recientemente los autores demostraron la ubicuidad del problema de Sturm-Lioville matricial en la Física de los sistemas a capas. En el presente trabajo se ejemplifican dos casos importantes, como son los modos elásticos y las oscilaciones electromagnéticas en medios bianisotrópicos. Para estos casos se dan las expresiones explícitas de las matrices del operador de Sturm-Liouville y se clasifican en correspondencia con la forma que adopta la función de Green regular en el infinito de estos operadores. A través de estos ejemplos, se analizan

(RPS) Instituto de Física, Benemérita Universidad Autónoma de Puebla -Calle 18 Sur y San Claudio, Edif. 110-A, Ciudad Universitaria, C.P. 72570, Puebla, México. (RPA) Universidad Autónoma del Estado de Morelos. Facultad de Ciencias. Ave. Universidad 1001, Cuernavaca, Morelos, Mexico. e-mail: rpernass@gmail.com, e-mail: rpa@uaem.mx.

también las propiedades generales del problema de Sturm-Liouville que son relevantes para el estudio de los sistemas de capas.

1 Introducción

La Física de los sistemas a capas plano paralelas es de gran actualidad y se estudia un número importante de excitaciones elementales muy diversas: estados electrónicos, modos elásticos, modos de oscilación ópticos, estados superconductores, modos electromagnéticos y un largo etcétera [1-7].

Llamemos $F_\nu(\mathbf{r},t)$ a una arreglo de N componentes representativo del campo que estudiamos (funciones de onda, elongaciones, potenciales electromagnéticos, etc.). Recientemente [8] hemos propuesto la siguiente densidad lagrangiana para describir de una vez todas estas situaciones

$$\begin{aligned}\mathscr{L} = &\frac{1}{2}\frac{\partial \mathbf{F}}{\partial t}\cdot\rho\cdot\frac{\partial \mathbf{F}}{\partial t}+\frac{1}{2}\frac{\partial \mathbf{F}}{\partial t}\cdot\Omega\cdot\mathbf{F}+\frac{1}{2}\mathbf{F}\cdot\gamma\cdot\mathbf{F}\\ &+\frac{1}{2}\nabla\mathbf{F}:\lambda:\nabla\mathbf{F}+\mathbf{F}\cdot\mu:\nabla\mathbf{F}+\nabla\mathbf{F}:\chi\cdot\frac{\partial \mathbf{F}}{\partial t}\,. \end{aligned} \tag{1}$$

No es difícil comprobar que esta densidad tiene como casos particulares las que usualmente encontramos en los libros para varias de estas excitaciones.

Suele suceder que los parámetros (masas efectivas, constantes dieléctricas, potenciales, constantes elásticas, etc.) son funciones de la coordenada perpendicular a las intercaras, digamos que z. Entonces la simetría respecto a las traslaciones en estos planos permite escoger el campo en cuestión $F_\nu(\mathbf{r},t)$ como

$$F_\nu(\mathbf{r},t) = F_\nu(z)\,e^{i(\kappa\cdot\rho-\omega t)}\,, \tag{2}$$

donde

$$\rho = (x,y)\,, \tag{3}$$

$$\kappa = (\kappa_x,\kappa_y)\,. \tag{4}$$

Si escribimos las ecuaciones de Euler-Lagrange correspondientes llegaremos al siguiente problema para el campo:

$$\frac{d}{dz}\left[\mathbf{B}(z)\cdot\frac{d\mathbf{F}(z)}{dz}+\mathbf{P}(z)\cdot\mathbf{F}(z)\right]+\mathbf{Y}(z)\cdot\frac{d\mathbf{F}(z)}{dz}+\mathbf{W}(z)\cdot\mathbf{F}(z)=\mathbf{0}, \tag{5}$$

donde las matrices $N\times N$ $\mathbf{B}(z),\mathbf{P}(z),\mathbf{Y}(z)$ y $\mathbf{W}(z)$ se expresan en términos de los parámetros que entran en $\mathscr{L}$ como sigue:

$$B_{\nu\alpha}=\frac{1}{2}(\lambda_{3\nu3\alpha}+\lambda_{3\alpha3\nu})\,, \tag{6}$$

$$P_{\nu\alpha}=\frac{1}{2}\sum_{i}^{2} i\,\kappa_i\,(\lambda_{3\nu i\alpha}+\lambda_{i\alpha3\nu})+\mu_{\alpha3\nu}-i\omega\,\chi_{3\nu\alpha}\,, \tag{7}$$

$$Y_{\nu\alpha}=\frac{1}{2}\sum_{k}^{2} i\,\kappa_k\,(\lambda_{k\nu3\alpha}+\lambda_{3\alpha k\nu})-\mu_{\nu3\alpha}-i\omega\,\chi_{3\alpha\nu}\,, \tag{8}$$

$$\begin{aligned}W_{\nu\alpha}=&-\frac{1}{2}\sum_{k}^{2}\sum_{i}^{2}\kappa_k\kappa_i\,(\lambda_{k\nu i\alpha}+\lambda_{i\alpha k\nu})\\&+i\sum_{k}^{2}\kappa_k\,\mu_{\alpha k\nu}-i\sum_{j}^{2}\kappa_j\,\mu_{\nu j\alpha}\\&-\frac{1}{2}\omega^2(\rho_{\nu\alpha}+\rho_{\alpha\nu})-\frac{1}{2}(\gamma_{\nu\alpha}+\gamma_{\alpha\nu})\\&+\omega\sum_{i}^{2}\kappa_i\,\chi_{i\alpha\nu}+\omega\sum_{k}^{2}\kappa_k\,\chi_{k\nu\alpha}+\frac{1}{2}i\omega(\Omega_{\alpha\nu}-\Omega_{\nu\alpha})\,.\end{aligned} \tag{9}$$

(5) no es otra cosa que una ecuación de Sturm-Lioville matricial. Si pedimos que el operador de esta ecuación sea formalmente hermítico tendremos que $\mathbf{B}$ y $\mathbf{W}$ son matrices hermíticas y que $\mathbf{Y}=-\mathbf{P}^{\dagger}$. [6, 9]

La forma lineal

$$\mathbf{A}(z)=\mathbf{B}(z)\cdot\frac{d\mathbf{F}(z)}{dz}+\mathbf{P}(z)\cdot\mathbf{F}(z) \tag{10}$$

es muy importante en la teoría y práctica de estos estudios, sobre todo porque se puede demostrar bajo condiciones bastante generales que es una función continua para todo valor de z. [6]

El objetivo del presente trabajo es estudiar cómo se expresan estos resultados generales en dos problemas concretos de suma trascendencia. En la sección 2 analizaremos el caso muy conocido de las excitaciones o modos elásticos mientras que en la sección 3 estudiaremos el caso menos visto de los modos electromagnéticos en sistemas cuyas capas están construidas con materiales bianisotrópicos. Esto nos permitirá deducir la forma o estructura de su función de Green regular en el infinito [10]. Como acabamos de decir, los modos elásticos son muy conocidos (ver, por ejemplo, [3] y las referencias que allí se dan), pero no deja de ser ilustrativo constatar cómo se manifiestan las propiedades generales. Por otra parte, los materiales bianisotrópicos constituyen una clase muy amplia y los modos electromagnéticos en sistemas a capas de estos materiales están siendo muy estudiados por sus múltiples aplicaciones [11-27].

2 Excitaciones elásticas en sistemas a capas

Como se conoce, las ecuaciones de la Elasticidad son tres ecuaciones acopladas, pero en el caso isótropo, escogiendo el eje z perpendicular a las intercaras y tomando $\kappa = (0, \kappa)$ estas tres ecuaciones se desacoplan en una correspondiente a los modos TH (Transversales Horizontales) y en otro sistema, ahora de dos ecuaciones para los llamados modos sagitales [3]. Estas últimas son las que estudiamos aquí. Para un medio homogéneo

$$\begin{pmatrix} \left(\mu \frac{d^2}{dz^2} + \Gamma q_L^2\right) & i\kappa(\Gamma - \mu)\frac{d}{dz} \\ i\kappa(\Gamma - \mu)\frac{d}{dz} & \left(\Gamma \frac{d^2}{dz^2} + \mu q_T^2\right) \end{pmatrix} \cdot \begin{pmatrix} u_y \\ u_z \end{pmatrix} = \begin{pmatrix} 0 \\ 0 \end{pmatrix} \qquad (11)$$

donde

$$\Gamma = \lambda + 2\mu \tag{12}$$

$$q_L = +\sqrt{\left(\frac{\omega}{v_L}\right)^2 - \kappa^2} \quad ; \quad v_L = \sqrt{\frac{\Gamma}{\rho}} \tag{13}$$

$$q_T = +\sqrt{\left(\frac{\omega}{v_T}\right)^2 - \kappa^2} \quad ; \quad v_T = \sqrt{\frac{\mu}{\rho}} \tag{14}$$

Estas son las ecuaciones (1.75) y (1.76) de [3]. λ y μ son los coeficientes de Lamé, ω es la frecuencia y v_T/v_L es la velocidad de las ondas transversales/longitudinales. En nuestro formato standard se tiene que

$$\mathbf{F} = \begin{pmatrix} u_y \\ u_z \end{pmatrix} \tag{15}$$

$$\mathbf{B} = \begin{pmatrix} \mu & 0 \\ 0 & \Gamma \end{pmatrix} \tag{16}$$

$$\mathbf{P} = i \begin{pmatrix} 0 & \mu\kappa \\ \lambda\kappa & 0 \end{pmatrix} \tag{17}$$

$$\mathbf{Y} = i \begin{pmatrix} 0 & \lambda\kappa \\ \mu\kappa & 0 \end{pmatrix} \tag{18}$$

$$\mathbf{W} = \begin{pmatrix} \Gamma q_L^2 & 0 \\ 0 & \mu q_T^2 \end{pmatrix} . \tag{19}$$

Estas son las ecuaciones (3.49), página 68 de [3]. Notar que se cumplen las condiciones de hermiticidad formal ($\mathbf{B} = \mathbf{B}^\dagger$, $\mathbf{Y} = -\mathbf{P}^\dagger$, $\mathbf{W} = \mathbf{W}^\dagger$), y que éste es uno de esos casos en que $\mathbf{P}$ no es nula ni hermítica. $\mathbf{P}$ aparece por el movimiento transversal; notar que se anula cuando $\kappa = 0$.

En la forma lineal es ineludible considerar los dos términos:

$$\begin{aligned} \mathbf{A}(z,z') &= \mathbf{B}(z) \cdot {}'\mathbf{G}(z,z') + \mathbf{P}(z) \cdot \mathbf{G}(z,z') \\ &= \begin{pmatrix} \mu & 0 \\ 0 & \Gamma \end{pmatrix} \cdot {}'\mathbf{G}(z,z') + i\kappa \begin{pmatrix} 0 & \mu \\ \lambda & 0 \end{pmatrix} \cdot \mathbf{G}(z,z') . \end{aligned} \tag{20}$$

Vale la pena notar los siguientes aspectos:

1. De (11) no se derivan estas formas de **P** y **Y**. Para llegar a ellas hay que discutir la forma de las ecuaciones del movimiento para un medio no homogéneo, o lo que es lo mismo, analizar qué forma lineal es continua a lo largo del sistema.
2. En [3], ecuaciones (3.49), página 68, la **P** no tiene el prefactor *i*. Esto parece ser un gazapo de este libro.
3. La condición del salto ($\mathscr{A}^+ - \mathscr{A}^- = -\mathbf{I}_2$) debe ser cumplida en todo momento por (20). En un medio homogéneo esto implica que

$$\Delta\,'\mathscr{G} = -\begin{pmatrix} \mu^{-1} & 0 \\ 0 & \Gamma^{-1} \end{pmatrix}$$

   Ecuación (1.78) de [3]. Esta forma simple del salto también ocurre en todo punto donde los parámetros de Lamé sean continuos ya que el término $\mathbf{P}\cdot\mathbf{G}$ toma el mismo valor a la derecha e izquierda del punto en cuestión. Si analizamos incidencia normal ($\kappa = 0$) tampoco este término aporta nada al análisis, aunque μ y λ tomen valores distintos a derecha e izquierda, pues $\mathbf{P} = \mathbf{0}_2$. Pero en una intercara, y a $\kappa \neq 0$, el segundo término de (20) cuenta pues λ y μ pueden tomar valores diferentes a ambos lados de la intercara. Sería peligroso olvidar este detalle. Para hallar la función de Green de un medio homogéneo no es importante pero al hacer empalmes es imprescindible tener en cuenta que *quien salta* es la proyección de la Forma Diferencial Lineal $\mathbf{A}(z,z')$ dada en (20); no $'\mathscr{G}(z)$.
4. Como $\mathbf{P}+\mathbf{Y} \neq \mathbf{0}$, la función de Green regular en el infinito adopta la segunda forma discutida en [10], o sea que contiene la función $\text{sign}(z-z')$ en ciertos elementos matriciales.

3 Modos electromagnéticos en sistemas a capas de materiales bianisotrópicos

3.1 Consideraciones generales

Los medios bianisotrópico se caracterizan por las siguientes relaciones constitutivas:

$$\overline{D} = \hat{\varepsilon} \cdot \overline{E} + \hat{\xi} \cdot \overline{H}; \tag{21}$$

$$\overline{B} = \hat{\zeta} \cdot \overline{E} + \hat{\mu} \cdot \overline{H}, \tag{22}$$

donde intervienen los vectores: intensidad del campo eléctrico ($\overline{E}$), intensidad del campo magnético ($\overline{H}$), densidad de flujo magnético ($\overline{B}$) y el desplazamiento eléctrico ($\overline{D}$). En este caso $\hat{\varepsilon}$, $\hat{\xi}$, $\hat{\zeta}$ y $\hat{\mu}$ son matrices de orden 3×3. A la matriz $\hat{\varepsilon}$ se le conoce como tensor permitividad y a $\hat{\mu}$ como tensor permeabilidad. A $\hat{\xi}$ y $\hat{\zeta}$ se le conocen como tensores de acoplamiento cruzado magnetoeléctrico. En general los cristales son descritos con tensores $\hat{\varepsilon}$ y $\hat{\mu}$ simétricos.

Las relaciones (21) y (22) pueden escribirse en la forma:

$$\overline{D} = \hat{\gamma} \cdot \overline{E} + \hat{\chi} \cdot \overline{B}; \tag{23}$$

$$\overline{H} = \hat{\nu} \cdot \overline{B} + \hat{\tau} \cdot \overline{E}, \tag{24}$$

donde:

$$\hat{\nu} = \hat{\mu}^{-1}; \tag{25}$$

$$\hat{\tau} = -\hat{\nu} \cdot \hat{\zeta}; \tag{26}$$

$$\hat{\chi} = \hat{\xi} \cdot \hat{\nu}; \tag{27}$$

$$\hat{\gamma} = \hat{\varepsilon} + \hat{\xi} \cdot \hat{\tau}. \tag{28}$$

Se asume que la heteroestructura a estudiar tiene geometría planar y que los tensores $\hat{\varepsilon}$, $\hat{\xi}$, $\hat{\zeta}$ y $\hat{\mu}$, solo dependerán de la coordenada z perpendicular a las intercaras de dicha heteroestructura. Estos significa que los modos normales pueden expresarse como una exponencial de $i(\kappa_1 x + \kappa_2 y - \omega t)$ multiplicado por una función de la variable z, siendo κ_1 y κ_2 las componentes del vector de onda en el plano de las interfaces. Consideremos un medio conductor gobernado por la ley de Ohm: $\overline{J}_c = \hat{\sigma} \cdot \overline{E}$. Al igual que el resto de los tensores $\hat{\sigma}$ dependerá solamente de la coordenada z.

En este trabajo presentamos un sistema de ecuaciones del tipo Sturm-Liouville matricial (ESLM) para el medio bianisotrópico cuyas incógnitas son las componentes transversales del campo eléctrico $E_1 \equiv E_x$ y $E_2 \equiv E_y$:

$$\frac{d}{dz}\left[B_{\gamma\eta}\,\frac{dE_\eta(z)}{dz}+P_{\gamma\eta}\,E_\eta(z)\right]+Y_{\gamma\eta}\,\frac{dE_\eta(z)}{dz}+W_{\gamma\eta}\,E_\eta(z)=\mathbf{0}$$
$$\gamma,\eta=1,2. \quad (29)$$

Los pasos para obtener esta ecuación son similares a los descritos en [27] donde se reportó una ESLM que describe la propagación de ondas electromagnéticas en un medio anisotrópico. Como es natural, en el desarrollo para obtener la ecuación (29) se deben tener en cuenta las nuevas relaciones constitutivas: Eq. (23) y Eq. (24). Esto implica que al aplicar la ley de Ampère (ver Ref. [27]) debemos hacer uso también de la ley de Faraday $\nabla\times\overline{E}=-\frac{\partial}{\partial t}\overline{B}$ para sustituir la derivada temporal de $\overline{B}$ por las derivadas espaciales presentes en el rotor de $\overline{E}$.

A continuación aparecen expresadas las matrices $\mathbf{B}(z)$, $\mathbf{P}(z)$, $\mathbf{Y}(z)$ y $\mathbf{W}(z)$ de orden 2×2 que forman parte de (29). Es fácil comprobar que estas matrices y la ESLM derivan en las correspondientes al caso anisotrópico [27] cuando los tensores $\hat{\xi}$ y $\hat{\zeta}$ son nulos. En los cálculos se consideraron no nulos los nueve elementos de cada uno de los tensores presentes en las relaciones (21) y (22) así como también los elementos del tensor de conductividad eléctrica $(\hat{\sigma})$. Los tensores $\hat{\varepsilon}$, $\hat{\mu}$ y $\hat{\sigma}$ fueron considerados simétricos. De esta forma, las expresiones obtenidas pueden ser utilizadas directamente, sin necesidad de llevar los tensores a ejes principales previamente.

$$\mathbf{B}(z)=\begin{pmatrix}(C_2+C_{2bb})\frac{(C_2+C_{2b})}{(C_1+C_{1b})}-\hat{\nu}_{22} & \hat{\nu}_{12}+(C_2+C_{2bb})\frac{(C_3+C_{3b})}{(C_1+C_{1b})}\\ \hat{\nu}_{12}+(C_2+C_{2b})\frac{(C_3+C_{3bb})}{(C_1+C_{1b})} & (C_3+C_{3bb})\frac{(C_3+C_{3b})}{(C_1+C_{1b})}-\hat{\nu}_{11}\end{pmatrix}; \quad (30)$$

$$\mathbf{P}(z)=\begin{pmatrix}i\left[\kappa_2\hat{\nu}_{23}-\omega\hat{\tau}_{21}-(C_2+C_{2bb})\frac{(C_4+C_{4b})}{(C_1+C_{1b})}\right] & -i\left[\kappa_1\hat{\nu}_{23}+\omega\hat{\tau}_{22}+(C_2+C_{2bb})\frac{(C_5+C_{5b})}{(C_1+C_{1b})}\right]\\ -i\left[\kappa_2\hat{\nu}_{13}-\omega\hat{\tau}_{11}+(C_3+C_{3bb})\frac{(C_4+C_{4b})}{(C_1+C_{1b})}\right] & i\left[\kappa_1\hat{\nu}_{13}+\omega\hat{\tau}_{12}-(C_3+C_{3bb})\frac{(C_5+C_{5b})}{(C_1+C_{1b})}\right]\end{pmatrix}; \quad (31)$$

$$\mathbf{Y}(z)=\begin{pmatrix}i\left[\kappa_2\hat{\nu}_{23}+\omega\hat{\chi}_{12}-(C_2+C_{2b})\frac{(C_4+C_{4bb})}{(C_1+C_{1b})}\right] & -i\left[\kappa_2\hat{\nu}_{13}+\omega\hat{\chi}_{11}+(C_3+C_{3b})\frac{(C_4+C_{4bb})}{(C_1+C_{1b})}\right]\\ -i\left[\kappa_1\hat{\nu}_{23}-\omega\hat{\chi}_{22}+(C_2+C_{2b})\frac{(C_5+C_{5bb})}{(C_1+C_{1b})}\right] & i\left[\kappa_1\hat{\nu}_{13}-\omega\hat{\chi}_{21}-(C_3+C_{3b})\frac{(C_5+C_{5bb})}{(C_1+C_{1b})}\right]\end{pmatrix}; \quad (32)$$

$$\mathbf{W}(z) = \begin{pmatrix} \left[(C_7 + C_{7b}) - (C_4 + C_{4bb})\frac{(C_4+C_{4b})}{(C_1+C_{1b})}\right] & -\left[(C_6 + C_{6b}) + (C_4 + C_{4bb})\frac{(C_5+C_{5b})}{(C_1+C_{1b})}\right] \\ -\left[(C_6 + C_{6bb}) + (C_4 + C_{4b})\frac{(C_5+C_{5bb})}{(C_1+C_{1b})}\right] & \left[(C_8 + C_{8b}) - (C_5 + C_{5bb})\frac{(C_5+C_{5b})}{(C_1+C_{1b})}\right] \end{pmatrix}. \tag{33}$$

Los coeficientes C_1 a C_8 corresponden con el de un sistema anisotrópico y fueron reportados en [27]:

$$\begin{aligned}
C_1 &= \kappa_2^2\hat{\nu}_{11} - 2\kappa_1\kappa_2\hat{\nu}_{12} + \kappa_1^2\hat{\nu}_{22} - \omega^2\left(\hat{\varepsilon}_{33} + i\frac{\hat{\sigma}_{33}}{\omega}\right);\\
C_2 &= \kappa_1\hat{\nu}_{22} - \kappa_2\hat{\nu}_{12};\\
C_3 &= \kappa_2\hat{\nu}_{11} - \kappa_1\hat{\nu}_{12};\\
C_4 &= \kappa_1\kappa_2\hat{\nu}_{23} - \kappa_2^2\hat{\nu}_{13} - \omega^2\left(\hat{\varepsilon}_{13} + i\frac{\hat{\sigma}_{13}}{\omega}\right);\\
C_5 &= \kappa_1\kappa_2\hat{\nu}_{13} - \kappa_1^2\hat{\nu}_{23} - \omega^2\left(\hat{\varepsilon}_{23} + i\frac{\hat{\sigma}_{23}}{\omega}\right);\\
C_6 &= \kappa_1\kappa_2\hat{\nu}_{33} + \omega^2\left(\hat{\varepsilon}_{12} + i\frac{\hat{\sigma}_{12}}{\omega}\right);\\
C_7 &= \kappa_2^2\hat{\nu}_{33} - \omega^2\left(\hat{\varepsilon}_{11} + i\frac{\hat{\sigma}_{11}}{\omega}\right);\\
C_8 &= \kappa_1^2\hat{\nu}_{33} - \omega^2\left(\hat{\varepsilon}_{22} + i\frac{\hat{\sigma}_{22}}{\omega}\right).
\end{aligned} \tag{34}$$

Nótese que considerar la conductividad es equivalente a sustituir el tensor permitividad $\hat{\varepsilon}$ por la permitividad compleja $\tilde{\varepsilon}$ que es un tensor cuyos elementos son $\tilde{\varepsilon}_{nm} = \hat{\varepsilon}_{nm} + i\frac{\hat{\sigma}_{nm}}{\omega}$.

Los coeficientes C_{1b} a C_{8b} y C_{2bb} a C_{6bb} se deben a la bianisotropía:

$$C_{1b} = -\omega^2(\hat{\xi}\cdot\hat{\tau})_{33} + \omega\kappa_1(\hat{\chi}_{32} - \hat{\tau}_{23}) + \omega\kappa_2(\hat{\tau}_{13} - \hat{\chi}_{31});$$

$$\begin{aligned} C_{2b} &= \omega\hat{\chi}_{32};\\ C_{2bb} &= -\omega\hat{\tau}_{23};\end{aligned}$$

$$\begin{aligned} C_{3b} &= -\omega\hat{\chi}_{31};\\ C_{3bb} &= \omega\hat{\tau}_{13};\end{aligned}$$

$$\begin{aligned} C_{4b} &= -\omega^2(\hat{\xi}\cdot\hat{\tau})_{31} - \omega\kappa_1\hat{\tau}_{21} + \omega\kappa_2\hat{\tau}_{11} + \omega\kappa_2\hat{\chi}_{33};\\ C_{4bb} &= -\omega^2(\hat{\xi}\cdot\hat{\tau})_{13} + \omega\kappa_1\hat{\chi}_{12} - \omega\kappa_2\hat{\chi}_{11} - \omega\kappa_2\hat{\tau}_{33}; \end{aligned} \tag{35}$$

$$\begin{aligned} C_{5b} &= -\omega^2(\hat{\xi}\cdot\hat{\tau})_{32} - \omega\kappa_1\hat{\tau}_{22} + \omega\kappa_2\hat{\tau}_{12} - \omega\kappa_1\hat{\chi}_{33};\\ C_{5bb} &= -\omega^2(\hat{\xi}\cdot\hat{\tau})_{23} + \omega\kappa_1\hat{\chi}_{22} - \omega\kappa_2\hat{\chi}_{21} + \omega\kappa_1\hat{\tau}_{33};\end{aligned}$$

$$\begin{aligned} C_{6b} &= \omega^2(\hat{\xi}\cdot\hat{\tau})_{12} + \omega\kappa_2\hat{\tau}_{32} + \omega\kappa_1\hat{\chi}_{13};\\ C_{6bb} &= \omega^2(\hat{\xi}\cdot\hat{\tau})_{21} - \omega\kappa_2\hat{\chi}_{23} - \omega\kappa_1\hat{\tau}_{31}; \end{aligned} \tag{36}$$

$$C_{7b} = -\omega^2(\hat{\xi}\cdot\hat{\tau})_{11} + \omega\kappa_2(\hat{\chi}_{13} - \hat{\tau}_{31});$$

$$C_{8b} = -\omega^2(\hat{\xi}\cdot\hat{\tau})_{22} + \omega\kappa_1(\hat{\tau}_{32} - \hat{\chi}_{23}). \tag{37}$$

A partir de las expresiones anteriores se pueden determinar condiciones de simetría para los tensores presentes en las relaciones (21) y (22) que de cumplirse darían lugar a un operador Sturm-Liouville formalmente hermítico es decir, se cumpliría que $\mathbf{B} = \mathbf{B}^\dagger, \mathbf{W} = \mathbf{W}^\dagger, \mathbf{Y} = -\mathbf{P}^\dagger$. Las siguientes condiciones son suficientes:

- $\hat{\varepsilon}$ y $\hat{\mu}$ reales y simétricos, $\hat{\xi} = \hat{\zeta}^\dagger$ y $\hat{\sigma} = \mathbf{0}$.

El símbolo † sobre la matrix significa su traspuesta conjugada. Si se cumplen las condiciones de hermiticidad formal, entonces los eigenvalores del operador Sturm-Liouville podrán ser reales o aparecerán en pares del tipo: k_ℓ y su complejo conjugado.

El cálculo de las correspondientes componentes de la forma diferencial lineal $A_\gamma = B_{\gamma\eta}\ \frac{dE_\eta(z)}{dz} + P_{\gamma\eta}\ E_\eta(z)$ presentes en la ecuación

(29) conduce a $A_1(z) = -i\omega H_2(z)$ y $A_2(z) = i\omega H_1(z)$. Este resultado asocia directamente la propiedad de continuidad de $\mathbf{A}(z)$ con la continuidad de las componentes transversales H_1, H_2 del campo magnético. El mismo resultado fue reportado en [27] para el caso del medio anisotrópico.

La búsqueda de soluciones linealmente independientes (LI) del sistema diferencial (29) en un dominio homogéneo conduce al planteamiento de un problema cuadrático de eigenvalores [28]. Un análisis detallado de la solución de este problema para la ESLM se puede encontrar en [10]. A continuación solo se presentan algunos elementos básicos que serán de utilidad para expresar una función de Green para los medios bianisotrópicos que abordamos a modo de ejemplo en la secciones siguientes.

Para un dominio homogéneo, las soluciones LI del sistema diferencial (29) pueden expresarse en forma de exponenciales:

$$\overline{E}_{\perp} = \overline{E}_{0\perp} e^{ikz}, \tag{38}$$

siendo $\overline{E}_{\perp} = [E_1, E_2]^T$ el vector que involucra las componentes transversales del campo eléctrico, en correspondencia con la Eq. (29). Los eigenvalores k se obtienen a partir de los ceros del determinante de la matriz secular:

$$\mathbf{Q}(k) = -k^2\mathbf{B} + ik(\mathbf{P} + \mathbf{Y}) + \mathbf{W}. \tag{39}$$

Si la matrix $\mathbf{B}$ es regular tendremos un conjunto $K = \{k_j, j = 1,2,3,4\}$ de cuatro eigenvalores ($\mathbf{Q}(k)$ resulta un polinomio de cuarto orden en k).

En [10] se reportó una forma general y compacta para la función de Green ($\mathbf{G}(z,z')$) regular en el infinito para el operador Sturm-Liouville matricial homogéneo. La homogeneidad significa que los parámetros que involucrados en los coeficientes matriciales ($\mathbf{B}$, $\mathbf{P}$, $\mathbf{Y}$ y $\mathbf{W}$) no dependen de la posición. Esta forma general de $\mathbf{G}(z,z')$ admite dos simplificaciones importantes cuando los eigenvalores k_j aparecen por pares del tipo $(k_j, -k_j)$, una para los problemas con $\mathbf{P} + \mathbf{Y} = \mathbf{0}$ y la otra para los problemas con $\mathbf{P} + \mathbf{Y} \neq \mathbf{0}$. En las secciones siguientes presentaremos ambas simplificaciones.

3.2 Medios magnetoeléctricos

Según Kong [24] los materiales magnetoeléctricos fueron predichos teóricamente por Dzyaloshinskii [12] y Landau y Lifshitz [14] y observados experimentalmente en 1960 por Astrov [11] en óxido de cromo antiferromagnético. Para estos medios Dzyaloshinskii propuso las siguientes relaciones constitutivas:

$$\overline{D} = \begin{pmatrix} \varepsilon & 0 & 0 \\ 0 & \varepsilon & 0 \\ 0 & 0 & \varepsilon_z \end{pmatrix} \cdot \overline{E} + \begin{pmatrix} \xi & 0 & 0 \\ 0 & \xi & 0 \\ 0 & 0 & \xi_z \end{pmatrix} \cdot \overline{H} \tag{40}$$

$$\overline{B} = \begin{pmatrix} \xi & 0 & 0 \\ 0 & \xi & 0 \\ 0 & 0 & \xi_z \end{pmatrix} \cdot \overline{E} + \begin{pmatrix} \mu & 0 & 0 \\ 0 & \mu & 0 \\ 0 & 0 & \mu_z \end{pmatrix} \cdot \overline{H} \,. \tag{41}$$

En este caso las matrices **B**, **P** y **Y** resultan:

$$\mathbf{B} = \begin{pmatrix} -\frac{1}{\mu} + \frac{{\kappa_1}^2}{\mu^2\left(\frac{{\kappa_1}^2}{\mu}+\frac{{\kappa_2}^2}{\mu}+\frac{{\xi_z}^2\omega^2}{\mu_z}-\left(\varepsilon_z+\frac{i\sigma_z}{\omega}\right)\omega^2\right)} & \frac{\kappa_1\kappa_2}{\mu^2\left(\frac{{\kappa_1}^2}{\mu}+\frac{{\kappa_2}^2}{\mu}+\frac{{\xi_z}^2\omega^2}{\mu_z}-\left(\varepsilon_z+\frac{i\sigma_z}{\omega}\right)\omega^2\right)} \\ \frac{\kappa_1\kappa_2}{\mu^2\left(\frac{{\kappa_1}^2}{\mu}+\frac{{\kappa_2}^2}{\mu}+\frac{{\xi_z}^2\omega^2}{\mu_z}-\left(\varepsilon_z+\frac{i\sigma_z}{\omega}\right)\omega^2\right)} & -\frac{1}{\mu} + \frac{{\kappa_2}^2}{\mu^2\left(\frac{{\kappa_1}^2}{\mu}+\frac{{\kappa_2}^2}{\mu}+\frac{{\xi_z}^2\omega^2}{\mu_z}-\left(\varepsilon_z+\frac{i\sigma_z}{\omega}\right)\omega^2\right)} \end{pmatrix}; \tag{42}$$

$$\mathbf{P} = \begin{pmatrix} -\frac{i\kappa_1\left(-\frac{\kappa_2\xi\omega}{\mu}+\frac{\kappa_2\xi_z\omega}{\mu_z}\right)}{\mu\left(\frac{{\kappa_1}^2}{\mu}+\frac{{\kappa_2}^2}{\mu}+\frac{{\xi_z}^2\omega^2}{\mu_z}-\left(\varepsilon_z+\frac{i\sigma_z}{\omega}\right)\omega^2\right)} & -i\left(-\frac{\xi\omega}{\mu}+\frac{\kappa_1\left(\frac{\kappa_1\xi\omega}{\mu}-\frac{\kappa_1\xi_z\omega}{\mu_z}\right)}{\mu\left(\frac{{\kappa_1}^2}{\mu}+\frac{{\kappa_2}^2}{\mu}+\frac{{\xi_z}^2\omega^2}{\mu_z}-\left(\varepsilon_z+\frac{i\sigma_z}{\omega}\right)\omega^2\right)}\right) \\ -i\left(\frac{\xi\omega}{\mu}+\frac{\kappa_2\left(-\frac{\kappa_2\xi\omega}{\mu}+\frac{\kappa_2\xi_z\omega}{\mu_z}\right)}{\mu\left(\frac{{\kappa_1}^2}{\mu}+\frac{{\kappa_2}^2}{\mu}+\frac{{\xi_z}^2\omega^2}{\mu_z}-\left(\varepsilon_z+\frac{i\sigma_z}{\omega}\right)\omega^2\right)}\right) & -\frac{i\kappa_2\left(\frac{\kappa_1\xi\omega}{\mu}-\frac{\kappa_1\xi_z\omega}{\mu_z}\right)}{\mu\left(\frac{{\kappa_1}^2}{\mu}+\frac{{\kappa_2}^2}{\mu}+\frac{{\xi_z}^2\omega^2}{\mu_z}-\left(\varepsilon_z+\frac{i\sigma_z}{\omega}\right)\omega^2\right)} \end{pmatrix}; \tag{43}$$

$$\mathbf{Y}=\begin{pmatrix} -\frac{i\kappa_1\left(-\frac{\kappa_2\xi\omega}{\mu}+\frac{\kappa_2\xi_z\omega}{\mu_z}\right)}{\mu\left(\frac{\kappa_1{}^2}{\mu}+\frac{\kappa_2{}^2}{\mu}+\frac{\xi_z{}^2\omega^2}{\mu_z}-\left(\varepsilon_z+\frac{i\sigma_z}{\omega}\right)\omega^2\right)} & -i\left(\frac{\xi\omega}{\mu}+\frac{\kappa_2\left(-\frac{\kappa_2\xi\omega}{\mu}+\frac{\kappa_2\xi_z\omega}{\mu_z}\right)}{\mu\left(\frac{\kappa_1{}^2}{\mu}+\frac{\kappa_2{}^2}{\mu}+\frac{\xi_z{}^2\omega^2}{\mu_z}-\left(\varepsilon_z+\frac{i\sigma_z}{\omega}\right)\omega^2\right)}\right) \\ -i\left(-\frac{\xi\omega}{\mu}+\frac{\kappa_1\left(\frac{\kappa_1\xi\omega}{\mu}-\frac{\kappa_1\xi_z\omega}{\mu_z}\right)}{\mu\left(\frac{\kappa_1{}^2}{\mu}+\frac{\kappa_2{}^2}{\mu}+\frac{\xi_z{}^2\omega^2}{\mu_z}-\left(\varepsilon_z+\frac{i\sigma_z}{\omega}\right)\omega^2\right)}\right) & -\frac{i\kappa_2\left(\frac{\kappa_1\xi\omega}{\mu}-\frac{\kappa_1\xi_z\omega}{\mu_z}\right)}{\mu\left(\frac{\kappa_1{}^2}{\mu}+\frac{\kappa_2{}^2}{\mu}+\frac{\xi_z{}^2\omega^2}{\mu_z}-\left(\varepsilon_z+\frac{i\sigma_z}{\omega}\right)\omega^2\right)} \end{pmatrix}; \tag{44}$$

En tanto que los elementos de $\mathbf{W}$ son:

$$\begin{aligned}
W_{11} &= \frac{\kappa_2{}^2}{\mu_z}+\frac{\xi^2\omega^2}{\mu}-\left(\varepsilon+\frac{i\sigma}{\omega}\right)\omega^2-\frac{\left(-\frac{\kappa_2\xi\omega}{\mu}+\frac{\kappa_2\xi_z\omega}{\mu_z}\right)^2}{\frac{\kappa_1{}^2}{\mu}+\frac{\kappa_2{}^2}{\mu}+\frac{\xi_z{}^2\omega^2}{\mu_z}-\left(\varepsilon_z+\frac{i\sigma_z}{\omega}\right)\omega^2}; \\
W_{12} &= -\frac{\kappa_1\kappa_2}{\mu_z}-\frac{\left(\frac{\kappa_1\xi\omega}{\mu}-\frac{\kappa_1\xi_z\omega}{\mu_z}\right)\left(-\frac{\kappa_2\xi\omega}{\mu}+\frac{\kappa_2\xi_z\omega}{\mu_z}\right)}{\frac{\kappa_1{}^2}{\mu}+\frac{\kappa_2{}^2}{\mu}+\frac{\xi_z{}^2\omega^2}{\mu_z}-\left(\varepsilon_z+\frac{i\sigma_z}{\omega}\right)\omega^2}; \\
W_{21} &= -\frac{\kappa_1\kappa_2}{\mu_z}-\frac{\left(\frac{\kappa_1\xi\omega}{\mu}-\frac{\kappa_1\xi_z\omega}{\mu_z}\right)\left(-\frac{\kappa_2\xi\omega}{\mu}+\frac{\kappa_2\xi_z\omega}{\mu_z}\right)}{\frac{\kappa_1{}^2}{\mu}+\frac{\kappa_2{}^2}{\mu}+\frac{\xi_z{}^2\omega^2}{\mu_z}-\left(\varepsilon_z+\frac{i\sigma_z}{\omega}\right)\omega^2}; \\
W_{22} &= \frac{\kappa_1{}^2}{\mu_z}+\frac{\xi^2\omega^2}{\mu}-\left(\varepsilon+\frac{i\sigma}{\omega}\right)\omega^2-\frac{\left(\frac{\kappa_1\xi\omega}{\mu}-\frac{\kappa_1\xi_z\omega}{\mu_z}\right)^2}{\frac{\kappa_1{}^2}{\mu}+\frac{\kappa_2{}^2}{\mu}+\frac{\xi_z{}^2\omega^2}{\mu_z}-\left(\varepsilon_z+\frac{i\sigma_z}{\omega}\right)\omega^2}.
\end{aligned} \tag{45}$$

A modo ilustrativo se consideró:

$$\hat{\sigma}=\begin{pmatrix}\sigma & 0 & 0\\ 0 & \sigma & 0\\ 0 & 0 & \sigma_z\end{pmatrix}. \tag{46}$$

Como es de esperar, para $\hat{\sigma}=\mathbf{0}$ se cumplen las condiciones de hermiticidad formal del operador Sturm-Liouville matricial:

$$\begin{aligned}
\mathbf{B} &= \mathbf{B}^\dagger; \\
\mathbf{W} &= \mathbf{W}^\dagger; \\
\mathbf{Y} &= -\mathbf{P}^\dagger.
\end{aligned} \tag{47}$$

Se puede verificar que en este caso el determinante de la matriz secular $\mathbf{Q}(k)$ solo contiene potencias pares de k, lo que significa que los eigenvalores también formarán pares del tipo $(k_j, -k_j)$. Para este ejemplo tenemos que $\mathbf{P} + \mathbf{Y} \neq \mathbf{0}$ de modo que la función de Green $\mathbf{G}(z, z')$ admite la siguiente simplificación [10]:

$$\mathbf{G}(z,z') = \sum_{k_j \in K_\uparrow;\ j=1,2} i \frac{\mathbf{C}_o^T(\mathrm{sgn}(z-z')\cdot k_j)}{D'(k_j)}\, e^{ik_j|z-z'|}\,, \qquad (48)$$

donde $\mathbf{C}_o(k)$ es la matriz de cofactores de la matriz secular $\mathbf{Q}(k)$ y $\mathbf{C}_o^T(k)$ es su traspuesta. Nótese que esta matrix es evaluada en k_j multiplicado por la función signo sgn de argumento $z - z'$. El denominador $D'(k)$ es el polinomio en k que resulta de derivar el polinimio secular $\mathrm{Det}[\mathbf{Q}(k)]$ con respecto a k. Los eigenvalores k_j generalmente son complejos, y el subconjunto $K_\uparrow$ incluye los eigenvalores con parte imaginaria positiva. Si alguna de las parejas $(k_j, -k_j)$ fuera real, se toma el eigenvalor positivo para evaluar (48).

3.3 Resonador de anillo partido

Un "Resonador de anillo partido" (Split-Ring Resonator, SRR) es una estructura producida artificialmente que consiste en dos anillos metálicos concéntricos abiertos en extremos opuestos y su diseño fue sugerido por Pendry et al. en 1999 [29] como un material que exhibe una permeabilidad magnética $\mu < 0$ alrededor de la frecuencia de resonancia magnética. Los metamateriales cuyos bloques básicos presentan estas estructuras pueden exhibir respuestas electromagnéticas efectivas exóticas que incluyen pero no se limitan a índices de refraccción negativos o cercanos a cero [30, 31, 32]. El SRR puede ser modelado como un medio bianisotrópico con las siguientes relaciones constitutivas [24, 33, 34]:

$$\overline{D} = \begin{pmatrix} \varepsilon_x & 0 & 0 \\ 0 & \varepsilon_y & 0 \\ 0 & 0 & \varepsilon_z \end{pmatrix} \cdot \overline{E} + \begin{pmatrix} 0 & 0 & 0 \\ 0 & 0 & 0 \\ 0 & -i\xi_0 & 0 \end{pmatrix} \cdot \overline{H}; \qquad (49)$$

$$\overline{B} = \begin{pmatrix} 0\,0 & 0 \\ 0\,0 & +i\xi_0 \\ 0\,0 & 0 \end{pmatrix} \cdot \overline{E} + \begin{pmatrix} \mu_x & 0 & 0 \\ 0 & \mu_y & 0 \\ 0 & 0 & \mu_z \end{pmatrix} \cdot \overline{H}. \tag{50}$$

En este caso las matrices **B**, **P**, **Y** y **W** resultan:

$$\mathbf{B} = \begin{pmatrix} -\frac{1}{\mu_y} + \frac{\left(\frac{\kappa_1}{\mu_y} - \frac{i\xi_0\omega}{\mu_y}\right)\left(\frac{\kappa_1}{\mu_y} + \frac{i\xi_0\omega}{\mu_y}\right)}{\frac{\kappa_2{}^2}{\mu_x} + \frac{\kappa_1{}^2}{\mu_y} - \varepsilon_z\omega^2 + \frac{\xi_0{}^2\omega^2}{\mu_y}} & \frac{\kappa_2\left(\frac{\kappa_1}{\mu_y} + \frac{i\xi_0\omega}{\mu_y}\right)}{\mu_x\left(\frac{\kappa_2{}^2}{\mu_x} + \frac{\kappa_1{}^2}{\mu_y} - \varepsilon_z\omega^2 + \frac{\xi_0{}^2\omega^2}{\mu_y}\right)} \\ \frac{\kappa_2\left(\frac{\kappa_1}{\mu_y} - \frac{i\xi_0\omega}{\mu_y}\right)}{\mu_x\left(\frac{\kappa_2{}^2}{\mu_x} + \frac{\kappa_1{}^2}{\mu_y} - \varepsilon_z\omega^2 + \frac{\xi_0{}^2\omega^2}{\mu_y}\right)} & -\frac{1}{\mu_x} + \frac{\kappa_2{}^2}{\mu_x{}^2\left(\frac{\kappa_2{}^2}{\mu_x} + \frac{\kappa_1{}^2}{\mu_y} - \varepsilon_z\omega^2 + \frac{\xi_0{}^2\omega^2}{\mu_y}\right)} \end{pmatrix}; \tag{51}$$

$$\mathbf{P} = \mathbf{0}; \tag{52}$$

$$\mathbf{Y} = \mathbf{0}; \tag{53}$$

$$\mathbf{W} = \begin{pmatrix} \frac{\kappa_2{}^2}{\mu_z} - \varepsilon_x\omega^2 & -\frac{\kappa_1\kappa_2}{\mu_z} \\ -\frac{\kappa_1\kappa_2}{\mu_z} & \frac{\kappa_1{}^2}{\mu_z} - \varepsilon_y\omega^2 \end{pmatrix}. \tag{54}$$

Se puede verificar de forma simple y directa que en este caso donde hemos considerado $\hat{\sigma} = \mathbf{0}$, también se cumplen las condiciones de hermiticidad formal del operador Sturm-Liouville matricial. Dado que $\mathbf{P} + \mathbf{Y} = \mathbf{0}$ queda claro que el determinante secular solo tendrá potencias pares de k, lo que significa que los eigenvalores también formarán pares del tipo $(k_j, -k_j)$. Para este problema donde $\mathbf{P} + \mathbf{Y} = \mathbf{0}$ la función de Green $\mathbf{G}(z, z')$ admite la siguiente simplificación [10]:

$$\mathbf{G}(z, z') = \sum_{k_j \in K_\uparrow;\ j=1,2} i\frac{\mathbf{C}_o^T(k_j)}{D'(k_j)} e^{ik_j|z-z'|}. \tag{55}$$

En este ejemplo las expresiones analíticas son más sencillas que en el ejemplo anterior, y se tiene que:

$$\mathbf{G}(z,z') = \frac{i}{k_1\left(4\mathrm{Det}[\mathbf{B}]k_1^2 - 2M\right)} \begin{pmatrix} -B_{22}k_1^2 + W_{22} & B_{12}k_1^2 - W_{12} \\ B_{21}k_1^2 - W_{21} & -B_{11}k_1^2 + W_{11} \end{pmatrix} e^{ik_1|z-z'|} + \frac{i}{k_2\left(4\mathrm{Det}[\mathbf{B}]k_2^2 - 2M\right)} \begin{pmatrix} -B_{22}k_2^2 + W_{22} & B_{12}k_2^2 - W_{12} \\ B_{21}k_2^2 - W_{21} & -B_{11}k_2^2 + W_{11} \end{pmatrix} e^{ik_2|z-z'|}, \tag{56}$$

con:

$$k_1 = +\sqrt{\frac{M + \sqrt{M^2 - 4\mathrm{Det}[\mathbf{B}]\mathrm{Det}[\mathbf{W}]}}{2\mathrm{Det}[\mathbf{B}]}}; \qquad k_2 = +\sqrt{\frac{M - \sqrt{M^2 - 4\mathrm{Det}[\mathbf{B}]\mathrm{Det}[\mathbf{W}]}}{2\mathrm{Det}[\mathbf{B}]}}, \tag{57}$$

donde $M = B_{22}W_{11} + B_{11}W_{22} - B_{21}W_{12} - B_{12}W_{21}$, involucra los cuatro elementos matriciales de $\mathbf{B}$ y $\mathbf{W}$. Con $\mathrm{Det}[\mathbf{B}]$ denotamos el determinante de la matrix $\mathbf{B}$ y de igual forma para $\mathbf{W}$.

4 Conclusiones

Como dijimos en la Introducción, hemos analizado dos excitaciones elementales de la mayor importancia en sistemas a capas plano paralelas para concluir que se describen mediante sendos problemas de Sturm-Liouville matriciales. Estas son las oscilaciones elásticas y los modos electromagnéticos cuando los materiales que componen la estructura tienen bianisotropía.

Para cada uno de ellos hemos reportado explícitamente las matrices $\mathbf{B}, \mathbf{P}, \mathbf{Y}, \mathbf{W}$ que entran en el problema de Sturm-Liouville y hemos analizado bajo qué condiciones estas matrices hacen que el operador sea formalmente hermítico. En los casos estudiados solo la presencia de mecanismos de pérdida como la conductividad hacen que el operador no tenga esta importante propiedad.

Las funciones de Green regulares en el infinito de estos problemas solo pueden tener dos formas o estructuras. [10] Estas vienen determinadas simplemente por el hecho de que la matriz $\mathbf{P} + \mathbf{Y}$ sea o no

sea nula. Para los dos casos estudiados hemos podido aportar este importante dato de sus funciones de Green regulares en el infinito.

Agradecimientos

R. Pérez-Álvarez agradece la hospitalidad de los colegas de la Universidad de La Habana (Cuba) y a F. García-Moliner de la Universidad Jaume I, Castellón, España, donde se esbozaron las primeras ideas del presente trabajo. R. Pernas-Salomón agradece el apoyo de la beca PRODEP No. DSA/103.5/16/9408 y la hospitalidad de los colegas del Instituto de Física "Luis Rivera Terrazas" de la Benemérita Universidad Autónoma de Puebla (BUAP).

Bibliografía

1. G. Bastard, *"Wave mechanics applied to semiconductor heterostructures"*, Éditions de Physique, Paris (1989).
2. B. Vinter and C. Weisbuch, *"Quantum Semiconductor Structures"*, Academic Press, San Diego (1991).
3. F García-Moliner and VR Velasco, *"Theory of Single and Multiple Interfaces"*, World Scientific, Singapore (1992).
4. F. García-Moliner, R. Pérez-Alvarez, J. Fernández-Velicia and L. Chico Gómez, *"Electrones y Fonones en Pozos Cuánticos"*, edited by Universidad Nacional de Educación a Distancia (UNED), Madrid, Spain (1994).
5. C Trallero-Giner, R Pérez-Álvarez and F García-Moliner, *"Long wave polar modes in semiconductor heterostructures"*, Elsevier Science (1998).
6. R Pérez-Álvarez and F García-Moliner, *"Transfer matrix, Green Function and related techniques: Tools for the study of multilayer heterostructures"*, Universitat Jaume I, Castellón de la Plana, Spain (2004).
7. R Pernas Salomón, *"Problema de sturm-liouville matricial en el estudio de diversas excitaciones elementales en sistemas a capas"*, Tesis de Doctorado, Universidad Autónoma del Estado de Morelos, México, junio de 2015.
8. R. Pérez-Álvarez and R. Pernas-Salomón, *"Ubiquity of the Sturm-Liouville problem in multilayer systems"*, EPL (Europhysics Letters) 115:1, pp 10 (2016).
9. B Friedman, *"Principles and techniques of applied mathematics"*, J Wiley, New York (1956).
10. René Pernas-Salomón and R. Pérez-Álvarez and V.R. Velasco, *"General form of the Greens function regular at infinity for the homogeneous SturmLiouville matrix operator"*, Appl. Math. and Comput. **269**, 824 - 833, (2015).
11. D.N. Astrov, *"The magnetoelectric effect in antiferromagnetics"*, Zh. Eksp. Teor. Fiz., vol. 38, 984-985 (1960).
12. I.E. Dzyaloshinskii, *"On the magnetoelectrical effect in antiferromagnets*, Soviet Physics JETP, vol. 10, 628-629 (1960).
13. V.L. Inderbom, *"Irreducible representations of the magnetic groups and allowance for magnetic symmetry"*, Soviet Phys. Crystallogr., vol. 5, 493 (1960).

14. L.D. Landau and E.M. Lifschitz, " *Electrodynamics of Continuous Media*", Addison Wesley, Massachusetts, USA, (1960).
15. R.R. Birss, *"Macroscopic symmetry in space-time"*, Rep. Prog. Phys., vol. 26, 307-310 (1963).
16. R.R. Birss and R.G. Shrubsall, *"The propagation of EM waves in magnetoelectric crystals"*, Phil. Mag., vol. 15, 687-700 (1967).
17. G.T. Rado, *"Observation and possible mechanisms of magnetoelectric effects in a ferromagnet"*, Phys. Rev. Lett., vol. 13, 355 (1967).
18. Kaiser S. Kunz, *"Plane electromagnetic waves in moving media and reflections from moving interfaces"*, Journal of Applied Physics, vol. 51, no. 2, 873-884 (1980).
19. D. Censor, *"Dispersion equations in moving media"*, Proceedings of the IEEE, vol. 68, no. 4, 528-529 (1980).
20. Friedrich W. Hehl and Yuri N. Obukhov and Jean-Pierre Rivera and Hans Schmid, *"Relativistic analysis of magnetoelectric crystals: Extracting a new 4-dimensional P odd and T odd pseudoscalar from Cr2O3 data"*, Physics Letters A, vol. 372, no. 8, 1141-1146 (2008).
21. Yuri N. Obukhov and Friedrich W. Hehl, *"Forces and momenta caused by electromagnetic waves in magnetoelectric media"*, Physics Letters A, vol. 372, no. 22, 3946 - 3952 (2008).
22. Young-Sea Huang, *"A new perspective on relativistic transformation versus the conventional Lorentz transformation illustrated by the problem of electromagnetic waves in moving media"*, Physica Scripta, vol. 81, no. 1, 015004 (2010).
23. J.A. Kong, *"Electromagnetic waves in moving media"*, PhD thesis, Syracuse University (1968).
24. J.A. Kong, *"Electromagnetic Wave Theory"*, Cambridge, Massachusetts, USA, EMW Publishing, isbn = 0-9668143-9-8 (2008).
25. Lei Chen, Zhenya Lei, Rui Yang, Xiaowei Shi, and Jiawei Zhang, *"Determining the effective electromagnetic parameters of bianisotropic metamaterials with periodic structures"*, Progress in Electromagneic Research M, Vol. 29, 79-93 (2013).
26. Po-Han Chang, Chih-Yu Kuo, and Ruey-Lin Chern, *"Wave propagation in bianisotropic metamaterials: angular selective transmission"*, Optics Express, Vol. 22, No. 21, 25710-25721 (2014).
27. R. Pernas-Salomón and R. Pérez-Álvarez, *"Sturm-liouville matrix equation for the study of electromagnetic waves propagation in layered anisotropic media"*, Progress In Electromagnetics Research M (PIER M) **40**, 79-90 (2014).
28. Tisseur, F. and Meerbergen, K., *"The Quadratic Eigenvalue Problem"*,SIAM Review **43**:2, 235-286, (2001).
29. J. B. Pendry, A. J. Holden, D. J. Robbins, and W. J. Stewart, *"Magnetism from Conductors and Enhanced Nonlinear Phenomena"*, IEEE TRANSACTIONS ON MICROWAVE THEORY AND TECHNIQUES **47**:11, 2075-2084, (1999).
30. D. R. Smith, Willie J. Padilla, D. C. Vier, S. C. Nemat-Nasser, and S. Schultz, *"Composite Medium with Simultaneously Negative Permeability and Permittivity"*, Phys. Rev. Lett. **84**:18, 4184-4187, (2000).
31. Linden, Stefan and Enkrich, Christian and Wegener, Martin and Zhou, Jiangfeng and Koschny, Thomas and Soukoulis, Costas M, *"Magnetic Response of Metamaterials at 100 Terahertz"*, Science **306**:5700, 1351-1353, (2004).
32. N. Katsarakis, G. Konstantinidis, A. Kostopoulos, R. S. Penciu, T. F. Gundogdu, M. Kafesaki, and E. N. Economou, *"Magnetic response of split-ring resonators in the far-infrared frequency regime"*, OPTICS LETTERS **30**:11, 1348-1350, (2005).
33. Xudong Chen, Bae-Ian Wu, Jin Au Kong, and Tomasz M. Grzegorczyk, *"Retrieval of the effective constitutive parameters of bianisotropic metamaterials"*, Phys. Rev. E. **71**, 046610, (2005).
34. Ugur Cem Hasar, Musa Bute, Joaquim J. Barroso, Cumali Sabah, Yunus Kaya, and Mehmet Ertugrul, *"Power analysis of multilayer structures composed of conventional materials and bi-anisotropic metamaterial slabs"*, J. Opt. Soc. Am. B **31**:5, 939-947, (2014).

Index